The Role of M2 Macrophages and their Product, HB-EGF, as Regulators of Lung Fibrosis

by

Elissa Mairen Barhite Hult

A dissertation submitted in partial fulfillment
of the requirements for the degree of
Doctor of Philosophy
(Molecular and Integrative Physiology)
in the University of Michigan
2022

Doctoral Committee:

Professor Howard C. Crawford, Co-Chair
Professor Bethany B. Moore, Co-Chair
Professor Marc B. Hershenson
Professor Marc Peters-Golden
Professor Rachel L. Zemans

Elissa M. Hult

emhult@umich.edu

ORCID iD: 0000-0002-6644-7134

Dedication

To my family and friends

Acknowledgements

It has been a great pleasure to spend the last five years at the University of Michigan completing my PhD. I want to take this opportunity to acknowledge the many people who have contributed to this work and helped me develop as a scientist and as a person. To my mentor, Dr. Bethany Moore; thank you for your tremendous encouragement and guidance throughout my scientific journey. You have helped me learn how to think scientifically, and your willingness to let me take the lead and lift me back up when experiments fail has helped build my resilience and develop my scientific confidence. Thank you for the countless hours discussing data, helping me with my papers, and providing feedback on my presentations. Your steady stream of support has been instrumental in making my time at Michigan both so successful and so positive, and I look forward to maintaining our relationship for many years to come.

To my co-mentor, Dr. Howard Crawford; thank you for welcoming me into your lab and for prioritizing mentorship even when we were located on different campuses, then different buildings, then different cities. In addition to providing fruitful feedback on my scientific work, I have appreciated your ability to recognize and validate the effort that I put into my scientific research. Your support has been instrumental to my success as a graduate student, and I am so appreciative for your tutelage.

I would also like to thank my committee members, Drs. Rachel Zemans, Marc Peters-Golden, and Marc Hershenson for their support, insights, and experiment suggestions. Your feedback has helped me become a better scientist and I am grateful for your guidance.

Additionally, I would like to thank the members of the Moore and Crawford laboratories. To the Moore lab, thank you for making the lab an enjoyable place to work. A special thank you to Carol Wilke, for providing technical expertise and a calming presence during my first few years as a PhD student, and to Helen Warheit-Niemi, who has been such a strong supporter, scientific collaborator, and wonderful friend. I am so glad we could experience our PhDs together. To the Crawford lab, thank you for welcoming me and for being willing to learn a new disease area in order to offer insightful comments and suggestions for all of my research projects. I have been so fortunate to have two lab spaces full of caring individuals.

I would also like to thank the Molecular and Integrative Physiology Department, both students and faculty. In addition to the many friends that I have made, the community of this department has made it a wonderful place to be a trainee and I'm very glad that I've been able to be a member of this department for five years.

To the beneficence that enabled my own research to be reported in this dissertation, I am grateful to the Immunology Program staff for the support on the Immunology Training grant and to NHLBI at the National Institutes of Health for my F31 dissertation fellowship award. These and other sources have provided funding throughout my graduate education.

Lastly, the biggest thank you to my family and friends. I am lucky to have wonderful friends both in Ann Arbor and in places further away, and I feel so fortunate to have so many people in my life who care about me and want to help me succeed. And, to my family, thank you for your unwavering support, care, and enthusiasm throughout my graduate career and in all other moments of my life. I am so grateful for all of you and to have such wonderful people always in my corner.

Table of Contents

Dedication ii

Acknowledgements iii

List of Figures ix

List of Tables xv

List of Abbreviations xvi

Abstract xviii

Chapter 1: Introduction 1

1.1 IPF: Epidemiology, Diagnosis, Pathogenesis and Treatment 1

1.1.1 Epidemiology 1

1.1.2 Diagnosis 3

1.1.3 Pathogenesis and Treatment 4

1.1.4 Animal Models of Fibrosis 6

1.2 Relevant Background Information for Chapter 2 8

1.2.1 Roles of Fibroblasts and AECs in Fibrosis 8

1.2.2 Inflammatory cells are important to understanding fibrosis 11

1.2.3 Types of Macrophages – Alveolar vs. Interstitial 12

1.2.4 Macrophages during fibrosis 13

1.2.5 Relevance of the M1/M2 model in fibrosis studies 14

1.3 Relevant Background Information for Chapter 3 16

1.3.1 Epidermal Growth Factor Receptor (EGFR): Function, Dimerization, and Signaling 16

1.3.2 EGFR Ligands 18

1.3.3 High-affinity binding ligands 19
1.3.4 Heparin-binding epidermal growth factor-like growth factor (HB-EGF) 19
1.3.5 Low-affinity binding ligands 20
1.3.6 EGFR in cancer 21
1.3.7 Erlotinib, an anti-EGFR therapy in cancer 22
1.3.8 Anti-EGFR therapies in cancer can lead to lung fibrosis 23
1.3.9 EGFR and its ligands in human pulmonary fibrosis 24
1.3.10 EGFR and its ligands in animal models of pulmonary fibrosis 25
Chapter 2: M2 Macrophages have Unique Transcriptomes but Conditioned Media does not Promote Profibrotic Responses in Lung Fibroblasts or Alveolar Epithelial Cells *in vitro* 27
Abstract 27
Introduction 28
Materials and Methods 29
Animals and Housing 29
RT-qPCR 29
Cell Isolation 31
RNAseq Analysis 32
Fibroblast Proliferation and Migration 33
AEC Apoptosis 34
Protease Inhibitor Studies 35
Flow Cytometry 35
Statistics 35
Results 36
RNAseq shows unique differences between M1 and M2 BMDMs 36
BMDM polarization in vitro shows accurate M1 and M2 phenotypes 38

The increased M2 effect on fibroblast migration is explained by M2 polarizing reagents, IL-4 and IL-13 40

The increased M2 CM effect on fibroblast mRNA transcript expression of key profibrotic and anti-apoptotic factors is explained by M2 polarizing reagents, IL-4 and IL-13 42

M2 polarization reagents, IL-4+IL-13, increase profibrotic and anti-apoptotic mediator expression in AECs 44

Although increased AEC apoptosis with M2 CM is not an effect of polarizing reagents, the phenomenon is likely due to a promiscuous protease 46

Transcriptome data for secreted proteins from RNAseq analysis suggests possible candidates for caspase-3/7 “lookalike” 49

Discussion 53

Chapter 3: Lyz2Cre-Mediated Deletion of HB-EGF in Myeloid and Lung Epithelial Cells Protects Against Lung Fibrosis 61

Abstract 61

Introduction 62

Materials and Methods 64

IPF patient study 64

Animals and Housing 65

Bleomycin Administration 65

Lung homogenate collection, bronchoalveolar lavage (BAL) and protein concentration assays 66

Total lung cell preparation, cell marker staining for flow cytometry, PrimeFlow staining, and tSNE analysis 66

Hydroxyproline Assays and Histology 69

RT-qPCR 70

Isolation of blood cells for flow cytometry 72

Bone Marrow Transplantation (BMT) 72

Type II alveolar epithelial cell isolation and apoptosis assay 73

Fibroblast isolation, proliferation, and migration assays 73

Statistics 74
Results 75
Increased levels of HB-EGF are associated with increased IPF disease progression and fibrosis in mice 75
Monocyte-derived alveolar macrophages (moAMs) express HB-EGF 77
Hbegf$^{f/f}$;Lyz2Cre mice are protected from bleomycin-induced fibrosis despite similar levels of acute lung injury 80
Hbegf$^{f/f}$;Lyz2Cre mice have decreased macrophage numbers during fibrosis initiation 82
Protection in Hbegf$^{f/f}$;Lyz2Cre mice correlates with impaired macrophage migration and decreased CCL2 expression 84
Lyz2Cre deletes HB-EGF in AECs which may also contribute to protection from fibrosis 87
rHB-EGF does not induce a profibrotic response in AECs 90
rHB-EGF induces fibroblast migration with little impact on proliferation or matrix gene expression 92
Discussion 95
Chapter 4: Discussion 102
Bringing It All Together 102
Significance of Chapter 2 103
Significance of Chapter 3 105
Study Caveats 107
Future Directions 110
Next Steps for Chapter 2 Studies 110
Next Steps for Chapter 3 Studies 112
Concluding Remarks 118
Bibliography 119

List of Figures

Figure 1: IPF has a poor survival rate compared to different types of cancer. From http://www.manageipf.com/about-ipf 2

Figure 2: High Resolution Axial CT images of Normal and IPF lungs. Arrow indicates UIP predominant basal abnormalities with sub-pleural honeycombing (adapted from www.PILOTforIPF.org). 4

Figure 3: Trichrome blue-stained lung histology sections of saline (A) and bleomycin-treated (B) C57Bl/6J mice after 21 days. While the lungs of saline-treated mice depict a healthy lung (A), bleomycin-treated mouse lungs have increased number of immune cells, increased collagen deposition (blue), and increased interstitial thickening by comparison (B). Adapted from Moore et al., 2013, Am J Respir Cell Mol Biol. 8

Figure 4: Schematic of IPF injury. Pulmonary fibrosis is thought to be the combined result of AEC injury, chronic immune cell recruitment and activation, and excessive deposition of fibroblast extracellular matrix proteins. 10

Figure 5: Schematic of a healthy and fibrotic lung 13

Figure 6: Macrophages can differentiate into M1-like and M2-like macrophages based on the presence of various growth factors. Adapted from Zhang et al., 2018, Respiratory Research. 15

Figure 7: EGFR (HER1) has 7 ligands and activation of any of the ErbB/HER receptors can lead to downstream changes in cell maintenance. Adapted from Vallath et al., 2014, Euro Resp Journal. 18

Figure 8: While there are many EGFR-specific tyrosine kinase inhibitors (TKIs), each EGFR-TKI acts in a different part of the signaling pathway. Adapted from Vallath et al., 2014, Euro Resp Journal. 23

Figure 9: M1 and M2 bone marrow-derived macrophages (BMDMs) have different gene expression profiles based on RNA sequencing (RNAseq) analysis. RNAseq analysis of the top 5% of genes (270 genes) using the ClueGO plugin of Cytoscape shows drastically different prominent biological themes in M1 (A) and M2 (B) BMDMs as analyzed by biological process. Additionally, M1 and M2 BMDMs exhibit different transcriptome profiles (C) and M2 BMDMs have an increased number of differentially expressed genes for secreted proteins than M1 BMDMs (D). In (C) and (D), negative log2 expression values correlate to genes enhanced in M2 BMDMs and positive log2 expression values correlate to genes enhanced in M1 BMDMs. 37

Figure 10: BMDMs achieve a reliable M1 or M2 polarization when given standard combinations of polarizing reagents LPS+IFNg (M1) or IL-4+IL-13 (M2). BMDMs were polarized to an M1-like (100ng/ml LPS + 50ng/ml IFNg) or M2-like (10ng/ml IL-13 + 10ng/ml IL-4) phenotype for 24 hours before being isolated for RNA extraction. Representative RT-qPCR data of M1 genes: (A) iNOS and (B) TNFa, and M2 genes: (C) Fizz1, (D) Arg1, (E) IL-10, (F) CD163, (G) CD206, and (H) HB-EGF. N.D.: Not Detected. *: $p<0.05$, ****: $p<0.0001$. All data representative of 3-7 experiments, n=4, 5. 38

Figure 11: iNOS labels M1 BMDMs reliably at the protein level. M1 (A) and M2 (B) BMDMs were stained with anti-Arg1 and anti-iNOS via flow cytometry. While Arg1 at the protein level appears ubiquitously expressed in M1s and M2s (C), only M1 BMDMs are positive for iNOS (D). Flow cytometry quantification by percentage of total macrophages. **: $p<0.01$, ****: $p<0.0001$. 40

Figure 12: Effects of macrophage CM on fibroblast proliferation and migration are recapitulated by polarization cytokines. M1 and M2 CM or their respective polarization growth media (LPS + IFNγ or IL-4 + IL-13) were put on untreated primary lung fibroblasts for proliferation and scratch wound assays. Fibroblasts treated with M1 (A) or M2 (B) CM show increased proliferation over SFM via MTT assay after 48 hours, though no difference was noted between CM and respective polarization media controls. Representative sample (2 experiments, n=6). (C) Representative scratch wound assay showing M2 CM and IL-4+IL-13 polarization media cause the fastest wound closure (migration) but that there is no difference between the two treatments. *: $p<0.05$, **: $p<0.01$. Data in (C) are representative of at least three experiments, n=5 per group. 41

Figure 13: While expression of profibrotic and anti-apoptotic mRNA transcript in fibroblasts is enhanced with M2 CM treatment, these effects are attributable to polarization reagents. qPCR fold change of key profibrotic genes (A) (collagen1, collagen3, fibronectin, periostin), or apoptosis-related genes (B) (Cox2, PGE synthase, EP2, EP4), and of anti-apoptotic genes (C) (BCL2, survivin, XIAP). *: $p<0.05$, **: $p<0.01$, ***: $p<0.001$, ****: $p<0.0001$. All figures show representative data from at least three experiments, n=3-4. 43

Figure 14: Although AECs treated with M2 CM show increased expression of profibrotic and anti-apoptotic genes, these differences are caused by IL-4 and IL-13 reagents in the CM. qPCR fold change of key profibrotic genes (A) (VEGF, CTGF, POSTN, PDGFa), of (B) apoptosis-related genes (Cox2, PGE synthase, EP2, EP4), and of anti-apoptotic genes (C) (BCL2, survivin, XIAP). *: $p<0.05$, **: $p<0.01$, ***: $p<0.001$, ****: $p<0.0001$. All figures show representative data from at least three experiments, n=3-4. 46

Figure 15: While M2 CM appears to induce greater AEC apoptosis than M1 CM as measured via Caspase-Glo Luminescence assay, further verification supports no difference in AEC apoptosis treated with M1 or M2 CM. (A) AECs topped with 50µl of M2 CM have robustly increased caspase 3/7 activation over AECs given M1 CM using Caspase-Glo assay, (B) AECs given M1 or M2 CM show no difference in viability as measured by MTT assay, and (C) flow cytometry of AECs plated on fibronectin show no differences in apoptotic phase or expression of apoptotic protein markers Apotracker and Zombie Violet after treatment with M1

or M2 CM for 24hrs. *: p<0.05, **: p<0.01, ***: p<0.001, ****: p<0.0001. Representative data shown, all experiments repeated 2-7 times, n=2-5. 47

Figure 16: M2 CM appears to induce AEC apoptosis more robustly than polarizing growth media using Caspase-Glo luminescence assay. Relative caspase-3/7 activation in AECs given different types of CM as measured by luminescence from Caspase-Glo 3/7 kit. (A) positive control TGF-β (4ng/ml) induces caspase 3/7 activation while LPS (20ng/ml) does not and (B) AECs topped with 50µl of M2 CM have robustly increased caspase 3/7 activation over AECs given serum-free media (SFM) or polarizing growth media containing IL4 (10ng/ml), IL13 (10ng/ml), or IL4+IL13. *: p<0.05, **: p<0.01, ***: p<0.001, ****: p<0.0001. Representative data shown, all experiments repeated between 2-7 times, n=3-5. 48

Figure 17: Caspase-Glo 3/7 false positive likely caused by a heat-sensitive peptidase present in the M2 CM. AECs given either unheated or heated (100°C for 10 minutes) M1 or M2 CM were compared to wells containing no AECs and unheated or heated CM to assess the ability of substances in the CM to activate the Caspase-Glo 3/7 reagent. Fold change data from combined experiments (2 experiments, n=3 each). *: p<0.05, **: p<0.01, ***: p<0.001, ****: p<0.0001. 49

Figure 18: M1 and M2 BMDMs have different transcriptome profiles for secreted proteins based on RNAseq analysis. (A) RNAseq data show an increased number of genes for secreted proteases in M2 BMDMs (negative log2 values) compared to M1 BMDMs (positive log2 values). BMDMs polarized to an M1-like (B) or M2-like (C) phenotype show differences in molecular function categories as calculated by the ClueGO plugin of Cytoscape. In (B) and (C), ClueGO analysis organized upregulated genes into groups by molecular function as described in Methods. Percentages were calculated by dividing the number of genes present in each molecular function group divided by the total number of all genes. 51

Figure 19: M2 transcriptome data highlights proteases that may be responsible for cleavage of Caspase-Glo 3/7 substrate in the AEC apoptosis assay. Peptidases defined in the M2 transcriptome for secreted proteins (Figure 18) were further characterized by molecular function (A) and biological process (B) and re-analyzed with ClueGO as described in Methods. Pre-treatment of M1 CM (C) or M2 CM (D) with protease inhibitors Pierce™ pan-cocktail (PC – 5x and 0.5x standard concentration), aprotinin (0.75µM), E-64 (1µM), or AEBSF (1µM) was done to quantify depletion of luminescence. *: p<0.05, **: p<0.01, ***: p<0.001, ****: p<0.0001. Experiments repeated twice, n=3-4. 53

Figure 20: Cytoscape and ClueGO software organizes genes for secreted proteins in the M1 and M2 transcriptome into defined groups by molecular function. Molecular function of upregulated genes by group and labeled by function in the (A) M1 and the (B) M2 transcriptome for secreted proteins. These images serve as the raw data for the pie charts in Figure 18. 57

Figure 21: Cytoscape and ClueGO software organizes genes for the secreted proteins in the M2 transcriptome into defined groups by molecular function and biological process. ClueGO-Cytoscape groups of peptidases, as determined by genes for secreted peptidases, in the M2 transcriptome by molecular function (A) and by biological process (B). These images serve as the raw data for the pie charts in Figure 19. 59

Figure 22: Representative flow gating of a d7 bleomycin-treated mouse. (A) all cells → (B) doublets removed → (C) $CD45^+$ cells → (D) myeloid cells ($CD11b^+CD11c^+$) → (E) removal of all $Ly6G^-$ cells (neutrophils) → (F) $CD64^+$ cells. From the $CD64^+$ cells, macrophage subsets can be identified (G): alveolar macrophages (AMs) ($CD11c^+CD11b^-SiglecF^{hi}$), monocyte-derived alveolar macrophages (moAMs) ($CD11c^+CD11b^+SiglecF^{int}$), and interstitial macrophages (IMs) ($CD11b^+CD11c^-SiglecF^{lo}$). Ly6C+ monocytes can also be identified ($CD64^{lo}CD11b^{hi}Ly6C^+$) (H, I). For PrimeFlow experiments, macrophages from (F) were gated to be HB-EGF^+ before looking at subsets (G). 68

Figure 23: Increased levels of HB-EGF are associated with increased risk of IPF disease progression in humans and fibrosis in mice. IPF patients with faster disease progression have higher levels of (A) HB-EGF and (B) its receptor, EGFR, in their bloodstream and worsened survival compared to IPF patients with slower disease progression. Sensitivity and specificity was determined for different thresholds of the measured biomarker, where high HB-EGF RFU values or high EGFR RFU values, respectively, were used to flag progression. The maximum sensitivity plus specificity of HB-EGF was achieved using a threshold of 810.2 RFU. Kaplan-Meier curves for groups above and below this threshold showed significantly worse progression for those below 810.2 RFU (logrank p=0.02, RMST p=0.03). The maximum sensitivity plus specificity of EGFR was achieved using a threshold of 34301.3 RFU. Kaplan-Meier curves for groups above and below this threshold showed significantly worse progression for those below 34301.3 RFU (logrank p=0.02, RMST p=0.02). Orange lines indicate patients below threshold and blue lines indicate patients above the threshold for faster-progressing disease. Wild type mice treated with bleomycin-treated (bleo) mice have increased levels of HB-EGF mRNA expression in the lung homogenate (C) and in bronchoalveolar lavage (BAL) cells compared to saline-treated mice. Representative RT-qPCR data in C (2 experiments, n=4-6) and D (1 experiment, n=4-6). **: $p<0.01$, ****: $p<0.0001$. 77

Figure 24: Monocyte-derived alveolar macrophages (moAMs) express HB-EGF. PrimeFlow RNA assays show the presence of HB-EGF^+ alveolar macrophages (AMs) ($CD11c^+SiglecF^{hi}$), HB-EGF^+ moAMs ($CD11c^+CD11b^+SiglecF^{int}$), and HB-$EGF^+$ interstitial macrophages (IMs) ($CD11b^+SiglecF^{lo}$) in C57Bl/6J mice in control animals (A). Oral-pharyngeal administration of bleomycin induces an expansion of HB-EGF^+ moAMs and interstitial macrophages (IMs) after 21 days (B) compared to mice treated with a saline control (A) in C57Bl/6J mice. tSNE data is representative of one experiment with three mice per group. All data representative of 3 experiments, n= 3. 79

Figure 25: $Hbegf^{f/f}$;Lyz2Cre mice are protected from bleomycin-induced fibrosis despite similar levels of acute lung injury. $Hbegf^{f/f}$;Lyz2Cre mice have lower levels of hydroxyproline (A), decreased (B) expression of profibrotic genes (B) Collagen 1, Collagen 3, and Fibronectin, and improved lung histology (C) 21 days post-bleomycin treatment compared to $Lyz2Cre^+$ control mice. Additionally, levels of total protein and albumin detected in the BAL fluid (BALF) is not different between $Lyz2Cre^+$ and $Hbegf^{f/f}$;Lyz2Cre mice (D) three days post-bleomycin treatment, suggesting initial lung injury between genotypes is the same. n.s.: not significant, *: $p<0.05$, **: $p<0.01$, ***: $p<0.001$, ****: $p<0.0001$. Lines in (C) are 100 µm length. All data representative of 2-4 experiments, n=4-6. 81

Figure 26: Hbegf$^{f/f}$;Lyz2Cre mice have decreased macrophage numbers during fibrosis initiation. (A) Hbegf$^{f/f}$;Lyz2Cre number at day 7 post-bleomycin. (B) Hbegf$^{f/f}$;Lyz2Cre mice also have lower levels of moAMs 21 days post-bleomycin treatment by total cell number. n.s.: not significant, *: p<0.05, **: p<0.01, ***: p<0.001, ****: p<0.0001. All data representative of 3-5 experiments, n=4-6. 83

Figure 27: Hbegf$^{f/f}$;Lyz2Cre mice also show decreased macrophage numbers during fibrosis initiation by fold change. (A) Hbegf$^{f/f}$;Lyz2Cre mice have lower levels of moAMs and IMs 7 days post-bleomycin treatment as determined by relative fold change (B) Hbegf$^{f/f}$;Lyz2Cre mice also have lower levels of moAMs 21 days post-bleomycin treatment by relative fold change. Data in Figure 27A correspond to data in Figure 26A; data in Figure 27B correspond to data in Figure 26B. t-tests performed comparing treatments within a single genotype. n.s.: not significant, *: p<0.05, **: p<0.01, ***: p<0.001, ****: p<0.0001. All data representative of 3-5 experiments, n=4-6. 84

Figure 28: Protection of Hbegf$^{f/f}$;Lyz2Cre mice from bleomycin-induced fibrosis is not caused by decreased proliferation in moAMs (A) or Ly6C+ monocytes (B) or increased moAM apoptosis (C). Data in panels (A-B) representative of two experiments (n=3-4) using t-tests to compare treatments within a single genotype, data in panel (C) shows a single experiment (n=3-4) using ANOVA comparisons. n.s.: not significant, *: p<0.05, **: p<0.01, ***: p<0.001, ****: p<0.0001. 85

Figure 29: Protection in Hbegf$^{f/f}$;Lyz2Cre mice correlates with impaired macrophage migration and decreased CCL2 expression. Hbegf$^{f/f}$;Lyz2Cre mice have decreased numbers of Ly6C^{+} monocytes in the lungs compared to wild type mice 7 days post-bleomycin treatment (A), but no difference in total Ly6C^{+} monocytes in the blood at the same time point (B). Hbegf$^{f/f}$;Lyz2Cre mice have lower levels of CCL2 in their BALF (C), in BAL cells (D), in AECs (E), and in BMDMs (F) 3 days post-bleomycin compared to Lyz2Cre^{+} controls. n.s.: not significant, *: p<0.05, **: p<0.01, ***: p<0.001, ****: p<0.0001. Data in (A), (C), (D), and (E) are representative data from 2-3 experiments with n=2-5, and data in (B) and (F) are representative of 1 experiment, n=2-3. 86

Figure 30: rHB-EGF (50ng/ml) treatment for 24hrs on AECs (A), BMDMs (B), or primary lung fibroblasts (C) does not cause an increase in CCL2 expression as measured by qPCR. Additionally, the combination of bleomycin (day 3) treatment followed by rHB-EGF (50ng/ml) administration (24hr) does not increase CCL2 expression (D). n.s.: not significant, *: p<0.05, **: p<0.01, ***: p<0.001, ****: p<0.0001..... 87

Figure 31: Lyz2Cre deletes HB-EGF in AECs which may also contribute to protection from fibrosis. (A) AECs from Hbegf$^{f/f}$;Lyz2Cre mice have highly decreased levels of HB-EGF at baseline (saline treatment) as well as 21 days post-bleomycin treatment. Representative data of two experiments, n=6. (B) Lethally-irradiated C57Bl/6J mice reconstituted with Hbegf$^{f/f}$;Lyz2Cre bone marrow showed no difference in overall hydroxyproline content compared to lethally-irradiated C57Bl/6J mice reconstituted with C57Bl/6J bone marrow. Representative of three experiments, n=3-7. (C) Lethally-irradiated Hbegf$^{f/f}$;Lyz2Cre mice reconstituted with C57Bl/6J bone marrow showed no difference in overall hydroxyproline compared to Hbegf$^{f/f}$;Lyz2Cre mice reconstituted with Hbegf$^{f/f}$;Lyz2Cre bone marrow, implying

HB-EGF derived from the epithelium is more important in fibrosis protection than immune cell-derived HB-EGF. Representative of one experiment, n=3-7. n.s.: not significant, *: p<0.05, **: p<0.01, ***: p<0.001, ****: p<0.0001..... 88

Figure 32: Removal of HB-EGF from AECs does not alter expression of other EGFR ligands 21 days post-bleomycin (EGF: epidermal growth factor, TGFa: transforming growth factor-alpha, AREG: amphiregulin, EREG: epiregulin, EPGN: epigen, BTC: betacellulin). n.s.: not significant, *: p<0.05, **: p<0.01, ***: p<0.001, ****: p<0.0001. 90

Figure 33: rHB-EGF does not induce a profibrotic response in AECs. (A) Primary lung fibroblasts treated with rHB-EGF (50ng/ml) do not show increases in expression of profibrotic genes periostin, PDGFa, CTGF, or VEGF or alterations in anti-apoptotic gene expression (B) BCL2, XIAP, or survivin. (C) rHB-EGF (50ng/ml) does not induce AEC apoptosis compared to positive control TGFb (4n/gml) as measured via caspase-glo 3/7 assay. Representative data shown of experiments repeated at least three times, n=3-5. *: p<0.05, **: p<0.01. Data in (C) are representative of at least three experiments, n=5 per group. 92

Figure 34: rHB-EGF induces fibroblast migration with little impact on proliferation or matrix gene expression. (A) Fibroblasts treated with rHB-EGF (25ng/ml, 50ng/ml) do not have increased proliferation as measured by MTT. (B) qPCR fold change of key profibrotic genes collagen1, collagen3, and fibronectin is not induced in fibroblasts after rHB-EGF (50ng/ml) administration. (C, D) rHB-EGF promotes fibroblast migration. Representative data shown of at least three experiments, n=3-6. In (C), all doses of HB-EGF from 6.25ng/ml-100ng/ml are significantly different from SFM control starting at 12 hours. p-values are given for HB-EGF (25ng/ml), HB-EGF (50ng/ml), and HB-EGF (100ng/ml) and represent differences between treatment group and SFM at final timepoint (68hr). n.s.: not significant, ***: p<0.001, ****: p<0.0001. 94

Figure 35: Hbegf$^{f/f}$;Lyz2Cre mice also show decreased neutrophil (PMN) numbers during fibrosis initiation. Hbegf$^{f/f}$;Lyz2Cre mice have lower levels of PMNs 7 days post-bleomycin treatment as determined by total number (A) and relative fold change (B). Data in Figure 35A/B correspond to data in Figure 26A and Figure 27A. ANOVA statistics in (A), in (B) t-tests performed comparing treatments within a single genotype. n.s.: not significant, *: p<0.05, **: p<0.01, ***: p<0.001, ****: p<0.0001. All data representative of 2-5 experiments, n=4-6..... 97

List of Tables

Table 1: Primers and Probes for Chapter 2 30

Table 2: Primers and Probes for Chapter 3 70

List of Abbreviations

AECs	Alveolar Epithelial Cells
AMs	Alveolar Macrophages
AREG	Amphiregulin
Arg1	Arginase 1
αSMA	Alpha Smooth Muscle Actin
AT1s	Type I Alveolar Epithelial Cells
AT2s	Type II Alveolar Epithelial Cells
AUC	Area Under Curve
BAL	Bronchoalveolar Lavage
BALF	Bronchoalveolar Lavage Fluid
BCL2	B-cell lymphoma 2
BM	Bone Marrow
BTC	Betacellulin
CCL2	Monocyte Chemoattractant protein 1
CCR2	Chemokine (C-C) Motif Receptor 2
CD163	Cluster of Differentiation 163
CD206	Cluster of Differentiation 206
CD45	Common Leukocyte Antigen
CM	Conditioned Media
COPD	Chronic Obstructive Pulmonary Disease
Col I	Collagen I
Col III	Collagen III
Cox2	Cyclooxygenase 2
CTGF	Connective Tissue Growth Factor
ECM	Extracellular Matrix
EGF	Epidermal Growth Factor
EGFR/ErbB1	Epidermal Growth Factor Receptor
ErbB2/HER2	(Human) Epidermal Growth Factor Receptor 2
ErbB3/HER3	(Human) Epidermal Growth Factor Receptor 3
ErbB4/HER4	(Human) Epidermal Growth Factor Receptor 4
EMT	Epithelial to Mesenchymal Transition
EP2	E prostanoid 2
EP4	E prostanoid 4
EPGN	Epigen
EREG	Epiregulin
FITC	Fluorescein Isothiocyanate

Fizz1/RELMα	Found in Inflammatory Zone 1/Resistin-like Molecule Alpha
FN	Fibronectin
FVC	Forced Vital Capacity
GM	Growth Media
H+E	Hematoxylin and Eosin
HB-EGF	Heparin-binding epidermal growth factor-like growth factor
HRCT	High-resolution Computed Tomography
i.p	Intraperitoneal
i.t	Intratracheal
i.v	Intravenous
IFNγ	Interferon Gamma
IL-4	Interleukin 4
IL-10	Interleukin 10
IL-13	Interleukin 13
IL-1β	Interleukin 1 beta
ILD	Interstitial Lung Disease
IMs	Interstitial Macrophages
IPF	Idiopathic Pulmonary Fibrosis
LPS	Lipopolysaccharide
MMP	Matrix Metalloproteinases
MoAMs	Monocyte-derived alveolar macrophages
MSC	Mesenchymal Stem Cells
MTT	Tetrazolium bromide
PDGFα	Platelet Derived Growth Factor Alpha
PGE2	Prostaglandin E2
PGE synthase	Prostaglandin E synthase
PMNs	Polymorphonuclear leukocytes
POSTN	Periostin
SOMAmer	Slow Off-rate Modified Aptamer
SPC	Surfactant Protein C
TGFα	Transforming Growth Factor Alpha
TGFβ	Transforming Growth Factor Beta
Th1	T helper cell 1
Th2	T helper cell 2
TKIs	Tyrosine Kinase Inhibitors
TNFα	Tumor Necrosis Factor alpha
UIP	Usual Interstitial Pneumonia
VEGF	Soluble Vascular Endothelial Growth Factor
WT	Wild Type
XIAP	X-linked inhibitor of Apoptosis

Abstract

Idiopathic Pulmonary Fibrosis (IPF) is a highly debilitating lung disease with no known cure[1–3]. Previous work has shown that monocytes and macrophages are critical in the development and progression of pulmonary fibrosis in animal models[4–7]. As such, the overarching theme of this dissertation is to further explore myeloid cell regulation of lung fibrosis and specifically, to better understand how macrophages and macrophage-associated factors may be regulating fibrosis.

This dissertation is comprised of two distinct but interrelated projects. The first set out to characterize the soluble products of proinflammatory (M1-like) and profibrotic (M2-like) macrophages to investigate how these factors mediate fibrosis and influence structural cells of the lung. Using M1- and M2-polarized bone marrow-derived macrophages (BMDMs) in an *in vitro* model, the data showed that M1-like and M2-like BMDMs have different gene expression profiles based on RNAseq analyses, with M2-like BMDMs containing gene clusters with higher enrichment for cell processing as well as increased expression for secreted proteins. While M2 supernatant increased profibrotic characteristics of fibroblasts and alveolar epithelial cells (AECs) compared to cells treated with M1 supernatant, all effects could be attributed to the lingering presence of IL-4 and IL-13, which was required to polarize the BMDMs to an M2 phenotype. The presence of a M2 protease(s) able to yield a false positive in an assay of AEC apoptosis by direct cleavage of the Caspase-Glo 3/7 substrate was also noted. Together, this work provides a novel M1-M2 transcriptome database, confirms profibrotic effects noted by M2

supernatant in pulmonary structural cells *in vitro*, and provides new evidence that profibrotic effects associated with M2 macrophages are likely related to polarization cytokines found in the fibrotic milieu.

In the second project, the aim was to characterize the role of a known M2-associated growth factor, heparin-binding epidermal growth factor-like growth factor (HB-EGF) to determine if it acts as a major myeloid-derived profibrotic effector. The findings demonstrated that faster-progressing IPF patients had higher levels of both HB-EGF and its receptor, epidermal growth factor receptor, using SOMAmer technology, and also showed that *HB-EGF* expression is increased in lung macrophages of fibrotic mice. In addition, the results proved that mice lacking HB-EGF from the myeloid compartment ($Hbegf^{f/f}$;Lyz2Cre mice) are protected from bleomycin-induced fibrosis as evidenced by decreased levels of hydroxyproline and profibrotic gene expression. This protection is likely multifactorial, caused by genotypic differences in CCL2-dependent monocyte migration, decreased fibroblast migration, and decreased contribution of HB-EGF from AEC sources when HB-EGF is removed under the Lyz2Cre promoter.

In summary, this work has explored the profibrotic impacts of M2-polarized macrophages and demonstrated a profibrotic effect of M2-derived HB-EGF on myeloid cell accumulation and fibroblast migration in lung fibrosis.

Chapter 1: Introduction

1.1 IPF: Epidemiology, Diagnosis, Pathogenesis and Treatment

Idiopathic pulmonary fibrosis (IPF) is a chronic fibrosing interstitial lung disease of unknown etiology with no known cure[8–10]. IPF accounts for 20% of all cases of ILD and is recognized as the ILD with the most severe manifestations and the poorest outcomes[11,12]. Experts consider IPF to be a form of aberrant wound healing where repeated microinjuries to the epithelium disrupt the epithelial barrier, promote fibroblast activation and lead to excessive deposition of extracellular matrix (ECM) proteins. Together, these culminate in scar formation, impaired gas exchange, and eventual death. Work in the last two decades has made great progress further categorizing IPF clinically and identifying possible risk factors, an important step towards understanding and developing a cure for this disease.

1.1.1 Epidemiology

The most lethal of the interstitial lung diseases, IPF causes mortality in over 50% of patients within three years of diagnosis, giving it a mortality rate higher than all cancers excepting pancreatic and lung[3,13–16] (Figure 1). Though IPF is often considered a rare disease, occurring at the same frequency as stomach, brain, and testicular cancers, it is estimated that over 3 million individuals worldwide are currently diagnosed with IPF and that its incidence and prevalence are on the rise[1,17]. For example, in 2010, the prevalence of IPF was estimated between 6-131 individuals per 100,000 persons with an incidence of 3-28 individuals per 100,000, nearly twice as high as the numbers recorded 10 years earlier[16,18,19]. As individuals worldwide continue

to live longer, the likelihood of increased IPF prevalence and the overall impact of IPF on patients, their families, and the healthcare system will continue to increase.

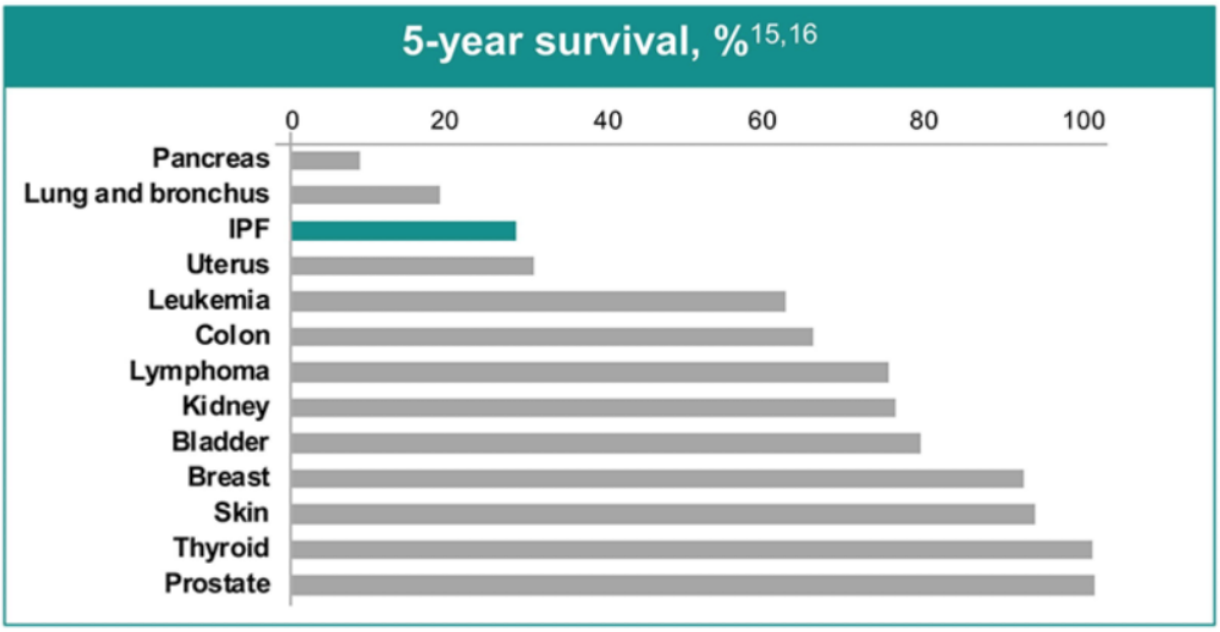

Figure 1: IPF has a poor survival rate compared to different types of cancer. From http://www.manageipf.com/about-ipf

Although IPF has no known cause, it does have associated risk factors. With a median diagnosis at age 65 years, age is arguably the most common and most important risk factor[1,20]. Though an IPF diagnosis is atypical for individuals under 50 years, the prevalence of IPF nearly doubles with every decade of life thereafter[21,22]. Like age, male sex is also significantly associated with higher incidence of IPF[17]. Other non-genetic risk factors of IPF include a history of cigarette smoking, chronic viral infections, and a family history of ILD[3,17,23]. Many genetic predispositions to IPF have been determined by examining families with high rates of pulmonary fibrosis. These include mutations in genes associated with surfactant dysfunction (e.g. *SFTPC, SFTPA2*), epithelial barrier function (e.g. *DSP*), host defense (e.g. *MUC5B, TOLLIP*), and telomere biology and maintenance (e.g. *TERT, TERC, OBFC1*)[1]. Of these categories, telomere biology and host defense have generated the most interest recently. Increased injury to alveolar

epithelial cells (AECs) prompts increased cell division, which in turn shortens AEC telomeres and ages the AECs prematurely in a manner that is sufficient to cause lung remodeling and fibrosis in animal models and in humans[24–27]. *MUC5B,* a secreted mucin protein associated with host defense, is also an area of interest as a mutation in this promoter is reported in 30-35% of IPF patients and associated with IPF risk[26,28].

1.1.2 Diagnosis

By definition, IPF is characterized by the presence of a histopathologic or radiographic pattern termed usual interstitial pneumonia (UIP) in the absence of any identifiable associated environmental or occupational exposures or conditions[10]. Clinically, patients may first present with shortness of breath during exercise, which eventually progresses to difficulty breathing at rest[1]. These patients are often plagued by a chronic unproductive/dry cough, fatigue, and may show signs of digital clubbing[1,23]. Physical exams of patients typically reveal a Velcro-like crackling in the lungs and pulmonary function tests demonstrate low forced vital capacity (FVC), abnormal gas exchange with reduced carbon monoxide diffusion, and resting hypoxemia[1,20].

The presence of UIP verified through high-resolution computed tomography (HRCT) is currently the most reliable indicator of IPF diagnosis[1,23,29]. At low magnification, IPF lungs display dense patches of fibrosis alongside histopathologically normal regions of tissue[29]. Radiographically, these patches of fibrosis show remodeled lung architecture including irreversible dilation of the bronchi and bronchioles, presence of ground-glass opacification, and fine reticulation[23]. Most notably, IPF lungs show honeycombing, which are clustered cystic airspaces with thick well-defined walls[23]. These characteristics can be seen in Figure 2. Despite defined disease characteristics, IPF can still be challenging to diagnose[20]. This is largely because the classic UIP radiologic pattern is also a hallmark of other idiopathic interstitial pneumonias

and interstitial lung diseases such as connective tissue disease, chronic hypersensitivity pneumonitis, drug toxicity, or asbestosis[20]. Misdiagnosis of IPF often leads to incorrect treatment of IPF with immunosuppressive therapy and is associated with a high mortality rate[20]. In cases where HRCT images do not reveal a definite diagnosis of UIP, clinicians may opt for lung biopsy to help exclude other fibrotic lung diseases presenting with only ground glass without a definitive UIP pattern[30]. Despite their reliability, lung biopsies are not always the best course of action, as the risks may outweigh the potential benefits of diagnostic information, particularly if the disease is presumed to be at an advanced state or is in an older individual.

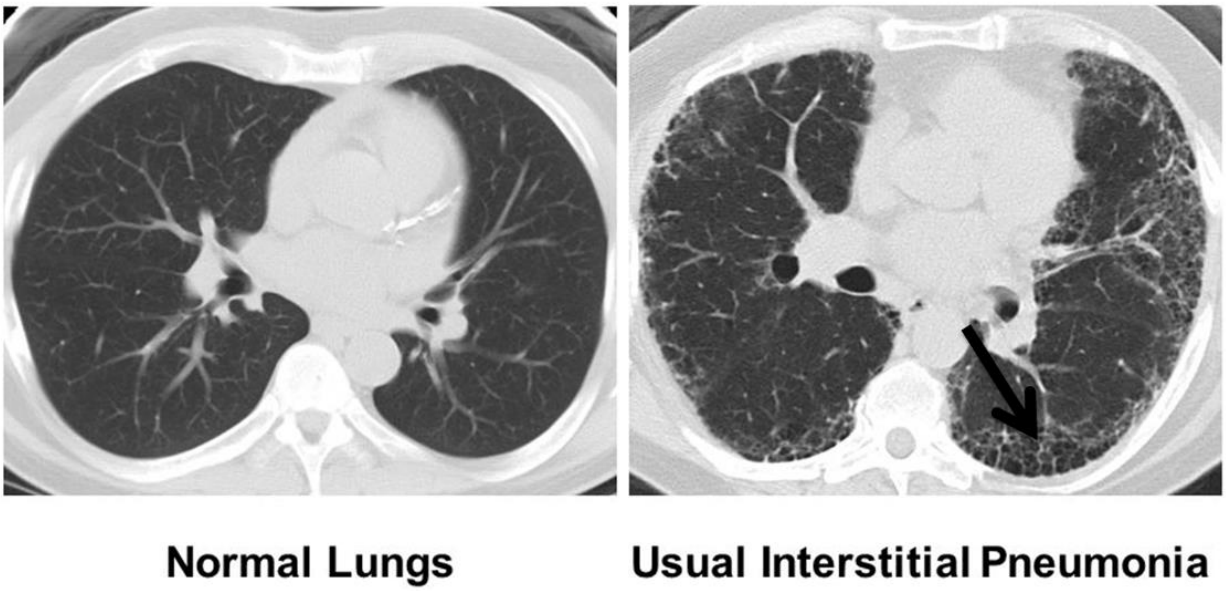

Figure 2: High Resolution Axial CT images of Normal and IPF lungs. Arrow indicates UIP predominant basal abnormalities with sub-pleural honeycombing (adapted from www.PILOTforIPF.org).

1.1.3 Pathogenesis and Treatment

IPF is a fatal lung disease with a disease course that is variable and unpredictable. While many patients with IPF will experience a gradual decline in lung function over several years, it is also possible for patients to either remain relatively stable or to decline rapidly. Patients who experience a rapid decline generally do so as a result of an acute exacerbation(s)[20]. These are often unpredictable, hard to anticipate, and idiopathic in nature[31].

Though IPF has no cure, there are several options available to patients that can help improve quality of life and sometimes length of life. Pulmonary rehabilitation has been shown to improve exercise capacity and health-related quality of life[20]. For some others, lung transplantation can also be an option. Although there have been no reported incidences of IPF development in transplanted lungs, transplants themselves come with many complications including primary graft dysfunction, acute or chronic allograft rejection, and risk of cytomegaloviral or other infections[20]. Consequently, only 66% of transplant recipients with IPF will survive for more than three years after transplantation and only 53% of patients remain in adequate health after five years[20,32].

Fortunately, there are two drugs on the market currently available to IPF patients: nintedanib and pirfenidone. Both FDA-approved in 2014, nintedanib and pirfenidone have demonstrated an ability to slow disease progression, though neither is curative[12,33–41]. Originally developed as a cancer treatment, nintedanib is a tyrosine kinase inhibitor that targets vascular endothelial growth factor (VEGF) receptors 1-3, fibroblast growth factor (FGF) receptors 1-3, and the platelet-derived growth factor (PDGF) receptor[20,42]. As each receptor has profibrotic capabilities, nintedanib's success is likely caused by its global inhibition of these highly similar pathways[42]. By inhibiting the FGFRs and PDGFRs, nintedanib helps decrease proliferation of fibroblasts and smooth muscle cells[42], and by inhibiting the VEGFRs, nintedanib helps alter a primary mediator of angiogenesis driving endothelial proliferation and vessel formation[43]. Pirfenidone is an organic compound with combined anti-inflammatory, antioxidant, and antifibrotic effects[1,20]. Although its precise mechanism of action is unknown, pirfenidone has shown to inhibit collagen synthesis, reduce fibroblast proliferation, and downregulate transforming growth factor (TGF)-β and tumor necrosis factor (TNF)-α in animal models[20,44,45].

In IPF patients, both nintedanib and pirfenidone have been shown to slow the rate of forced vital capacity (FVC) decline in one year by 50% and reduce severe respiratory events such as acute exacerbations and hospitalizations for respiratory events[36,37,46]. Studies suggest that one effect of these drugs might be to limit the development of further lung injuries in IPF patients[29]. Though clinicians also hope to see development and characterization of biomarkers that could be used for diagnosis, progression, and response to therapy, no biomarkers have yet been verified for clinical practice[1].

1.1.4 Animal Models of Fibrosis

Because human fibrotic lung disease is often advanced at diagnosis and effective therapies are limited, there is a critical need for experimental models that will allow for mechanistic studies of factors regulating fibroproliferation, AEC injury, immune cell infiltration, and crosstalk between many cell types. Although animal models are not typically progressive, nor are they able to replicate all of the disease features seen in human patients, these models are extremely valuable for their ability to provide insight into cell-specific lung injury and mechanisms leading to inflammation and fibroproliferation[5]. To that end, numerous rodent models have been described which mimic features of human fibrotic lung disease. The best characterized and most widely used model is bleomycin administration (described below). However, other models are also prevalent. These include use of particulates such as fluorescein isothiocyanate (FITC), silica, asbestos, and carbon nanotubes, which are particularly useful in inducing a more lasting fibrotic phenotype[5,47–55]. Other models induce overexpression of cytokines either genetically or through adenoviral vector transduction: in addition to interleukin (IL)-1β and IL-13 overexpression, TGFβ, TNFα, and TGFα overexpression models are favored, as these cytokines are known to be elevated in lung fibrosis and other forms of lung

injury[5,56,65,57–64]. Targeted AT2 injury, where the diphtheria toxin receptor is genetically expressed under the AT2-specific promoter for surfactant protein C (SPC), is an effective fibrosis model for studying downstream effects of perpetual and wide-spread lung epithelium injury[66]. Other approaches can use radiation, viral-mediated models of fibrosis, or humanized models of fibrosis[24,65,67–70].

Bleomycin administration is the most commonly employed murine model of fibrotic lung disease and causes obvious fibrosis in C57Bl/6 mice, seen in hydroxyproline accumulation (a surrogate for collagen deposition) and/or lung histology (Figure 3)[48,71]. Bleomycin is used in the clinic as a chemotherapeutic agent; however, its resulting lung toxicity acts as a limiting factor in its effectiveness for human patients. Delivery of bleomycin directly to the lung results in injury via induction of DNA strand breaks, generation of free radicals, and induction of oxidative stress[48,71,72]. Cell death then occurs (both necrosis and apoptosis), stimulating chronic inflammation, deposition of provisional matrix and eventual development of fibrosis[48]. In mice, bleomycin can be delivered by multiple methods, including intratracheal (i.t), intraperitoneal (i.p.), subcutaneous, intravenous (i.v.), and inhalational methods[48,73]. A single i.t. dose of bleomycin generally elicits a disease course characterized by lung injury (days 1-5), acute inflammation (days 3-10), fibroproliferation (days 7-14) and deposition of ECM, alveolar distortion and chronic inflammation by day 21[74]. The disease course is self-limiting and may start to show resolution starting at day 35, but there are some conflicting reports on the timing of resolution[75–80]. Because of changing animal welfare guidelines, many laboratories have shifted to oropharyngeal (o.p.) administration as it eliminates the need for surgical cut-down of the trachea for direct lung delivery. Few if any changes in fibrotic onset and development have been noted between the two methods[81]. Consequently, I use single o.p. administration of bleomycin

throughout this dissertation exclusively, both to keep with best animal practice recommendations and to provide novel data in a context most usable to others working in the field of fibrosis.

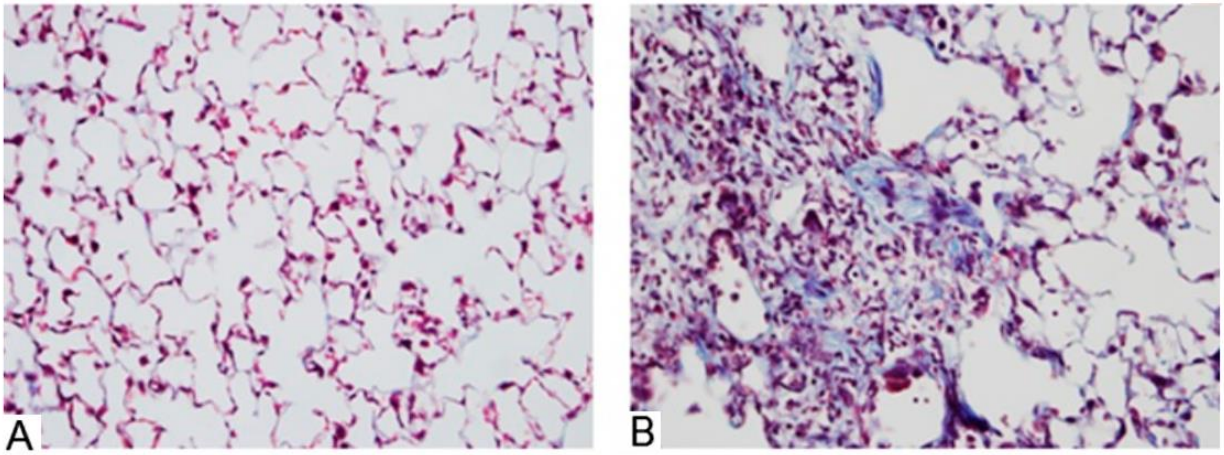

Figure 3: Trichrome blue-stained lung histology sections of saline (A) and bleomycin-treated (B) C57Bl/6J mice after 21 days. While the lungs of saline-treated mice depict a healthy lung (A), bleomycin-treated mouse lungs have increased number of immune cells, increased collagen deposition (blue), and increased interstitial thickening by comparison (B). Adapted from Moore et al., 2013, *Am J Respir Cell Mol Biol.*

1.2 Relevant Background Information for Chapter 2

1.2.1 Roles of Fibroblasts and AECs in Fibrosis

One of the major challenges of IPF research is its being a disease of unknown etiology. Historically, IPF was thought to be an exclusively fibroblast-epithelial disease, where multiple cycles of epithelial cell injury and activation prompted the migration, proliferation, and activation of fibroblasts that then led to excessive extracellular matrix protein (ECM) deposition and abnormal wound repair[15]. Research conducted throughout the last two decades has expanded and refined this paradigm to also include immune cells in the development and progression of fibrosis[3,4,6,9,82,83]. Monocytes and macrophages have received particular attention because of their plasticity, proximity to the epithelium, and their abilities to crosstalk with these structural cells of interest[3,14,83–85]. A primary goal of this dissertation work is to further elucidate the role of macrophages in fibrosis and more on this topic will be described below. However, the

importance of fibroblasts and AECs to the development, progression, and perpetuation of fibrosis cannot be understated.

Fibroblasts are a mesenchymal cell type present in many organs including the lung. A structural cell, fibroblasts help maintain normal tissue architecture in the lung through the deposition of ECM proteins including multiple forms of collagen (I, III, IV, V, VI), glycoproteins, and proteoglycans (fibronectin, hyaluronan, laminin)[86]. Injury to the lung epithelium prompts AECs to release many soluble factors such as TGF-β, PDGF, connective tissue growth factor (CTGF), IL-4, and IL-13 that induce immune cell recruitment and expansion of fibroblasts[85]. These fibroblasts are thought to both proliferate and migrate and produce ECM proteins to restore the integrity of the epithelium. Though beneficial in a normal wound-healing model, in IPF there is excessive ECM protein deposition that causes destruction of normal lung architecture (Figure 4). At the same time, α–smooth muscle actin (SMA)-positive myofibroblasts are activated and contract the lung tissue, which stiffens the lung and further impedes gas exchange[87]. To model these changes *in vitro* and probe questions relating to causative factors and timing of these events, researchers commonly use proliferation assays, migration assays (scratch wound), and western blots that examine the amount of profibrotic protein (periostin, αSMA, collagen I) produced in pulmonary fibroblasts[85,88].

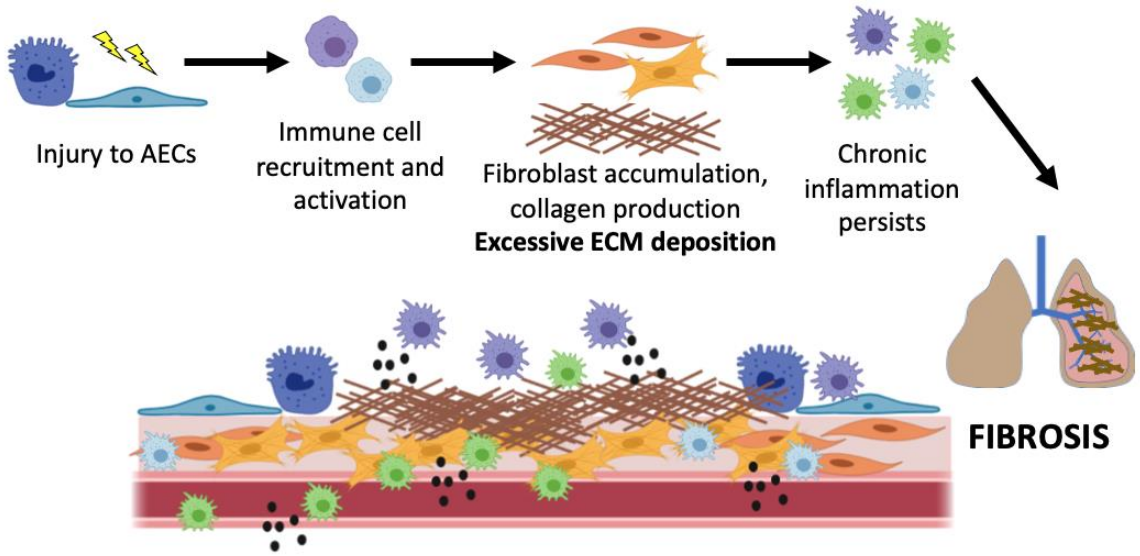

Figure 4: Schematic of IPF injury. Pulmonary fibrosis is thought to be the combined result of AEC injury, chronic immune cell recruitment and activation, and excessive deposition of fibroblast extracellular matrix proteins.

AECs compose the epithelial lining of the lungs. There are two types of AECs. AT1s cover over 90% of the alveolar surface area in the lung and are primarily responsible for gas exchange in concert with pulmonary capillaries[15]. AT2s are known for their role in surfactant secretion, stem-like progenitor function, and regenerative roles in the alveolus to maintain lung homeostasis[12,15]. In IPF, the integrity of the epithelium is highly diminished and re-epithelialization is relatively disordered[15]. Apoptosis is likely an essential feature of IPF: studies show that IPF patients have a depleted AT2 population as well as increased levels of AT2 apoptosis compared to healthy controls[15,89–91]. The precise mechanism of AEC apoptosis has yet to be determined. In IPF lungs and murine models, the Fas-FasL pathway has several components that are upregulated in the epithelium, suggesting the that this pathway is involved in AEC apoptosis[91–93]. However, other reports highlight the likelihood of other mechanisms, including increased ER stress, increased mitochondrial dysfunction, and repercussions from accelerated AT2 aging[94–99]. Though increased AEC injury in IPF has never been in doubt, recent work suggests that rather than function as only collateral damage in the disease state, persistent

injury to AECs may cause irreversible alterations in the capacity of these cells to carry out their reparative functions[12]. Consequently, AECs may acquire a dysfunctional phenotype that places them as a central driver of fibrosis[12,100,101].

1.2.2 Inflammatory cells are important to understanding fibrosis

Macrophages are a type of phagocytizing myeloid cell involved in many regulatory processes including the inflammatory response, homeostatic maintenance, and tissue regeneration[102]. Under homeostatic conditions, macrophages comprise nearly 70% of the total immune cell population in the lung[8,13]. Macrophages play a key role in the pathogenesis of fibrotic lung disease, though their specific role is still incompletely understood[83]. Both monocytes and macrophages are known to be important for fibrosis development; mice lacking CCR2 are unable to recruit monocytes and macrophages to the lung and are protected from fibrosis[4]. However, the role of these innate immune cells is highly nuanced, as the deletion of macrophages during fibrosis progression reduces the severity of fibrosis, but depleting macrophages during resolution delays overall fibrosis resolution[103]. In general, IPF patients show an increased number of lung macrophages compared to healthy controls[104], and patients with faster-progressing IPF have increased numbers of $CD14^{hi}$ $CD16^{hi}$ monocytes in their circulation compared to patients with slower-progressing IPF[105–107]. In addition to these broad associations between macrophages and IPF, macrophages are also of interest because of their proximity to the lung epithelium and their ability to crosstalk with AECs and fibroblasts. For example, AT2s produce cytokines and chemokines that attract inflammatory cells like macrophages to areas of injury and promote fibroblast activation[15,85], while macrophages themselves can also stimulate fibroblasts, regulate AEC activation, and produce angiogenic factors like VEGF that can be both pro- or anti-fibrotic depending on the timing of expression and target cell[3,84,108,109]. General

consensus in the field is that inappropriate communication between macrophages, epithelial/endothelial cells, fibroblasts, and stem cells can contribute to a state of persistent injury as seen in IPF[83].

1.2.3 Types of Macrophages – Alveolar vs. Interstitial

A highly dynamic and plastic cell type, macrophages can be categorized into many different groups based on their location, physiology, and gene expression profile. Macrophages are often defined into two populations by their location and expression of CD11c, CD11b, and SiglecF: alveolar macrophages (AMs; $CD11c^{hi}CD11b^{lo}SiglecF^{+}$) located in the alveolar space, and interstitial macrophages (IMs; $CD11c^{lo}CD11b^{hi}SiglecF^{-}$) located in the lung interstitium[8] (Figure 5). In addition to their different geographical location in the lungs under homeostatic conditions, AMs and IMs have different origin sites and replication abilities. AMs are yolk-sac derived and colonize the empty alveolar niche within the first few days of life[14,110,111]. They have self-renewal properties and play a critical role in turnover of surfactant and efferocytosis[110,112]. Given their location, AMs are thought to be inherently suppressive by directly sensing immunological stimuli and helping to maintain immune tolerance in the airways[8,14]. The interstitial compartment, on the other hand, contains cells derived from both yolk-sac monocytes and bone marrow-derived macrophages (BMDMs)[13,14,113,114]. While AMs are considered chief effector cells of the pulmonary immune response, IMs are thought to have a larger role in maintaining homeostasis[8,13,14,115]. That said, there is less information on IMs in the literature, as their location and somewhat heterogeneous phenotype makes them much more challenging to isolate cleanly and confidently compared to AMs[14,110].

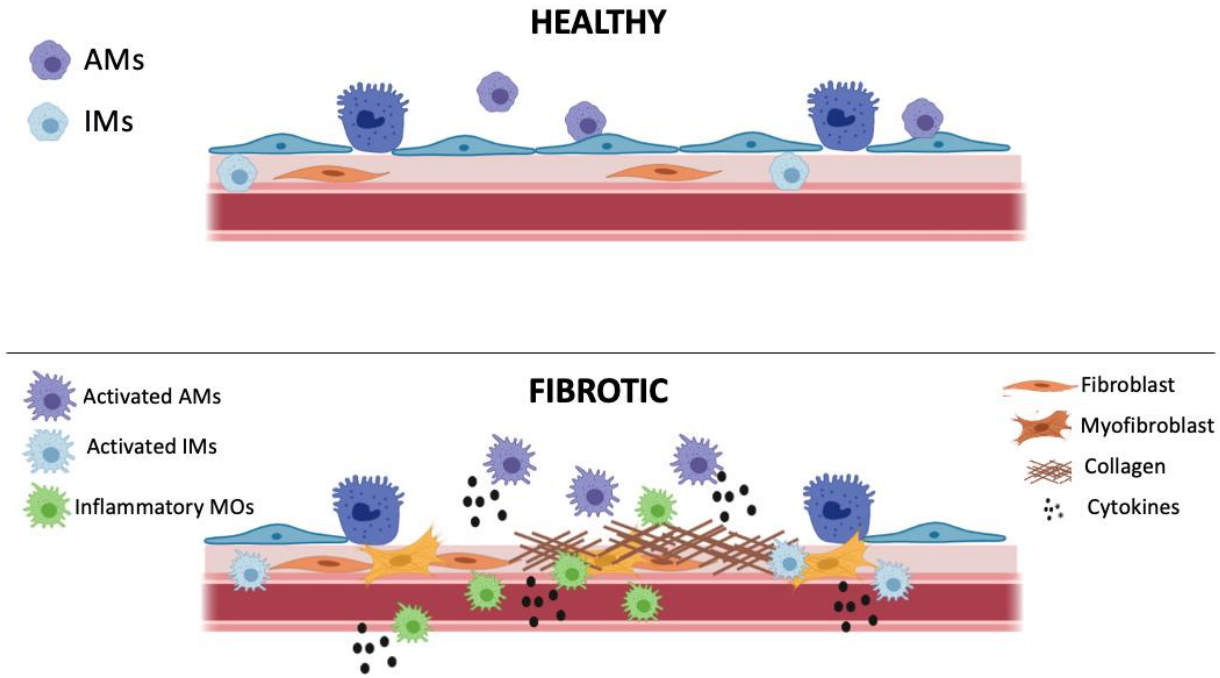

Figure 5: Schematic of a healthy and fibrotic lung

1.2.4 Macrophages during fibrosis

While both AMs and IMs exist and are considered local resident cell types in the lung under homeostatic conditions, macrophage populations become hard to define in the presence of acute or chronic lung injury as both the relative number and general phenotypes of these cells can change drastically[14,82,83,102]. For example, AMs are long-lived and self-populate under homeostatic conditions, but they become depleted during fibrosis[14,82,116]. There is massive recruitment of bone marrow-derived monocytes and non-resident $CD11b^+$ inflammatory macrophages to the lungs via a chemokine gradient[14,117–119]. Although a lack of unique differentiation markers makes it challenging to identify subsets of inflammatory macrophages responsible for specific aspects of the fibrotic response, recent work has shown that macrophages recruited to the lung are able to adjust their phenotype based on the lung microenvironment and relative population of surrounding cells[82,120]. For example, work in 2017 by Misharin et al. demonstrates that recruited monocytes are able to differentiate towards an AM-like phenotype

over time[6]. Termed "moAMs", these monocyte-derived AMs are most obviously different from AMs by their expression of SiglecF, which is high in AMs and only intermediately expressed in moAMs[82,116]. In their work, Misharin et al. discovered that while tissue-resident AMs did not contribute to fibrosis, moAMs are responsible for fibrosis in a bleomycin mouse model as genetic deletion of moAMs after their recruitment to the lung ameliorated fibrosis[4,6,120]. Interestingly, during the fibrotic phase, moAMs differ significantly from AMs in their expression of profibrotic genes and their capacity to be programmed by their environment[6,8,121]. However, moAMs persist for at least one year after initial injury at which time they are phenotypically and transcriptionally indistinguishable from tissue-resident AMs[6,116]. In both cases, the environment of the injured lung can reshape the transcriptome of moAMs and tissue-resident AMs[116].

1.2.5 Relevance of the M1/M2 model in fibrosis studies

Pulmonary macrophages are a heterogeneous and highly plastic population and given the influx of recruited cells amongst tissue-resident macrophages, studying and isolating precise populations of macrophages *in vivo* can be very challenging. As such, researchers in the field broadly classify macrophages into a spectrum of phenotypes ranging from "M1-like" to "M2-like" (Figure 6). M1-like macrophages, termed "classically activated," are proinflammatory and are activated by Th1 cytokines, including IFNγ, TNFα, and bacterial components such as LPS[102,122,123]. These M1-like macrophages have increased phagocytic capacity, release high levels of TNFα, IL-6, IL-1β, and can be characterized by increased gene expression of iNOS and MHC II[102,122–124]. M2-like macrophages, known also as "alternatively activated," are profibrotic and are activated by Th2 cytokines such as IL-4, IL-10, and IL-13[122]. M2-like macrophages are characterized by high expression of arginase1, Ym1, Ym2, Fizz1/RELMα, and CD206 and are highly associated with wound healing, asthma, and fibrosis[13,102,125,126]. Despite the

oversimplification that the M1/M2 classification brings, there is undeniable value in this system, both in order to group macrophages by function rather than name and for *in vitro* modeling and replicability.

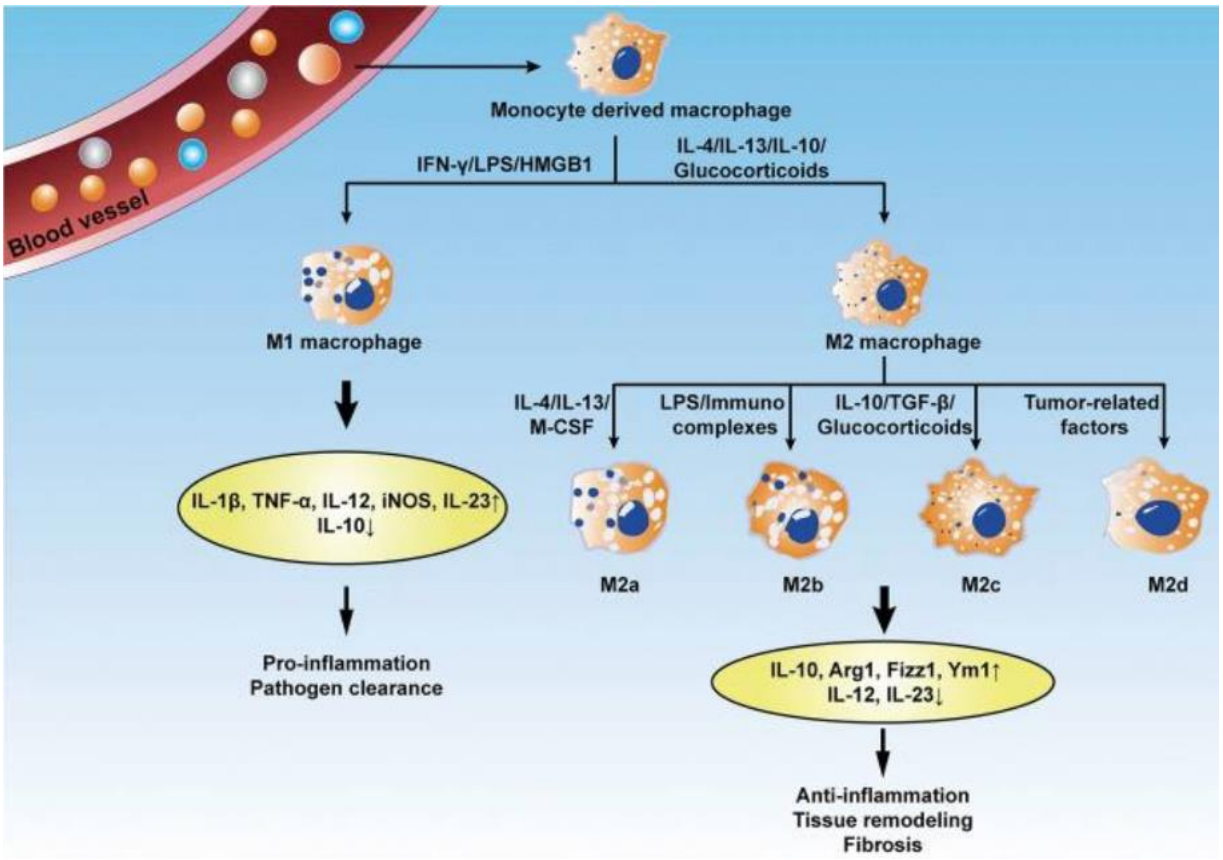

Figure 6: Macrophages can differentiate into M1-like and M2-like macrophages based on the presence of various growth factors. Adapted from Zhang et al., 2018, *Respiratory Research.*

The M1/M2 system is highly relevant because tissue-resident and recruited macrophages are known to be defined by factors that originate from their microenvironment[13,127,128], and M2-like polarization factors IL-4 and IL-13 are highly increased in the wounded lung[85,129,130]. For example, as mentioned, the injured lung epithelium produces TGFβ, PDGF, CTGF, and IL-4 and IL-13, which are crucial for the establishment and persistence of M2-like macrophages[85]. Further, both IL-4 and IL-13 are associated with profibrotic responses themselves. IL-13 is known to increase matrix metalloproteinase (MMP) activity in macrophages[83] and prolonged IL-13 leads to imbalances in production and catabolism in macrophages, both of which are known

to promote fibrosis[131]. Similarly, IL-4 effects SHIP1 and SHIP2, phosphatases responsible for contributing to M2-like macrophage polarization[132], and induction of Arg1 by IL-4 and IL-13 has been implicated in collagen deposition[133].

Previous work supports a strong role for M2-like macrophages in fibrosis. For example, macrophages in IPF patients are associated with M2-like markers: both CD206 and Arginase1 expression are enhanced in bleomycin-treated mice and elevated in AMs of IPF patients[14,82,115]. During IPF development and progression, predominant infiltration of M2 macrophages act as vital regulators of fibrogenesis in lung fibrosis[83,134]. Other work shows that M2 macrophages directly stimulate collagen production in myofibroblasts and enhance expression of tissue inhibitors of metalloproteinases (TIMPs) that block degradation of ECM[122,135,136]. M2-derived chemokines also play a role in fibrosis: CCL18 promotes collagen production in lung fibroblasts and high CCL18 levels correlate with fibrosis severity in IPF patients[137–139]. Additionally, the IPF FDA-approved drug, perfinidone, exerts anti-fibrotic effects in part by suppressing TGF-β expression, a cytokine associated with M2 polarization[13,140]. Despite these advances, little is known about the potential paracrine effects of M2 macrophages on primary AECs and fibroblasts in the lung. Further understanding of these M2-specific effects on local lung cells could present opportunities for development of diagnostic markers or future clinical therapies.

1.3 Relevant Background Information for Chapter 3

1.3.1 Epidermal Growth Factor Receptor (EGFR): Function, Dimerization, and Signaling

Growth factor receptors are often receptor tyrosine kinases (RTKs) with functional roles in angiogenesis, proliferation, mitosis, and wound healing. Epidermal growth factor receptor (EGFR) is a RTK expressed in tissues derived from epithelial, mesenchymal, and neuronal

origins with key downstream effector pathways that regulate a wide variety of cellular functions, including MEK/ERK, PI3K/AKT, STAT, and mTOR[141–145]. EGFR signaling regulates wound healing and repair in normal tissues, and its proper signaling is especially important in tissues that undergo extensive turnover of cells such as in epithelial layers of the skin, lungs, and gut[145]. In the lungs, EGFR signaling plays a role in controlling cell turnover and mucus production and acts as mediators of airway and alveolar homeostasis[141,145].

EGFR (ErbB1/HER1) is part of the ErbB family of receptor proteins (ErbB1-4; HER1-4), all of which contain a glycosylated extracellular domain, a single hydrophobic transmembrane segment, and an intracellular portion with a juxtamembrane segment, a protein kinase domain, and carboxyterminal tail[146]. Ligand-bound ErbB receptors can either homodimerize or heterodimerize with a different member of the ErbB family, and this dimerization causes reciprocal tyrosine phosphorylation of both receptors, autophosphorylation of c-terminal specific tyrosine-containing residues, and recruitment of signaling molecules at Src Homology 2 (SH2) or phosphotyrosine binding (PTB) motifs that enables the activation of key signaling cascades[141,147,148]. These pathways are intrinsically involved in cell proliferation, differentiation, and apoptosis, and thus help regulate physiological processes like organ development, growth, regeneration, and ion transport[144,147]. EGFR has seven ligands that have been documented in the literature (described below), three of which also bind to ErbB4 (HER4)[149–152] (**Figure 7**). Given the importance of EGFR in many critical cell pathways, the differing affinities and kinetics of each ligand, and the variations in signaling caused by each ligand, the study of EGFR and its ligands remains a highly complex and dynamic field[141,149,153].

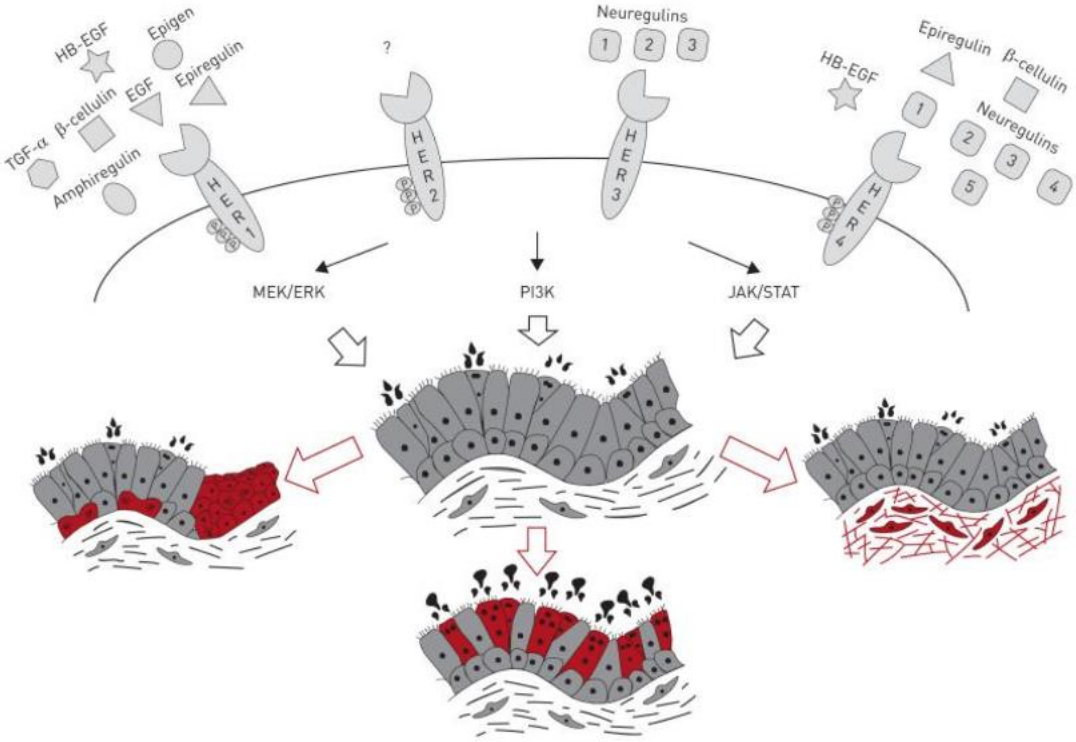

Figure 7: EGFR (HER1) has 7 ligands and activation of any of the ErbB/HER receptors can lead to downstream changes in cell maintenance. Adapted from Vallath et al., 2014, *Euro Resp Journal.*

1.3.2 EGFR Ligands

As previously mentioned, EGFR has seven ligands: epidermal growth factor (EGF), heparin-binding epidermal growth factor-like growth factor (HB-EGF), transforming growth factor alpha (TGFα), betacellulin (BTC), epiregulin (EREG), epigen (EPGN), and amphiregulin (AREG)[149,154]. Each member contains one or more EGF motifs in their extracellular domain and is able to bind to and fully activate EGFR[147]. All EGFR ligands are first synthesized in a membrane-bound form but are then cleaved by proteinases to become soluble in a process called ectodomain shedding. Members of the α disintegrin and metalloprotease (ADAM) family are key regulators of EGFR ligand shedding and though there is some redundancy, ADAM10 is considered the primary cleaving protease for EGF and BTC and ADAM17 cleaves the other ligands[141,149,150,155]. Although all seven ligands bind to EGFR, the ligands produce quantitatively

and qualitatively distinct cellular responses[156–158] and each varies in receptor affinity, concentration, preferred dimerization, and primary target cells, some of which will be explored below.

1.3.3 High-affinity binding ligands

Of the seven EGFR ligands, four are considered to have high affinity for EGFR: EGF, TGFα, HB-EGF, and BTC[149]. EGF is the ligand with highest affinity to EGFR and the prototypical member of the family of peptide growth factors that activate EGFR[147,154]. EGF has roles in tissue regeneration, ion transport including sodium and magnesium transport, and ulcer/wound healing[147]. Interestingly, the presence of EGF varies depending on the type of wound injury: EGF is upregulated after acute injury and enhances re-epithelialization, but is downregulated in chronic wounds and so thought to be a strong reason behind delayed healing in these injuries[147,159]. Like EGF, TGFα is an EGFR ligand that is well-studied[154]. Expressed by epithelial cells, TGFα stimulates proliferation of cultured epithelial cells, fibroblasts, and endothelial cells and induces the expression of matrix metalloproteinases (MMP)-1, -2, -3, and -9[160]. Additionally, TGFα has been implicated in the fibroproliferative response to acute lung injury in both mouse models and in human patients[160,161]; bronchoalveolar lavage fluid (BALF) samples taken from patients with IPF or acute lung injury had higher levels of TGFα than those taken from healthy controls[162]. Initially identified as a mitogen associated with a mouse pancreatic β-cell tumor cell line, BTC is expressed by a variety of cell types and tissues, though very little has been documented about the role of BTC in the lung[163]. BTC is one of the three EGFR ligands than can also bind to HER4[163]. To date, no studies report a phenotype for fibrosis in a BTC or EGF mouse model[145].

1.3.4 Heparin-binding epidermal growth factor-like growth factor (HB-EGF)

HB-EGF is an EGFR and HER4 ligand with high affinity to EGFR surpassed only by EGF[150,154]. Considered a critical molecular component to many physiological processes such as angiogenesis and adipogenesis, HB-EGF is most well-studied in the context of wound healing as it is the predominant growth factor involved in epithelialization in skin wound healing and induction of keratinocyte migration and invasiveness[150]. HB-EGF also has essential roles in tissue healing, proliferation, differentiation, and epithelial-mesenchymal transition[151,164,165]. Unlike some other EGFR ligands, both the membrane-bound (pro-HB-EGF) and soluble form (sHB-EGF) of HB-EGF are biologically active. Studies show biologically distinct roles for each form of HB-EGF in the kidney, pancreas, and liver[166–170] and HB-EGF can act in a juxtacrine, autocrine, paracrine, or endocrine signaling capacity[150]. In addition to pro-HB-EGF and sHB-EGF, ectodomain shedding also releases a nuclear fragment, HB-EGF-c, that is capable of binding to BAG-1 and BCL-2, interfering with apoptosis and increasing HB-EGF secretion[150]. Upon binding to EGFR, HB-EGF is highly efficient at inducing EGFR internalization and its degradation following ubiquitination, unlike other EGFR ligands TGFα, EREG, and AREG[153]. As HB-EGF provides a beneficial role in tissue healing and can contribute to the progression of several pathological conditions, it is a ligand of considerable interest as a therapeutic target[150].

1.3.5 Low-affinity binding ligands

The remaining three EGFR ligands – AREG, EREG, and EPGN – have low affinity for EGFR[149]. AREG, the ligand with the least affinity, is biologically active both in its soluble and membrane-bound state[155]. AREG is constitutively present in the lung and is known to modulate lung branching and morphogenesis[155]. It has gained much interest in recent years because its expression can be induced by many stimuli including inflammatory lipids, cytokines, hormones, and other growth factors and its overexpression is increasingly associated with many

pathological conditions[155,171]. For example, AREG expression is increased in damaged lung epithelium of COPD patients and AREG was recently identified as an essential mediator of pro-fibrogenic activity of TGFβ in a murine model[172,173]. In contrast, recent work also shows that AREG produced by group 2 innate lymphoid cells (ILC2s) promotes epithelial cell proliferation and tissue regeneration following virus-induced tissue damage[174]. Together, these data suggest high levels of AREG could be a result of pathologic conditions or a beneficial pathway towards injury resolution. Like BTC and HB-EGF, EREG can also bind to both EGFR and HER4[148]. Studies show that EREG contributes to inflammation, wound healing, and tissue repair by regulating angiogenesis and vascular remodeling and stimulating cell proliferation[148]. Finally, EPGN is a low-affinity EGFR ligand that is expressed in the liver and heart and in lower levels in the lung and kidney[175]. As the most recent addition to the EGFR ligand family, the biological functions of EPGN remain relatively unclear[175]. To date, no studies report a phenotype for fibrosis in an EREG or EPGN mouse model[145].

1.3.6 EGFR in cancer

Lung cancer is the foremost cause of cancer-related deaths worldwide[152]. 85% of these patients have non-small cell lung cancer (NSCLC) and of these patients, EGFR mutations are observed in nearly half[176]. The EGFR mutations in these patients are often either point mutations in exon 21 or short in-frame deletions in exon 19 and both cause constitutive activation of tyrosine kinases, leading to unrestricted cell growth, proliferation, and invasion[151,177,178]. EGFR ligands have also been highly associated with cancer and its further progression. HB-EGF is highly expressed in many forms of cancer[151] and efforts to reduce the effects of HB-EGF such as through its inhibition or neutralizing antibodies have been used as a therapeutic against glioblastoma, multiple myeloma, and cell lines of ovarian, breast, and colorectal cancer[179–181].

Additionally, HB-EGF is the most predominantly expressed EGFR ligand in EGFR-mutant lung cancer cells, and HB-EGF small molecule inhibitor CRM197 has already demonstrated utility by inducing cell apoptosis and suppression of tumorigenicity in lung cancer cells[176].

1.3.7 Erlotinib, an anti-EGFR therapy in cancer

EGFR mutations are present in a large percentage of lung cancer patients and thus a significant amount of research has been done trying to develop effective anti-EGFR therapeutics[176]. There are many drugs that target specific components of EGFR and its signaling pathway (Figure 8). EGFR-neutralizing antibodies such as cetuximab and bevacizumab, for example, have shown competency in attenuating doxycycline-inducible tumors in animal models but neither proved clinically beneficial in phase II clinical trials of patients with EGFR mutations[152,182,183]. EGFR-specific tyrosine kinase inhibitors (EGFR-TKIs) such as gefitinib and erlotinib, on the other hand, have had great success in many cancer patients[184–187]. As a result, these two drugs are some of the most studied EGFR-RTK inhibitors[152,188,189]. They have a similar mechanism of action: both act as inhibitors of the tyrosine kinase domain by blocking the intracellular ATP binding site of EGFR[141,152,190]. Erlotinib in particular is a well-established therapeutic for metastatic lung carcinoma[141,152,186]. Typically prescribed as a second or third-line treatment or in combination therapy with other chemotherapy drugs[152], erlotinib has shown increased life expectancy, increased progression-free survival, controlled rate of cancer metastasis, and improved tumor-related symptoms when compared with best supportive care in patients with NSCLC[184–187]. In addition to being effective, erlotinib is often well-tolerated by patients when used in combination therapy[152,185–187] although like other therapeutics, eventual erlotinib resistance or more adverse side effects may develop with time[185,191,192].

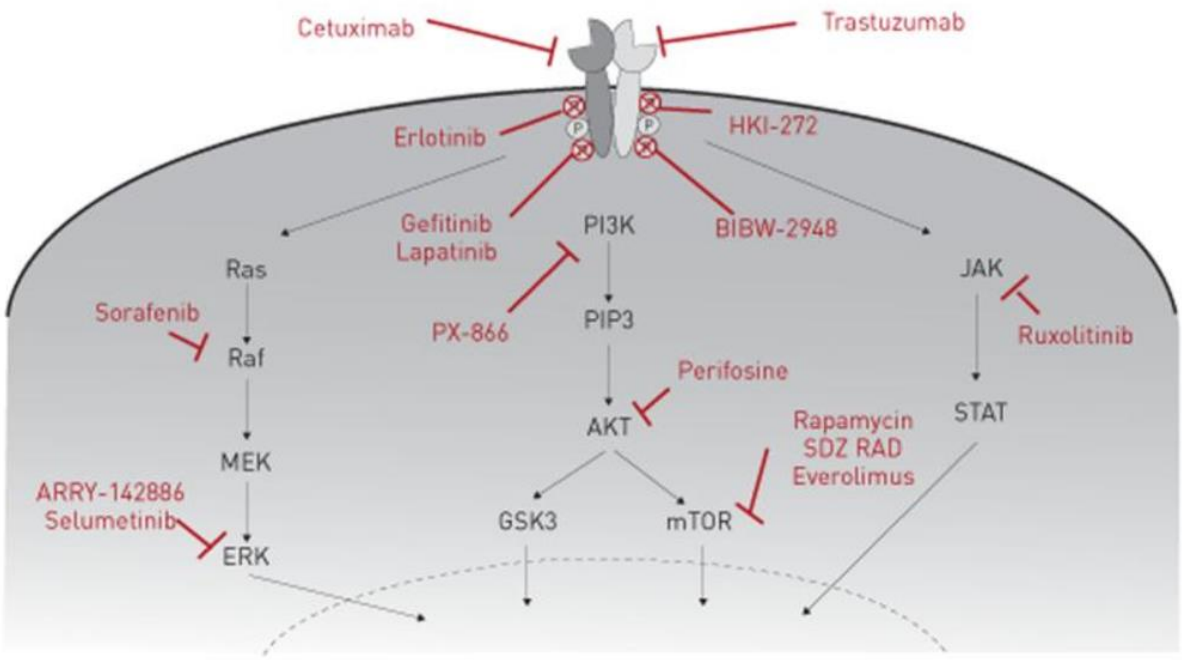

Figure 8: While there are many EGFR-specific tyrosine kinase inhibitors (TKIs), each EGFR-TKI acts in a different part of the signaling pathway. Adapted from Vallath et al., 2014, *Euro Resp Journal.*

1.3.8 Anti-EGFR therapies in cancer can lead to lung fibrosis

Despite the overall success of EGFR-TKIs like erlotinib and gefitinib in prolonging life and halting tumor progression in lung cancer patients, use of these therapies has also been associated with serious adverse health consequences including pneumonitis, increased incidence of pulmonary fibrosis and other interstitial lung diseases (ILD), and even death[184,193–195]. In one study, 7.7% of EGFR-TKI patients had to discontinue treatment due to unmanageable severe adverse events[193]. Despite widespread and global use of gefitinib and erlotinib, development of ILD in NSCLC patients after EGFR-TKI treatment appears to be most highly prevalent in the Japanese population[196]. Although researchers have not yet determined if this is due to genetic differences and/or consequence of ILD diagnosis practice, interstitial pneumonia and acute lung injury have been reported in 6% of Japanese patients treated with gefitinib[195,197,198], correlating to an ILD incidence of 1.9% in Japan and only 0.3% of all other cases globally[195].

Although many retrospective studies and clinical trials associate that associate treatment of cancer patients on an EGFR antagonist with later development of lung fibrosis, a direct causal link between the EGFR-RTI and fibrosis has not yet been determined. This is likely the consequence of several factors. For one, drug-associated ILD is not uncommon itself – treatment of NSCLC with combination chemotherapy has been associated with development of ILD, as has increases in drug dose and alteration in combination of chemotherapy drugs, use of radiation, and sequential use of radiotherapy and chemotherapy[195,199]. Additionally, clinicians face great challenges when trying to diagnose ILD. Clinical, radiological, and pathological observations are all necessary to exclude other conditions with similar symptoms such as pneumonia, allergy, cardiogenic edema or pulmonary hemorrhage[200], and identification of drug-associated ILD is made more complex as clinical imaging and pathological patterns are not diagnostically reliable[195]. For example, one study of high-resolution computed tomography (HRCT) and histopathology showed that pathological pattern and imaging did not correspond in over 40% of cases[201].

1.3.9 EGFR and its ligands in human pulmonary fibrosis

In addition to cancer, EGFR dysfunction is highly associated with lung fibrosis and diseases like COPD, asthma, and cystic fibrosis[202–204]. There is significant EGFR upregulation in all three forms of idiopathic interstitial pneumonias (IIPs): IPF, cryptogenic organizing pneumonia (COP), and nonspecific interstitial pneumonia (NSIP)[205], and patient samples showed that EGFR was primarily localized to hyperplastic alveolar epithelium surrounding areas of fibrosis in each diseased individual[205]. Fibroblasts taken from IPF patients also express high levels of EGFR and downstream target pAKT, further suggesting the presence of EGFR overactivation in human fibrosis[206]. In addition to EGFR dysfunction, fibrotic diseases are also

characterized by the presence of abnormal levels of EGFR ligands. Both TGFα and EGF stimulate fibroblast proliferation and play a role in the pathogenesis of IPF[197] and TGFα expression is increased in the lung tissue of patients with IPF compared with control lung tissue[207]. The increased expression of HB-EGF has also been noted in a variety of airway and fibrotic diseases. Studies show that levels of HB-EGF are positively correlated in sputum with chronic obstructive pulmonary disease (COPD) severity, epithelial-mesenchymal transition and airway remodeling, and is thought to have a role in the early inflammatory stage of scleroderma and systemic sclerosis[150,151,164,176,208].

Recent preliminary work in the Moore lab also demonstrates a connection between HB-EGF and IPF progression. Using SOMAmers (short, single-stranded deoxyoliognucleotides that can bind to discrete molecular targets with high affinity), Dr. David O'Dwyer measured the relative concentration of proteins in the ErbB pathway in the plasma proteome in two cohorts of IPF patients. He concluded that IPF patients who have levels of EGFR or HB-EGF in plasma that are above the identified threshold have higher incidence of disease progression (logrank test, p=0.02; logrank test, p=0.02, respectively) (*O'Dwyer et al.,*unpublished data). These data further implicate both EGFR and HB-EGF in the progression of IPF and perhaps its development as well.

1.3.10 EGFR and its ligands in animal models of pulmonary fibrosis

Like IPF in humans, animal models of pulmonary fibrosis also show increased prevalence of EGFR expression and several of the EGFR ligands. TGFα, for example, is detected in higher amounts in rats treated with bleomycin to induce lung injury compared to those receiving saline control, and chronic epithelial expression of TGFα in transgenic mice caused the progression of bleomycin-induced pulmonary fibrosis, supporting a role for this ligand in fibrosis

development[161,207,209]. Interestingly, EGFR antagonism has had varied effects. The use of the EGFR-TKI gefitinib has been shown both to worsen and to protect against pulmonary fibrosis in other animal work[197,210]. These discrepancies are likely the consequence of differential cell specific effects of ligands or of receptor actions, but their overall complexity and the lack of consensus in the field suggests a need for the further study of specific EGFR-TKIs in a simplified *in vitro* cell system. Very few animal studies have been performed that use erlotinib to investigate its effects on fibrosis. To date, there are only two studies of relevance. The first, by Hardie et al. in 2008 demonstrated that daily administration of erlotinib prevented the development of fibrosis in a doxycycline-inducible lung-specific TGFα overexpression fibrosis mouse model and the second, by Adachi et al. in 2010 showed that simultaneous administration of bleomycin and erlotinib to rats neither exacerbated nor ameliorated the overall amount of fibrosis compared to rats receiving bleomycin alone[211,212]. Consequently, as very few studies have explored the role of erlotinib in animal models of fibrosis, it follows that this EGFR-TKI is a valuable place to start.

Chapter 2: M2 Macrophages have Unique Transcriptomes but Conditioned Media does not Promote Profibrotic Responses in Lung Fibroblasts or Alveolar Epithelial Cells *in vitro*

Abstract

Macrophages are critical regulators of pulmonary fibrosis. Their plasticity, proximity, and ability to crosstalk with structural cells of the lung make them a key cell type of interest in the regulation of lung fibrosis. Macrophages can express a variety of phenotypes which have been historically represented through an "M1-like" to "M2-like" delineation. In this classification, M1-like macrophages are proinflammatory and have increased phagocytic capacity compared to alternatively activated M2-like macrophages that are profibrotic and are associated with wound healing. Extensive evidence in the field in both patients and animal models align pulmonary fibrosis with M2 macrophages. In this paper, we performed RNAseq to fully characterize M1 vs. M2-skewed bone marrow-derived macrophages (BMDMs) and investigated the profibrotic abilities of M2 BMDM conditioned media (CM) to promote fibroblast migration, proliferation, alveolar epithelial cell (AEC) apoptosis, and mRNA expression of key fibrotic genes in both fibroblasts and in AECs. Although M2 CM-treated fibroblasts had increased migration and M2 CM-treated fibroblasts and AECs had increased expression of profibrotic proteins over M1 CM-treated cells, all differences can be attributed to M2 polarization reagents IL-4 and IL-13 also present in the CM. Collectively, these data suggest that the profibrotic effects associated with M2 macrophage CM *in vitro* are attributable to effects of polarization cytokines rather than additional factors secreted in response to those polarizing cytokines.

Introduction

Idiopathic pulmonary fibrosis (IPF) is a chronic fibrosing interstitial lung disease of unknown etiology[8–10]. The most lethal of the interstitial lung diseases, IPF causes mortality in over 50% of patients within 3 years of diagnosis[3,13,14]. Experts consider IPF to be a form of aberrant wound healing where repeated microinjuries to the epithelium disrupt the epithelial barrier, promote fibroblast activation and lead to excessive deposition of extracellular matrix (ECM) proteins, and culminate in scar formation and eventual death. Historically, IPF was thought to be an exclusively fibroblast-epithelial disease, but work in the last two decades points to innate immune cells as having a critical role in the development and progression of fibrosis[3,4,6,9,82,83].

Monocytes and macrophages have received particular attention for their role in IPF because of their plasticity, proximity to the epithelium, and their abilities to crosstalk with structural cells of interest[3,14,83–85]. Studies have shown that alveolar epithelial cells (AECs) secrete cytokines that attract inflammatory cells to areas of injury and that these cytokines promote migration, proliferation, and activation of fibroblasts[85]. Macrophages are also able to communicate with fibroblasts through juxtacrine and paracrine signaling[213].

Bone marrow-derived macrophages (BMDMs) are often used as a cell source to study cellular crosstalk systems *in vitro*. To mirror the range of macrophage phenotypes in a simplified version, researchers often use the M1/M2 dichotomy. In this model, lipopolysaccharides (LPS) and interferon (IFN)-γ are added to BMDM media to create proinflammatory M1 macrophages, characterized by increased phagocytic capacity and increased iNOS and TNFα expression[102,122–124], and IL-4 and IL-13 are added to BMDM media to create "alternatively activated" M2 macrophages, associated with fibrosis and characterized by high expression of Arginase1 (Arg1),

Fizz1/RELMα, and CD206[13,102,122,125,126]. Despite frequent use, many studies fail to consider the implications of treatment conditions needed to differentiate or maintain macrophages in the M1/M2 phenotype *in vitro.* In this paper, we used the classically described model of M1/M2 polarization to systematically determine whether fibroblast or alveolar epithelial cell responses were attributable to unique factors in M1/M2 macrophage conditioned media (CM) that were distinct from the factors used for polarization in the growth media. In particular, we sought to determine if strongly M2 polarized BMDM CM promote fibroblast migration, proliferation, AEC apoptosis, and mRNA expression of key fibrotic genes in both fibroblasts and in AECs. Surprisingly, all differences can be attributed to the presence of IL-4 and IL-13 as the polarizing reagents, but no additional effects from the M2-skewed BMDM CM are present.

Materials and Methods

Animals and Housing

6-to 8-week-old C57Bl/6 male and female mice were purchased from The Jackson Laboratory (Bar Harbor, ME) and housed in specific pathogen-free conditions within the University of Michigan Animal Care Facility (Ann Arbor, MI). 6-to 8-week-old house-bred male and female Lyz2Cre^{+} mice (C57Bl/6 background, parent pair purchased from The Jackson Laboratory), considered a functional wildtype, were housed similarly to purchased C57Bl/6 mice and were used synonymously as wildtype alongside C57Bl/6 mice. All animal experiments were approved by the Institutional Animal Committee on Use and Care (IACUC) at the University of Michigan and were performed in accordance with the National Institutes of Health policies on the humane care and use of laboratory animals.

RT-qPCR

RNA for RT-qPCR experiments was obtained from isolated cells via Trizol (ThermoFisher, Waltham, MA) extraction following the manufacturer's protocol. Equivalent RNA was subjected to qRT-PCR performed on an ABI StepOnePlus real-time thermocycler (ThermoFisher) using a TaqMan® RNA-to-Ct™ 1-Step Kit (ThermoFisher) following the manufacturer's protocol. The gene of interest was normalized between samples to GAPDH expression using delta CT values. All primers and probes used in this study are listed in Table 1 below.

Table 1: Primers and Probes for Chapter 2

Gene	Direction	Sequence
Fizz1	Forward	5′-TCCAGCTAACTATCCCTCCACTGT-3′
	Reverse	5′-AGCCACAAGCACACCCAGTAG-3′
	Probe	5′-ATGAACAGATGGGCCTCCTGCCCT-3′
Arg1	Forward	5′-ACCACAGTCTGGCAGTTGGAA-3′
	Reverse	5′-GCATCCACCCAAATGACACA-3′
	Probe	5′-CTGGCCACGCCAGGGTCCAC-3′
IL10	Forward	5′-GGGTTGCCAAGCCTTATCG-3′
	Reverse	5′-CACCCAGGGAATTCAAATGC-3′
	Probe	5′-CAGGCAGAGAAGCATGGCCCAGAA-3′
Hbegf	Forward	5′-CGGTGATGCTGAAGCTCTTT-3′
	Reverse	5′-GCTGGTTTGTGGATCCAGTG-3′
	Probe	5′-ACGCGGACAACACTGCGGCC-3′
Tnfα	Forward	5′-CCAGACCCTCACACTCAGATCA-3′
	Reverse	5′-CCTCCACTTGGTGGTTTGCT-3′
	Probe	5′-TCGAGTGACAAGCCTGTAGCCCACG-3′
iNOS	Forward	5′-ACATCAGGTCGGCCATCACT-3′
	Reverse	5′-CGTACCGGATGAGCTGTGAAT-3′
	Probe	5′-CCCCAGCGGAGTGACGGCA-3′
Col1	Forward	5′-TGACTGGAAGAGCGGAGAGTACT-3′
	Reverse	5′-GGTCTGACCTGTCTCCATGTTG-3′
	Probe	5′-CTGCAACCTGGACGCCATCAAGG-3′
Col3	Forward	5′-GGATCTGTCCTTTGCGATGAC-3′
	Reverse	5′-GCTGTGGGCATATTGCACAA-3′
	Probe	5′-TGCCCCAACCCAGAGATCCCATTT-3′
Fibronectin	Forward	5′-TCGAGCCCTGAGGATGGA-3′
	Reverse	5′-GTGCAAGGCAACCACACTGA-3′
	Probe	5′-CTGCAGGGCCTCAGGCCGG-3′
Periostin	Forward	5′-GGGGTTGTCACTGTGAACTG-3′
	Reverse	5′-CGGCTGCTCTAAATGATGAA-3′
	Probe	5′-CGTGTCCTGACACAAATTGG-3′
Cox2	Forward	5′-TGACCCCAAGGCTCAAAT-3′
	Reverse	5′-GAACCCAGGTCCTCGCTTATG-3′
	Probe	5′-TTTGCCCAGCACTTCACCCATCAG-3′
EP2	Forward	5′-CAGTCCTCTGTTGTCGGACT-3′
	Reverse	5′-CATGAAGCGCATCCTCACAA-3′
	Probe	5′-CCTGTTCTACCCAGTCCAGTGCCA-3′
EP4	Forward	5′-TCTCTGGTGGTGCTCATCTG-3′
	Reverse	5′-GTCTTTCACCACGTTTGGCT-3′
	Probe	5′-ACACTCGCACCACGAGCGGA-3′
PGE synthase	Forward	5′-AACCTGGGCGAGTGGATCT-3′
	Reverse	5′-CTGTAAGTGGCTCCAAATGGG-3′
	Probe	5′-ACATGTGTGTTTCTTAGCCTTTTG-3′
survivin	Forward	5′-GATCTGGCAGCTGTACCTCA-3′
	Reverse	5′-ATCAGGCTCGTTCTCGGTAG-3′
	Probe	5′-CTGGAGGACTGCGCCTGCAC-3′
XIAP	Forward	5′-ACCCTGCCATGTGTAGTGAA-3′
	Reverse	5′-TCTCTGGGGGTTAAATGAGC-3′
	Probe	5′-TGAAGTCATTTCAGAACTGGCCGG-3′
BCL2	Forward	5′-GGAGTGTGAGGACCCAATCT-3′
	Reverse	5′-CAACCACACCATCGATCTTC-3′
	Probe	5′-AGCCCCAGACCCCAACTCC-3′
VEGF	Forward	5′-CTTGCAGATGTGACAAGCCA-3′
	Reverse	5′-GAGAGGTCTGGTTCCCGAAA-3′
	Probe	5′-TGCAGCCTGGCTCACCGCCT-3′
CTGF	Forward	5′-GAGTGTGCACTGCCAAAGAT-3′
	Reverse	5′-GGCAAGTGCATTGGTATTTG-3′
	Probe	5′-CGCAGCGGTGAGTCCTTCCA-3′
PDGFα	Forward	5′-CGAAGTCAGATCCACAGCAT-3′
	Reverse	5′-GGGCTCTCAGACTTGTCTCC-3′
	Probe	5′-CCGGGACCTCCAGCGACTCT-3′
GAPDH	Forward	5′-GGGCCACGCTAATCTCATTT-3′
	Reverse	5′-ATACGGCCAAATCCGTTCAC-3′
	Probe	5′-CTCCTCGAGCCTCGTCCCGT-3′

Cell Isolation

To isolate fibroblasts, mice were euthanized under CO_2 and their lungs perfused with sterile PBS via the right ventricle. Lungs were excised under aseptic conditions and minced with scissors. The lung mince was then placed in a T175 tissue culture treated plastic flask with ~30ml Dulbecco's Modified Eagle Medium (DMEM)+10% fetal bovine serum (FBS). Fibroblasts were allowed to grow 14 days with media changes every 3-4 days before use.

BMDMs were isolated as described previously[214,215]. Briefly, bone marrow cells were collected from mice after CO_2 euthanasia by flushing their femurs and tibias with 10% DMEM. These cells were cultured in bone marrow medium (30% L-cell supernatant, 70% DMEM+10% FBS media) for 6 days, with fresh media added every 2 days. On day 6, cells were counted and replated at 1 million cells/well in a 12-well plate overnight in complete DMEM. On day 7, BMDMs were treated with recombinant murine (rm)IFNγ (50ng/ml, R&D Systems, Minneapolis, MN) and *E.coli*-derived lipopolysaccharide (LPS; 100ng/ml, Sigma Aldrich, St. Louis, MO) in serum-free media (SFM) for "M1-like" polarization, or were treated with rmIL-4 (10ng/ml, R&D Systems) and rmIL-13 (10ng/ml, R&D Systems) in SFM for "M2-like" polarization. M1 or M2 polarization reagents placed in SFM were considered "polarizing growth media" and placed on BMDMs for 24 hours to polarize BMDMs to an M1 or M2 phenotype. BMDMs were considered fully polarized at the conclusion of 24 hours. Cells and/or supernatant from M1 or M2 BMDMs were collected at the end of this 24-hour polarization period. As M1 or M2 BMDMs are presumed to secrete additional factors into the media during this polarization period, the supernatant removed from M1/M2 BMDMs is considered to be different from the polarizing growth media and is referred to as "conditioned media" (CM). In experiments using

heated BMDM CM, CM was thawed from frozen, put in 1ml aliquots, and heated at 100°C on a heat block for 10 minutes.

Alveolar epithelial cells (AECs) were isolated using a whole lung dispase digestion after casting airways in low melt agarose as previously described[216]. After isolation, AECs were plated overnight at 500,000 cells/well on 24-well plates coated in undiluted Matrigel (BD Biosciences, San Jose, CA) for RNA extraction or at 50,000 cells/well on opaque 96-well plates for apoptosis assays. AECs were treated for 24 hours total after initial overnight plating. As AECs were used within 48 hours of isolation, these AECs were considered undifferentiated type 2-like cells.

RNAseq Analysis

RNAseq analysis was performed on BMDMs isolated and polarized to either an M1-like or an M2-like phenotype, as described above. Polarized BMDMs were isolated and RNA was extracted using a RNeasy column kit (Qiagen, Germantown, MD) per the manufacturer's directions. RNA integrity was assessed on an Agilent Bioanalyzer (Agilent, Santa Clara, CA). Only samples with an RNA integrity value of at least 8 were used in RNA sequence analysis. RNA sequencing was performed by Genewiz (South Plainfield, NJ) using their standard RNA sequencing pipeline. In short, sequence reads (30-50 million read depth) were trimmed to remove likely adapter sequences and nucleotides with poor quality using Trimmomatic v.0.36. Reads were mapped to the ENSEMBL mouse reference genome using the STAR aligner v.2.5.2b. Unique gene hit counts were calculated by using feature Counts from the Subread package v.1.5.2. Only unique reads that fell within exon regions were counted. Transcript counts were normalized, and differential expression statistics were calculated using DESeq2 (Supplemental Table 1, all Supplemental Tables available at:

https://doi.org/10.6084/m9.figshare.14818545). RNAseq data was visualized using Python 3.7 and a combination of Matplotlib, Scikitlearn, and Seaborn packages. Both raw and processed RNAseq data are available in total through the Gene Expression Omnibus (GEO), accession number GSE167982. For further analysis, all candidate genes identified during Python visualization were run through the ClueGO Plug-In (version 2.5.7) for Cytoscape (version 3.8.0) to group data by molecular function (Figures 18, 19) or by biological process (Figures 9, 19) into biological nodes determined by ClueGO. The specific p-values used to place these genes into thematic groups and sub-thematic nodes based on component similarity ranged between $p<0.05$ and $p<0.0001$. For analysis in Figures 9A and 9B (Supplemental Table 2), Figures 18B (Supplemental Table 3), 18C (Supplemental Table 4), and Figures 19A (Supplemental Table 5) and 19B (Supplemental Table 6), all subtheme nodes were combined under their thematic group name and all gene duplicates were removed. The overall percentage prevalence of each group as labeled in pie charts in Figures 18B, 18C, 19A, and 19B was determined by dividing the number of unique genes present in one group by the total number of genes summed across all groups. Overall enrichment score was calculated by taking the negative log of the each term's p-value, then averaging all enrichment scores within a functional group (i.e., log(averaged p-value)*-1).

Fibroblast Proliferation and Migration

Fibroblasts were plated at 10,000 cells/well in a 96-well plate in complete DMEM for 4hrs, followed by overnight treatment in SFM. 90µl of macrophage CM or polarizing growth media without cells were added to their respective wells for 48hrs before 10µl of MTT solution was added to each well and allowed to incorporate for another 24hrs. After mixing in MTT stop

solution with a multichannel pipette, the plate was read according to manufacturer's instruction (Sigma Aldrich).

To investigate fibroblast migration using a scratch wound assay, fibroblasts were plated at 20,000 cells/well in clear bottomed 96-well plates (Essen Biosciences, catalog #4378, Ann Arbor, MI) overnight in DMEM+10% FBS. After fibroblast adherence, complete media was washed away and replaced with SFM overnight (200µl volume). The next day, the Wound Maker was used to create a uniform scratch in each well. Cells were rinsed 2x in SFM and replaced with corresponding CM/polarizing growth media (50-100µl) and the plate was placed at 37ºC. Pictures were taken using Incucyte software every 4hr for up to 5 days. In all figures M1 or M2 is used to denote M1 or M2 CM respectively and LPS+IFNγ or IL-4+IL-13 is used to denote the respective M1 or M2 polarization growth media.

AEC Apoptosis

Isolated AECs were plated overnight at 50,000 cells/well in a white-bottomed 96-well plate (Corning, NY) in complete small airway growth media (SAGM; Lonza, Morristown, NJ) plus human keratinocyte growth factor (KGF; Peptro Tech Inc, Cranbury, NJ). The 96 well plate had previously been coated with undiluted Matrigel to retain a type 2 AEC phenotype of cultured cells. After initial cell sit-down, media was aspirated, and cells were rinsed in SFM prior to addition of BMDM CM or polarizing growth media for 24hrs. Upon completion of the assay, Caspase-Glo 3/7 (Roche, Indianapolis, IN) was added in a 1:1 dilution and activation of caspase-3/7 was measured according to the manufacturer's guidelines. Samples were analyzed using an M3 Microplate Luminometer and the value expressed in relative luminescence units compared with control AECs maintained in SFM alone. In some experiments recombinant cathepsin-D

(R&D Systems) was tested for ability to cleave the caspase 3 substrate but results were negative (data not shown).

Protease Inhibitor Studies

M1 or M2 BMDM CM was thawed from frozen and used in protease inhibitor studies (Figure 19). BMDM CM was treated with either serine protease inhibitor AEBSF (1µM; Sigma Aldrich #SBR00015), serine protease inhibitor aprotinin (0.75µM; Sigma Aldrich, #A1153), cysteine inhibitor E-64 (1µM; Sigma Aldrich #E3132), or pan-protease inhibitor Pierce™ Protease Inhibitor (5x and 0.5x standard concentration; Mini Tablets ThermoFisher, #A32955). CM+inhibitors were allowed to incubate together for one hour before being plated on a white-bottomed 96-well plate. CaspaseGlo3/7 was added in a 1:1 dilution and samples were measured and analyzed as described above.

Flow Cytometry

AECs were isolated and plated at 2 million cells/well in a 6-well plate on fibronectin-coated plates overnight. Fibronectin-coated plates were used to increase technical feasibility for the assay, as dissociating AECs from Matrigel resulted in very low cell yields. The next day, cells were rinsed and media was replaced with BMDM CM for 24hrs. For flow analysis, nonspecific Fc binding was blocked with a CD16/32 antibody. Subsequently, primary antibodies were added to cell samples and incubated for 30 min in the dark at 4^{o}C. Primary antibodies used were anti-CD45 and anti-Epcam/CD326 (BD Biosciences) to identify AECs and Zombie Violet and Apotracker (Biolegend, San Diego, CA) for apoptosis. Total cell number was compared between samples using one-way ANOVA analysis with GraphPad Prism.

Statistics

Statistical analyses were performed using GraphPad Prism software package (GraphPad Software, La Jolla, CA). Following a normality test, differences between experimental groups were determined using one-way ANOVA with a Tukey post-test (for comparing 3 or more groups) if normally distributed. Non-normally distributed data was analyzed by Kruskal-Wallis test and Dunn's multiple comparison post-test. Differences were considered statistically significant when $p<0.05$. All data are represented as mean +/- SEM. All experiments were repeated, at least, in duplicate with similar results. Pertinent statistical information, i.e., n-values, experiment number, and p-values, are given in individual figure legends.

Results

RNAseq shows unique differences between M1 and M2 BMDMs

In order to determine whether M2 secreted factors were responsible for profibrotic effects of macrophages in the lung, we first wanted to understand the M1 v. M2 transcriptome in an unbiased fashion. To do this, we performed RNAseq on BMDMs polarized to an M1 or M2 phenotype. As an initial overview analysis, we inputted the top 5% (top 270 genes) of the most highly upregulated or downregulated genes from the RNAseq analysis into the ClueGO plug-in of Cytoscape (Supplemental Table 1, all Supplemental Tables available at: https://doi.org/10.6084/m9.figshare.14818545). We chose to use this plug-in to organize all inputted genes into family gene group clusters based on biological process. ClueGO analysis demonstrated that gene group clusters with the highest enrichment values in M1 BMDMs were related to inflammation, particularly the cell response to cytokine, to virus, to protozoan, and to interferon-β (Figure 9A). In contrast, clusters with the highest enrichment values in M2 BMDMs were related to cell processing, including categories of chondrocyte differentiation, connective

tissue development, and positive regulation of myelination (Figure 9B). To visualize these differences in genes pertaining to molecular function between M1 and M2 BMDMs, we employed the Matplotlib, Scikitlearn, and Seaborn packages from Python. Visualization in Python confirmed a large number of genes whose expression differs significantly between M1 and M2 BMDMs (Figure 9C). The RNAseq data also indicate that M2 BMDMs have a higher number of genes encoding for secreted proteins than M1 BMDMs (Figure 9D), providing additional rationale to further probe how M1/M2 secreted proteins initiate a profibrotic response in lung structural cells.

A

GO biological theme	GO categories (n=75)	Genes (n=58)	Enrichment score
Response to Cytokine	2	41	29.71
Response to Virus	3	22	15.17
Cellular response to interferon-beta	6	24	12.89
Defense response to protozoan	4	14	10.51
Defense response to Virus	66	41	9.86

B

GO biological theme	GO categories (n=31)	Genes (n=47)	Enrichment score
Chondrocyte differentiation	14	23	4.98
Connective tissue development	8	22	3.72
Positive regulation of myelination	4	11	4.18
Regulation of inflammatory response	1	15	4.67

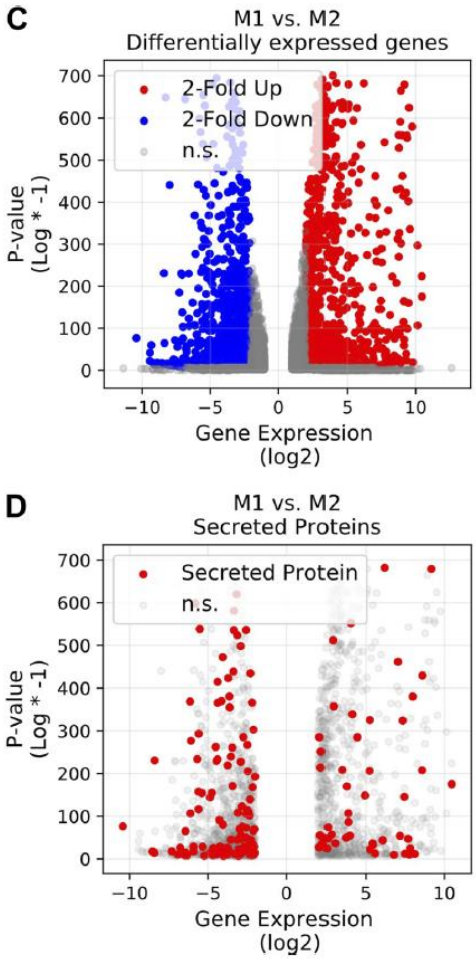

Figure 9: M1 and M2 bone marrow-derived macrophages (BMDMs) have different gene expression profiles based on RNA sequencing (RNAseq) analysis. RNAseq analysis of the top 5% of genes (270 genes) using the ClueGO plugin of Cytoscape shows drastically different prominent biological themes in M1 (A) and M2 (B) BMDMs as analyzed by biological process. Additionally, M1 and M2 BMDMs exhibit different transcriptome profiles (C) and M2 BMDMs have an increased number of differentially expressed genes for secreted proteins than

M1 BMDMs (D). In (C) and (D), negative log2 expression values correlate to genes enhanced in M2 BMDMs and positive log2 expression values correlate to genes enhanced in M1 BMDMs.

BMDM polarization in vitro shows accurate M1 and M2 phenotypes

As our RNAseq data yielded notable differences in gene expression between M1 and M2 BMDMs, we next wondered how differences in expressed genes can alter macrophage function and phenotype in pulmonary fibrosis. As data from the literature assert that profibrotic macrophages are M2-like, we chose to use BMDMs and polarize them *in vitro* to an M1 or M2 phenotype for further study. BMDMs are an ideal cell candidate as they are (1) an accessible macrophage population that can be isolated in abundance[217–219] and (2) recent work has shown that monocyte-derived alveolar macrophages (moAM)s, derived from bone marrow precursors[220], are pathogenic and that their recruitment to the lung along with Ly6Ci^{hi} monocytes are highly responsible for fibrosis development and progression[6].

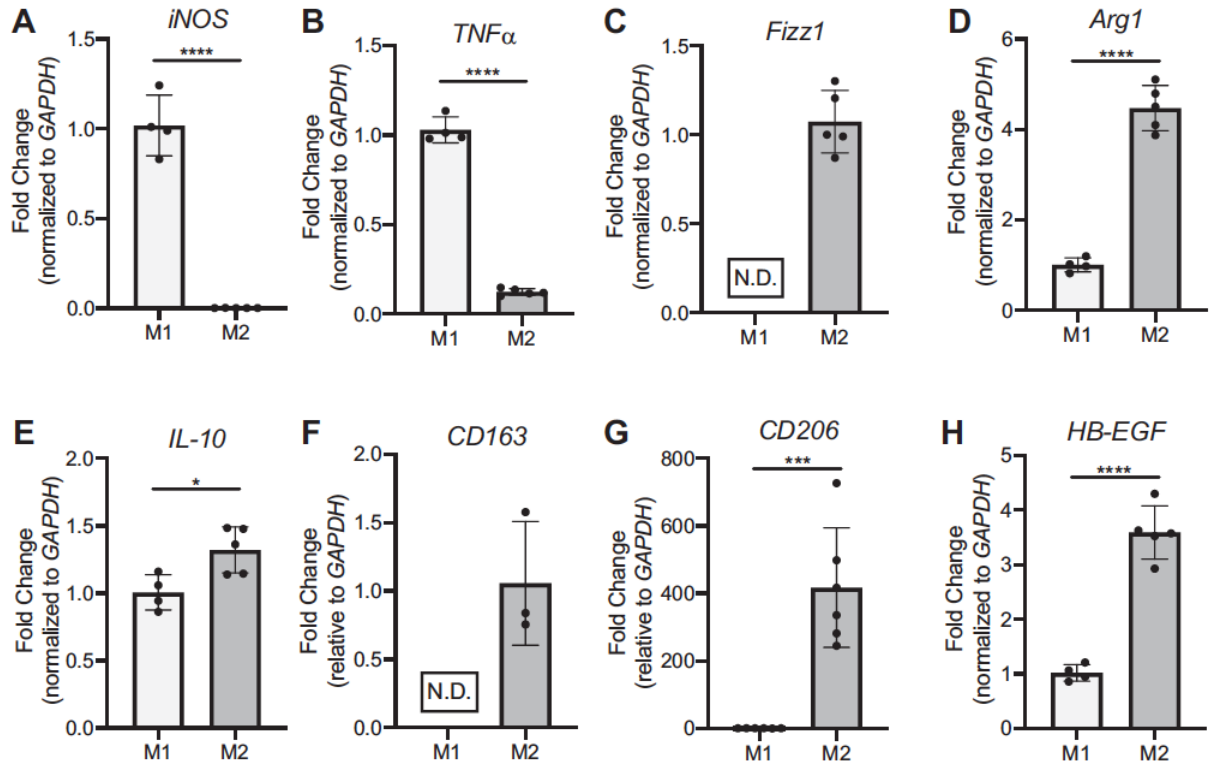

Figure 10: BMDMs achieve a reliable M1 or M2 polarization when given standard combinations of polarizing reagents LPS+IFNg (M1) or IL-4+IL-13 (M2). BMDMs were polarized to an M1-like (100ng/ml LPS + 50ng/ml IFNg) or M2-like (10ng/ml IL-13 + 10ng/ml IL-4) phenotype for 24 hours before being isolated for RNA extraction.

Representative RT-qPCR data of M1 genes: (A) iNOS and (B) TNFa, and M2 genes: (C) Fizz1, (D) Arg1, (E) IL-10, (F) CD163, (G) CD206, and (H) HB-EGF. N.D.: Not Detected. *: $p<0.05$, ****: $p<0.0001$. All data representative of 3-7 experiments, n=4, 5.

BMDMs polarized to M1 (100ng/ml LPS+50ng/ml IFNγ) or M2 (10ng/ml IL-4+10ng/ml IL-13) showed a highly consistent and differential phenotype (Figure 10). M1 BMDMs exhibited high iNOS and TNFα expression (Figures 10A, 10B) compared to M2 BMDMs, which more highly expressed Fizz1 (Figure 10C), Arg1 (Figure 10D), and IL-10 (Figure 10E) as well as CD163 (Figure 10F) and CD206 (Figure 10G). The relative expression of these key markers in the M1 and M2 BMDMs match those of other published work in the field[13,102,122,221]. M2 BMDMs also showed increased expression of heparin binding epidermal growth factor-like growth factor (HB-EGF) (Figure 10H). Though a lesser-known marker in the lung field, HB-EGF is used widely as an M2 marker in the pancreas literature[222]. In addition to clear fold change differences at the transcript levels, these M1-M2 phenotypes also hold at the protein level (Figure 11) as M2 BMDMs exhibit increased $Arg1^+$ protein expression and M1 BMDMs exhibit increased $iNOS^+$ protein expression via flow cytometry.

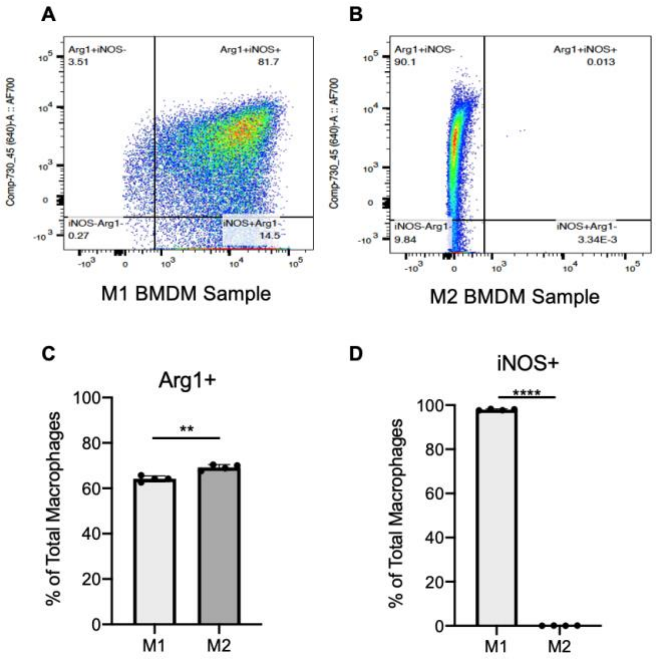

Figure 11: iNOS labels M1 BMDMs reliably at the protein level. M1 (A) and M2 (B) BMDMs were stained with anti-Arg1 and anti-iNOS via flow cytometry. While Arg1 at the protein level appears ubiquitously expressed in M1s and M2s (C), only M1 BMDMs are positive for iNOS (D). Flow cytometry quantification by percentage of total macrophages. **: p<0.01, ****: p<0.0001.

The increased M2 effect on fibroblast migration is explained by M2 polarizing reagents, IL-4 and IL-13

Fibroblasts are located adjacent to alveolar epithelial cells (AECs) along the basement membrane in the healthy lung, where they serve as key structural cells by maintaining normal tissue architecture through the deposition and maintenance of extracellular matrix (ECM) proteins[85]. Microinjuries to the epithelium can lead to AEC apoptosis, causing gaps in the epithelial lining that can be closed by activated fibroblasts proliferating and migrating to the wound site[85]. We investigated the effects of M1 and M2 CM on the ability of primary lung fibroblasts to proliferate and migrate. MTT assays showed that fibroblasts treated with either M1 or M2 CM had increased proliferation over the serum-free media control (Figures 12A, 12B). However, this level of increased proliferation with macrophage CM was not different compared to the respective polarization growth media controls; fibroblasts given M1 CM showed the same

amount of proliferation as those given LPS+IFNγ polarization growth media and treatment with M2 CM or IL-4+IL-13 polarization growth media yielded the same amount of proliferation (Figures 12A, 12B).

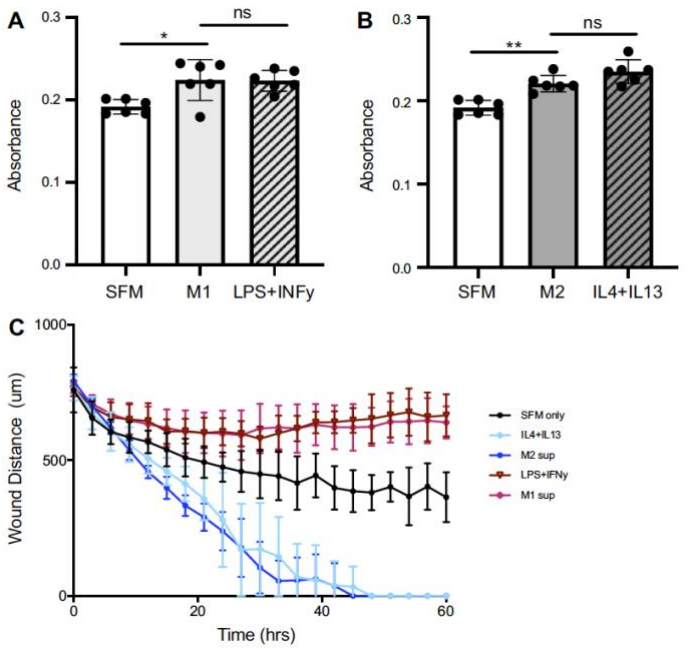

Figure 12: Effects of macrophage CM on fibroblast proliferation and migration are recapitulated by polarization cytokines. M1 and M2 CM or their respective polarization growth media (LPS + IFNγ or IL-4 + IL-13) were put on untreated primary lung fibroblasts for proliferation and scratch wound assays. Fibroblasts treated with M1 (A) or M2 (B) CM show increased proliferation over SFM via MTT assay after 48 hours, though no difference was noted between CM and respective polarization media controls. Representative sample (2 experiments, n=6). (C) Representative scratch wound assay showing M2 CM and IL-4+IL-13 polarization media cause the fastest wound closure (migration) but that there is no difference between the two treatments. *: $p<0.05$, **: $p<0.01$. Data in (C) are representative of at least three experiments, n=5 per group.

To determine fibroblast migration capabilities, we seeded fibroblasts at a set density and performed a scratch wound assay, using Incucyte image software to quantify the wound distance over time (Figure 12C). Fibroblasts given M2 CM closed the scratched area faster than either the control or fibroblasts given M1 CM. Interestingly, fibroblasts given M1 CM post-scratch failed to close the wound. Similar to fibroblast proliferation, polarization growth media controls in the scratch wound assay show that differences in fibroblast migration are explained by their respective polarizing reagents present in the CM, as overall migration was not different between fibroblasts given M2 CM or IL-4+IL-13, nor between fibroblasts given M1 CM or LPS+IFNγ.

The increased M2 CM effect on fibroblast mRNA transcript expression of key profibrotic and anti-apoptotic factors is explained by M2 polarizing reagents, IL-4 and IL-13

In addition to increased accumulation and migration, lung fibroblasts also become highly activated during fibrosis[223]. Their increased activation promotes production of ECM proteins, leading to scar formation that reduces overall lung elasticity[85]. Additionally, primary lung fibroblasts from IPF patients have been shown to be resistant to apoptosis[85,224,225].

ECM components secreted by fibroblasts include collagens, glycoproteins, and proteoglycans[85]. Fibroblasts given M2 CM had increased expression of collagen 1, collagen 3, fibronectin, and periostin (Figure 13A) compared to cells given M1 CM, consistent with the rationale that M2 macrophages cause profibrotic effects in fibroblasts. When these fold changes induced by M1 and M2 CM were compared to their polarization growth media controls however, no statistical difference was noted, implying that the increased M2 effect on fibroblast expression of these ECM genes is explained by polarizing reagents present in the CM.

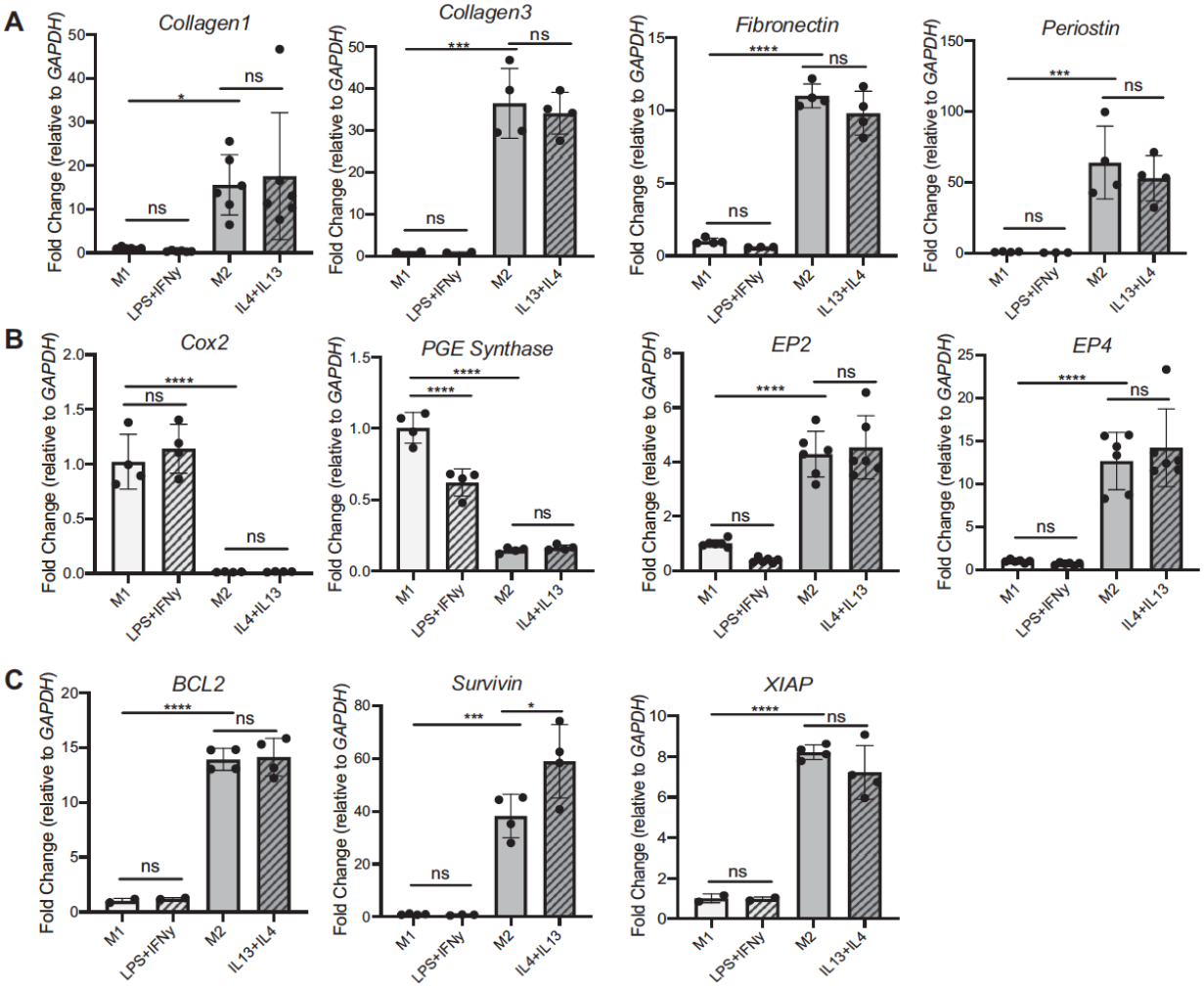

Figure 13: While expression of profibrotic and anti-apoptotic mRNA transcript in fibroblasts is enhanced with M2 CM treatment, these effects are attributable to polarization reagents. qPCR fold change of key profibrotic genes (A) (collagen1, collagen3, fibronectin, periostin), or apoptosis-related genes (B) (Cox2, PGE synthase, EP2, EP4), and of anti-apoptotic genes (C) (BCL2, survivin, XIAP). *: $p<0.05$, **: $p<0.01$, ***: $p<0.001$, ****: $p<0.0001$. All figures show representative data from at least three experiments, n=3-4.

Previous work in our laboratory suggests that prostaglandin (PG) $E(_2)$ signaling is an important regulator of fibroblasts and fibrosis[226,227]. All cells can produce arachidonic acid, which is metabolized to eicosanoids. Cyclooxygenase (COX)-2 is a rate-limiting enzyme to initiate prostaglandin synthesis[226]. In the healthy lung, high levels of PGE_2 limit fibroblast proliferation, migration, and collagen synthesis. However, the lungs of pulmonary fibrosis patients have decreased levels of PGE_2. In Figure 13B, fibroblasts given M2 CM have much lower levels of COX-2 and the enzyme responsible for PGE_2 production, PGE synthase,

compared to fibroblasts given M1 CM. Perhaps as a compensatory response to the lower production of PGE_2, M2 CM-treated fibroblasts show increased expression of PGE receptors E prostanoid (EP)2 and EP4. However, expression of COX-2, PGE synthase, and EP2 and EP4 is not different between the macrophage CM and its associated polarization growth media control.

Data in the literature support the concept that profibrotic fibroblasts are often resistant to apoptosis[33,224,225]. Thus, we next examined the expression of classic apoptosis markers BCL2, survivin, and XIAP. As expected, M2 CM on fibroblasts induced a multiple-fold increase in BCL2, survivin, and XIAP expression compared to M1 CM treatment (Figure 13C). However, the increased M2 effect on fibroblast mRNA transcript expression of these anti-apoptotic factors is explained by M2 polarizing reagents, IL-4 and IL-13, as these reagents induced a fold change either comparable or not statistically different from fibroblasts receiving M2 CM alone.

M2 polarization reagents, IL-4+IL-13, increase profibrotic and anti-apoptotic mediator expression in AECs

As the first physical line of defense against inhaled insults, AECs communicate with fibroblasts and macrophages and are the primary cell type to experience perpetuated microinjuries during fibrosis[3,15]. As homeostasis within a healthy lung microenvironment is dependent on AEC-mesenchymal cell crosstalk[226], we investigated if AECs receiving M2 supernatant increased expression of fibrotic genes. While there is no difference in the expression of vascular endothelial growth factor (VEGF), both connective tissue growth factor (CTGF) and platelet-derived growth factor alpha (PDGFα) were increased in AECs given M2 CM compared to those receiving M1 CM (Figure 14A). Increased levels of these genes were not different between AECs receiving M2 CM and those receiving M2 polarizing growth media controls, however.

In AECs given M2 CM, expression of COX-2 and PGE synthase are decreased compared to cells treated with M1 CM (Figure 14B) while expression of anti-apoptotic markers BCL2, survivin, and XIAP are increased in AECs treated with M2 CM (Figure 14C). Interestingly, EP2 expression is not different between M1 CM- or M2 CM-treated AECs and EP4 expression is increased in M2 CM-treated compared to M1 CM-treated AECs (Figure 14B). Across nearly all genes, expression differences between AECs given M2 CM and AECs given M2 polarizing growth media controls were not statistically different.

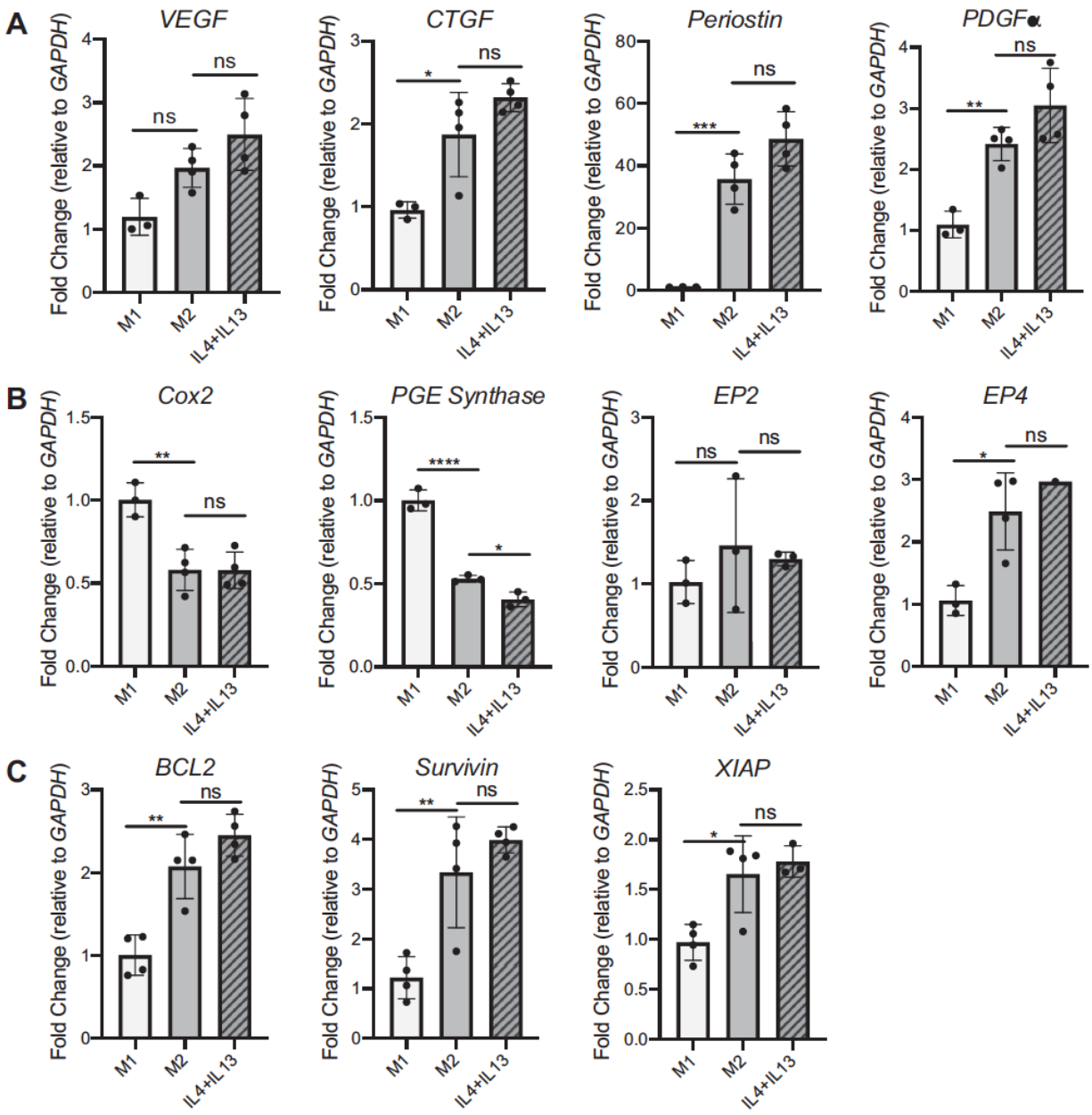

Figure 14: Although AECs treated with M2 CM show increased expression of profibrotic and anti-apoptotic genes, these differences are caused by IL-4 and IL-13 reagents in the CM. qPCR fold change of key profibrotic genes (A) (VEGF, CTGF, POSTN, PDGFa), of (B) apoptosis-related genes (Cox2, PGE synthase, EP2, EP4), and of anti-apoptotic genes (C) (BCL2, survivin, XIAP). *: p<0.05, **: p<0.01, ***: p<0.001, ****: p<0.0001. All figures show representative data from at least three experiments, n=3-4.

Although increased AEC apoptosis with M2 CM is not an effect of polarizing reagents, the phenomenon is likely due to a promiscuous protease

Repeated microinjuries to the lining of the lung cause AECs to apoptose during fibrosis[3,228–230]. We used the Caspase-Glo 3/7 assay to quantify differences in AEC apoptosis

after AEC treatment with M1 or M2 macrophage CM. In this assay, the kit provides a substrate that luminesces when it is cleaved by activated caspase 3/7. While AEC treatment with M1 CM increased caspase-3/7 activation over the serum free control, AECs given M2 CM exhibited a nearly five-fold increase in activation compared to the negative control (Figure 15A) and this difference was not recapitulated by the polarization growth media (Figure 16).

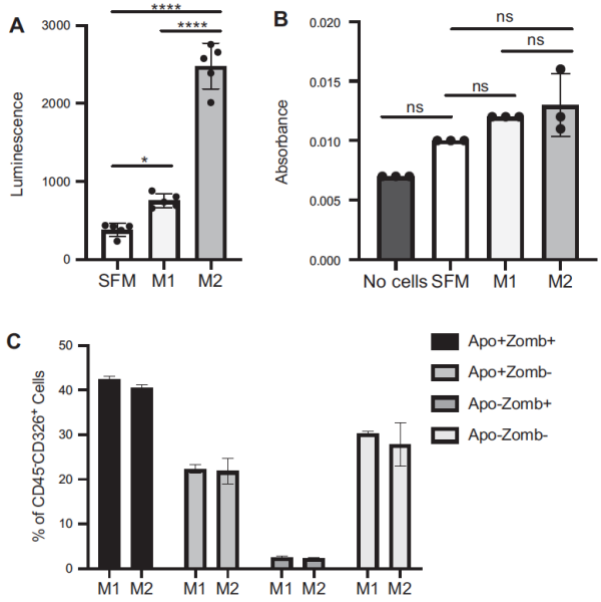

Figure 15: While M2 CM appears to induce greater AEC apoptosis than M1 CM as measured via Caspase-Glo Luminescence assay, further verification supports no difference in AEC apoptosis treated with M1 or M2 CM. (A) AECs topped with 50µl of M2 CM have robustly increased caspase 3/7 activation over AECs given M1 CM using Caspase-Glo assay, (B) AECs given M1 or M2 CM show no difference in viability as measured by MTT assay, and (C) flow cytometry of AECs plated on fibronectin show no differences in apoptotic phase or expression of apoptotic protein markers Apotracker and Zombie Violet after treatment with M1 or M2 CM for 24hrs. *: $p<0.05$, **: $p<0.01$, ***: $p<0.001$, ****: $p<0.0001$. Representative data shown, all experiments repeated 2-7 times, n=2-5.

To further quantify these differences in apoptosis rate, we performed a MTT cell viability assay with AECs given either M1 or M2 CM. Surprisingly, this experiment yielded no difference in overall viability between M1 CM-treated or M2 CM-treated cells (Figure 15B). As such, we sought to re-validate our caspase-glo 3/7 AEC apoptosis assay through a secondary method.

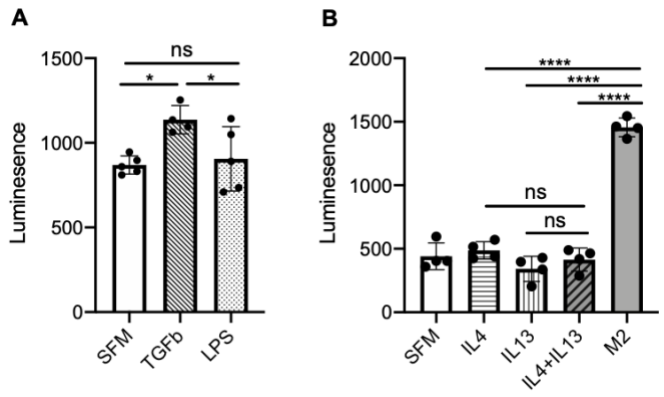

Figure 16: M2 CM appears to induce AEC apoptosis more robustly than polarizing growth media using Caspase-Glo luminescence assay. Relative caspase-3/7 activation in AECs given different types of CM as measured by luminescence from Caspase-Glo 3/7 kit. (A) positive control TGF-β (4ng/ml) induces caspase 3/7 activation while LPS (20ng/ml) does not and (B) AECs topped with 50µl of M2 CM have robustly increased caspase 3/7 activation over AECs given serum-free media (SFM) or polarizing growth media containing IL4 (10ng/ml), IL13 (10ng/ml), or IL4+IL13. *: $p<0.05$, **: $p<0.01$, ***: $p<0.001$, ****: $p<0.0001$. Representative data shown, all experiments repeated between 2-7 times, n=3-5.

Using flow cytometry to perform a live/dead stain and to quantify the amount of apoptotic cells present in our CM-treated AECs, we found no difference in total apoptosis nor differences in stage-specific apoptosis between M1 CM and M2 CM-treated AECs (Figure 15C). Consequently, we were forced to consider the likely possibility that the increased luminescence detected in Figure 15A was not the result of AEC-derived active caspase-3/7, but rather, because of a caspase-3/7 "look-alike" endopeptidase present in the M2 CM that was also able to cleave the substrate present in the Caspase-Glo 3/7 kit and yield a false positive result. Figure 17 demonstrates that M2 CM alone in wells without AECs is able to activate the Caspase-Glo 3/7 reagent, further supporting the presence of an imposter cell factor. As wells with heat-inactivated M2 CM have approximately 245-fold decreased luminescent activity compared to wells with non-heated M2 supernatant (Figure 17), we conclude that the masquerading mediator is likely a protein or peptidase.

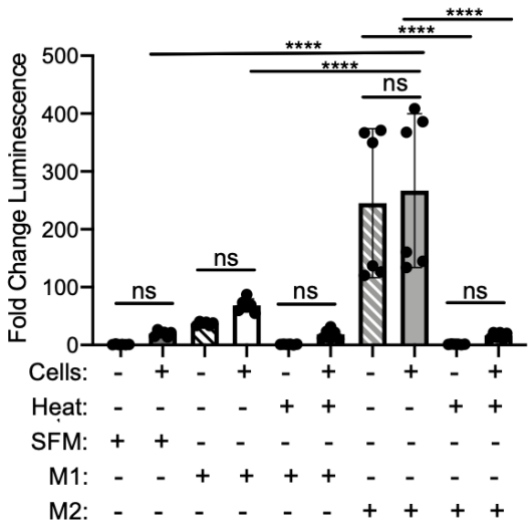

Figure 17: Caspase-Glo 3/7 false positive likely caused by a heat-sensitive peptidase present in the M2 CM. AECs given either unheated or heated (100°C for 10 minutes) M1 or M2 CM were compared to wells containing no AECs and unheated or heated CM to assess the ability of substances in the CM to activate the Caspase-Glo 3/7 reagent. Fold change data from combined experiments (2 experiments, n=3 each). *: $p<0.05$, **: $p<0.01$, ***: $p<0.001$, ****: $p<0.0001$.

Transcriptome data for secreted proteins from RNAseq analysis suggests possible candidates for caspase-3/7 "lookalike"

To winnow down the protein/peptidase candidates likely responsible for this unexpected caspase-3/7 cleavage, we returned to our M1-M2 RNAseq dataset and used Python to visualize categories of genes for secreted proteins that are differentially expressed in M1 and M2 BMDMs. We noticed that M2 BMDMs have an increased number of differentially expressed genes for secreted proteases compared to M1 BMDMs (Figure 18A) (23 upregulated genes for secreted proteins in M2s compared to only 5 upregulated in M1s), further implicating the presence of a secreted protease causing the false positive signals in Figure 15A, 16B, and 17. Using the ClueGO plug-in within Cytoscape, we organized all genes for secreted proteins into family gene group clusters based on molecular function for the M1 (Figure 18B) and M2 transcriptomes (Figure 18C) (See Figure 20 for pictorial depiction of groups and nodes from Figures 18A-B, see Supplemental Tables 3-6 for complete gene list by category). As expected,

the M1 transcriptome for secreted proteins contains gene families related to the immune response including cytokine binding (5%), cytokine receptor binding (26%), and receptor ligand activity (30%) with a total of 9 distinct molecular function groups. In contrast, the M2 transcriptome for secreted proteins contains 19 groups covering a wider array of molecular function (Figure 18C). A sizeable percentage of genes are present in molecular functions including integrin binding (6%), heparin binding (8%), growth factor binding (8%), peptidase activity (13%)/positive regulation of peptidase activity (2%), receptor regulator activity (21%), and signaling receptor regulator activity (12%).

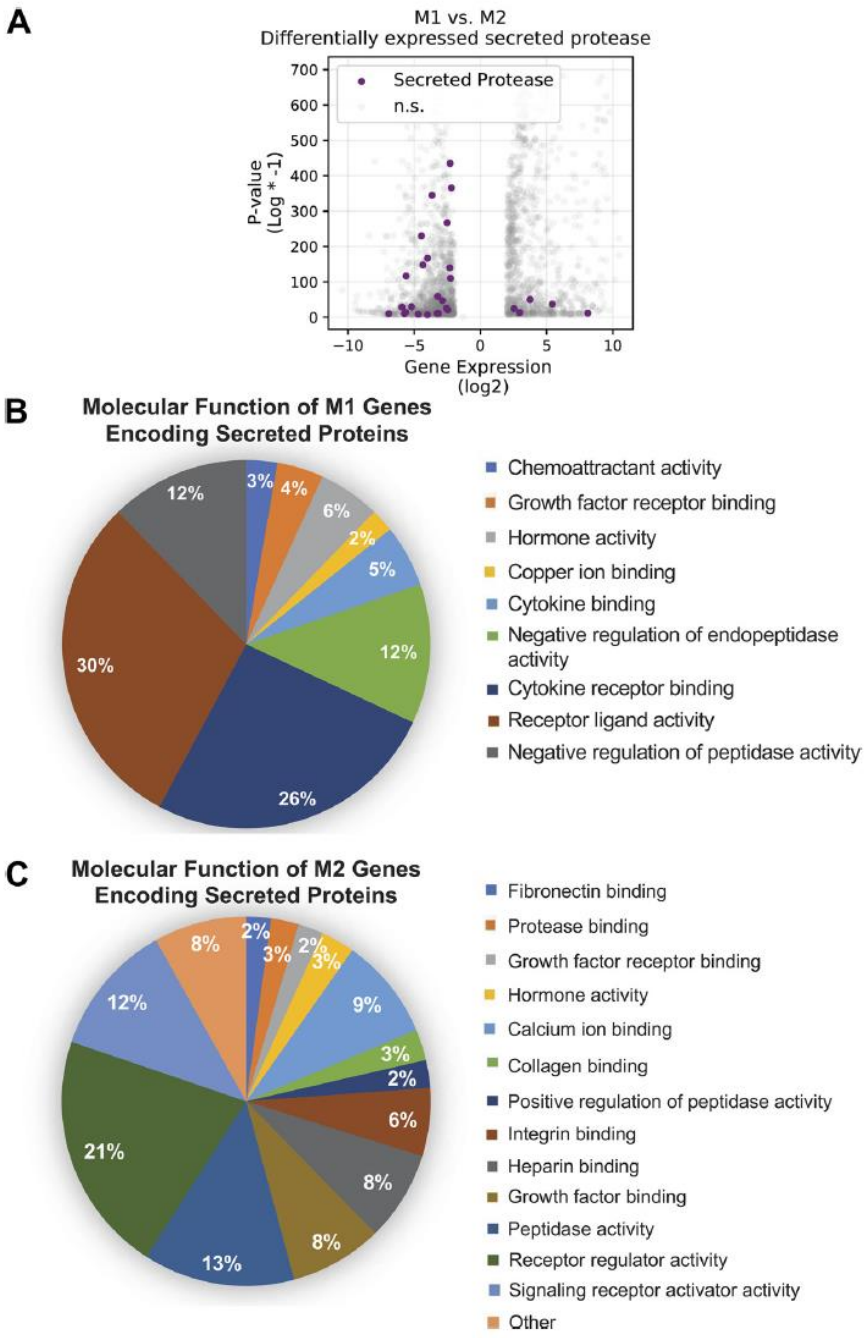

Figure 18: M1 and M2 BMDMs have different transcriptome profiles for secreted proteins based on RNAseq analysis. (A) RNAseq data show an increased number of genes for secreted proteases in M2 BMDMs (negative log2 values) compared to M1 BMDMs (positive log2 values). BMDMs polarized to an M1-like (B) or M2-like (C) phenotype show differences in molecular function categories as calculated by the ClueGO plugin of Cytoscape. In (B) and (C), ClueGO analysis organized upregulated genes into groups by molecular function as described in Methods. Percentages were calculated by dividing the number of genes present in each molecular function group divided by the total number of all genes.

As the most robust phenotypic effect was noted in the M2 CM (Figures 15A) and heat inactivation of the macrophage CM effectively reduced the false positive signal (Figure 17), we

further refined our analysis to genes listed in the “peptidase activity” molecular function group of the M2 genes encoding secreted proteins. ClueGO analysis of the molecular function (Figure 19A) and biological processes (Figure 19B) of the listed peptidases from the M2 genes encoding secreted proteins of Figure 18C showed hits for peptidase activity (32%), endopeptidase activity (26%), and metalloendopeptidase activity (10%). Interestingly, additional hits included both negative regulation of cysteine-type endopeptidase activity involved in the apoptotic process (3%) and serine-type peptidase activity (13%). We consequentially used inhibitors against cysteine-type peptidases and against serine-type peptidases with the M1 and M2 CM to investigate which family of peptidases was responsible for cleaving the luminescent substrate. Inhibiting protease activity in M1 CM unsurprisingly had no effect on luminescence, as overall caspase-3/7 substrate cleavage was already low with this CM (Figure 19C). Interestingly, the Pierce™ pan-protease cocktail inhibitor was most successful at reducing luminescence in M2 CM compared to serine peptidase inhibitors or cysteine peptidase inhibitors alone and it inhibited peptidase activity in a dose-dependent manner (Figure 19D). Although the exact formula is proprietary, this protease cocktail includes E64, aprotinin, AEBSF, leupeptin, bestatin, and pepstatin A. As neither E64, aprotinin, or AEBSF alone altered caspase-3/7 substrate cleavage in the M2 CM, it is unlikely that one of these inhibitors is responsible for decreased enzyme activity noted with the pan-peptidase inhibitor. Decreased caspase-3/7 substrate cleavage is also not likely caused by leupeptin, as leupeptin is a serine and cysteine protease inhibitor and thus targets the same protease families as E64, apoprotin, and AEBSF together. As bestatin targets amino-peptidases and pepstatin A targets aspartic acid proteases, it is likely that the M2 CM contains either an amino-peptidase or aspartic acid protease that is cleaving our luminescent substrate.

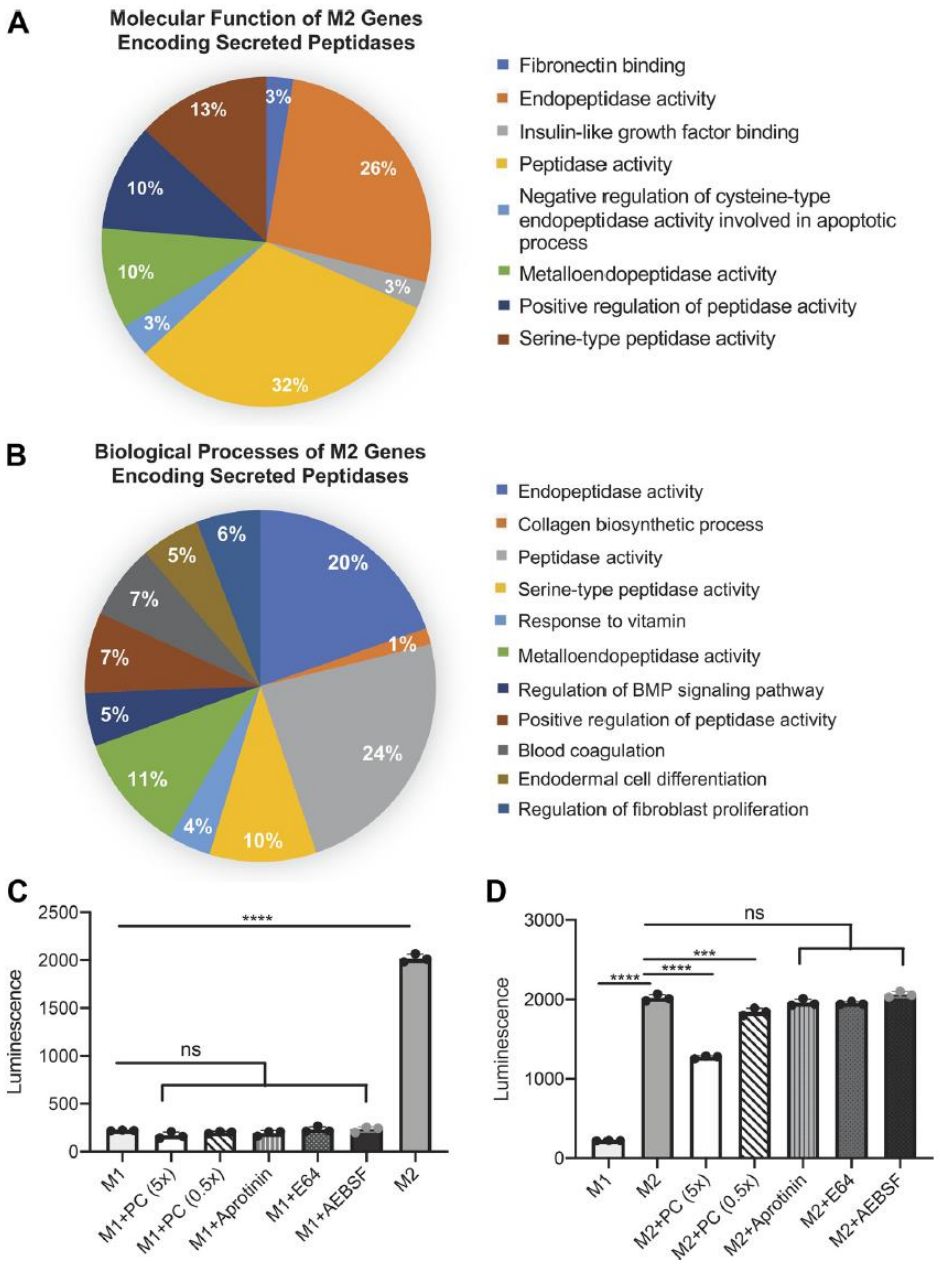

Figure 19: M2 transcriptome data highlights proteases that may be responsible for cleavage of Caspase-Glo 3/7 substrate in the AEC apoptosis assay. Peptidases defined in the M2 transcriptome for secreted proteins (Figure 18) were further characterized by molecular function (A) and biological process (B) and re-analyzed with ClueGO as described in Methods. Pre-treatment of M1 CM (C) or M2 CM (D) with protease inhibitors Pierce™ pan-cocktail (PC – 5x and 0.5x standard concentration), aprotinin (0.75µM), E-64 (1µM), or AEBSF (1µM) was done to quantify depletion of luminescence. *: $p<0.05$, **: $p<0.01$, ***: $p<0.001$, ****: $p<0.0001$. Experiments repeated twice, n=3-4.

Discussion

Evidence in the literature over the last two decades has shown that macrophages are critical in fibrosis development and that their secreted factors are important in cell crosstalk. In

this paper, we used RNAseq to confirm BMDM polarization to accepted M1/M2 phenotypes. Although no paper to our knowledge has performed RNAseq on polarized wild type mouse BMDMs, our data reveal similarities to gene expression profiles found in polarized rat BMDMs by Guo et al., 2019[231]. Like Guo et al., we detected increased pathway enrichment for chemokine/cytokine pathways in M1 BMDMs and increased enrichment for cell processing in M2 BMDMs. We also noted high levels of CCR7, CD86 and low Arg1 in M1 BMDMs compared to high CD68, CD163, Arg1 and low expression of CD86 and CCR7 in M2 BMDMs. These similarities in both enrichment pathways and genes associated with a polarized BMDM phenotype confirm the utility of this RNAseq dataset for further interrogation by other members of the scientific community.

In addition to the polarization differences yielded in our RNAseq dataset, qPCR analysis of M1 and M2 BMDMs depicted expected differences in Arg1, iNOS, TNFα, IL-10, Fizz1, CD163, CD206 and HB-EGF concordant with other studies in the literature[13,14,102,131] (Figure 10). Although we restricted our macrophage polarization to the broad "M2" phenotype, it is important to note that others have determined that use of different polarization cytokines can beget a wider range of macrophage phenotypes. Although existing work shows that these subgroups may have different functions from each other *in vivo*[232,233], there is inconsistent evidence of strong transcriptional differences between the subsets[13,233,234]. As such, we decided to use the conventional IL-4+IL-13 polarization conditions to create the M2 BMDM phenotype.

Fibroblast treatment with M2 CM yielded expected profibrotic changes in overall migration and expression of ECM and anti-apoptotic proteins (Figure 12, Figure 13). Although these profibrotic effects of increased fibroblast migration with M2 CM had not been previously reported, there was a lack of statistical difference in fibroblast functional outcomes for

fibroblasts treated with macrophage CM compared to those treated with polarizing growth media containing IL-4+IL-13. Evidence from the literature shows that IFNγ is a strong inhibitor of fibroblast proliferation in human lung fibroblasts[235–238], while other studies show that IL-4 may promote fibroblast proliferation, though in different organs[61,239–241]. These data together provide evidence to conclude that the polarizing reagents are likely wholly responsible for M1-M2 CM-mediated proliferation differences (Figures 12A, B). There is scant evidence connecting any of our polarization cytokines to fibroblast migration; consequently, our observation that IL-4+IL-13 enhances lung fibroblast migration is a novel and potentially unexpected finding.

Fibroblast treatment with M2 CM also yielded increased expression in ECM and anti-apoptotic proteins (Figure 13). While IL-4 has been shown previously to increase levels of pro-alpha collagen 1 in human fibroblasts, it is surprising that the IL-4+IL-13 combination appears responsible for all increases in profibrotic protein expression in fibroblasts receiving M2 CM. This is in part because many different mediators have been shown to increase expression of ECM proteins, including TGF-β, CCL18/PARC, Arg1, and Fizz1[122,131,242,243]. That IL-4+IL-13 can induce the same phenotype as M2 macrophage CM that itself contains an even wider plethora of profibrotic mediators suggests the dominance of IL-4 and IL-13 in the lung milieu and that their effects supersede those of other mediators that could also be present in fibrotic macrophages.

AEC production of profibrotic mediators (Figure 14) and apoptosis are common indicators of fibrosis. Surprisingly, MTT and flow cytometry analysis (Figure 15) indicated no statistical differences in AEC apoptosis between cells that had received M1 or M2 CM. This lack of difference put alongside the well-accepted theory that AECs apoptose in the fibrotic lung, could suggest that AEC apoptosis requires juxtacrine signaling from macrophages. If this is

correct, it could be that for the most robust apoptotic response, cells adjacent to AECs are primed by injury cytokines such as IL-4, which have been documented previously to be more prevalent in the fibrotic lung from M2-like macrophages[244]. These local cytokines may then promote a juxtacrine signal in an adjacent cell that is responsible for AEC apoptosis. Future experiments can determine whether cell-cell contact with M2 macrophages alters AEC apoptosis.

Given that our M2 CM contained a protease able to cleave a Caspase 3/7 substrate, we sought to understand the specific molecular function of the protease genes upregulated in the M2 secreted transcriptome. We performed a similar analysis to Figure 18 but limited our inputted data to the 49 unique genes present in "peptidase activity" (Figure 19A, Supplemental Table 5**,** Figure 21; Figure 19B, Supplemental Table 6, Figure 21). Within this second analysis, functional categories included variants of peptidase activity (endopeptidase activity, peptidase activity, metalloendopeptidase activity) but interestingly, it also included "negative regulation of cysteine-type endopeptidase activity involved in the apoptotic process." Despite the prominence of serine and cysteine proteases in the RNAseq data, treatment of M1 and M2 CM with serine protease inhibitors AEBSF and aprotinin and cysteine protease inhibitor E64 did not yield any reduction in caspase-3/7 substrate cleavage (Figures 19C, 19D). This is contrary to our expectations, particularly because caspase 3 is a cysteine-aspartic protease which would have indicated a likely submission to a cysteine-specific inhibitor[245]. Our collective data implicate an aspartic acid protease in the M2 supernatant responsible for cleaving the luminescent substrate.

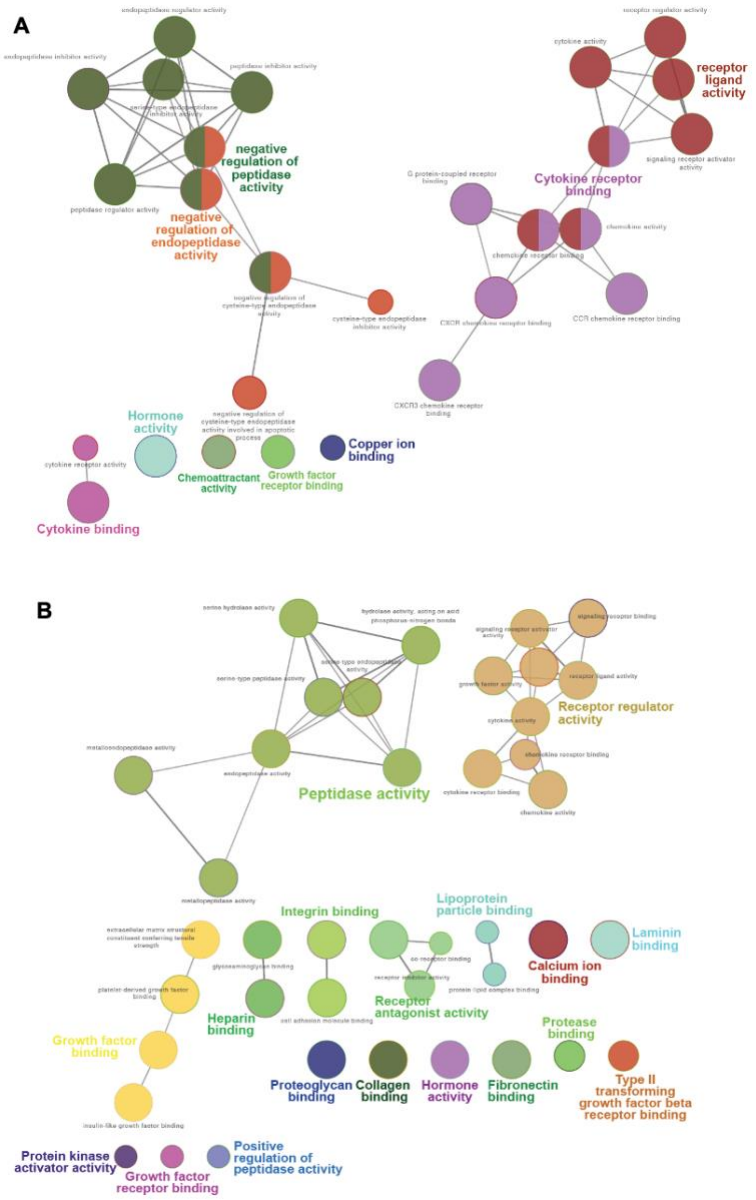

Figure 20: Cytoscape and ClueGO software organizes genes for secreted proteins in the M1 and M2 transcriptome into defined groups by molecular function. Molecular function of upregulated genes by group and labeled by function in the (A) M1 and the (B) M2 transcriptome for secreted proteins. These images serve as the raw data for the pie charts in Figure 18.

BLASTing the list of 22 differentially expressed secreted proteases from Figure 18A against the MEROPS peptidase database (https://www.ebi.ac.uk/merops/) (Supplemental Table 7) yielded a list of 14 metalloproteinases, 13 serine proteases/endopeptidases, and the aspartic acid protease cathepsin D (*Ctsd*). Of the 22 proteases, we considered cathepsin D to be the most likely candidate based on its function as an aspartic acid protease and its known role in animal

models of pulmonary fibrosis[246–250]. However, use of recombinant mouse cathepsin D in our caspase-glo assay revealed no increase in substrate-cleavage-based luminescence over the SFM control, despite doses ranging from 50µg/ml to 6.25ng/ml (data not shown). Of the remaining 21 proteases, 12 remain that are upregulated in M2 BMDMs and are not serine proteases (Supplemental Table 7). These proteases include members of the matrix metalloproteinase (MMP) family (*Mmp11, -17, -23*) and members of a disintegrin and metalloproteinase with thrombospondin motif (Adamts) family (*Adamts1, -10, -12, -2, -5*). Though evidence connecting *Adamts* genes to pulmonary fibrosis is limited[251], MMPs have been highly implicated in IPF and animal models of pulmonary fibrosis[252]. Thus, it is possible the substrate cleavage detected in the M2 CM is a result of a combinatorial effect of these proteases or to a different protease that was not detected in our analysis of the 5% most upregulated genes.

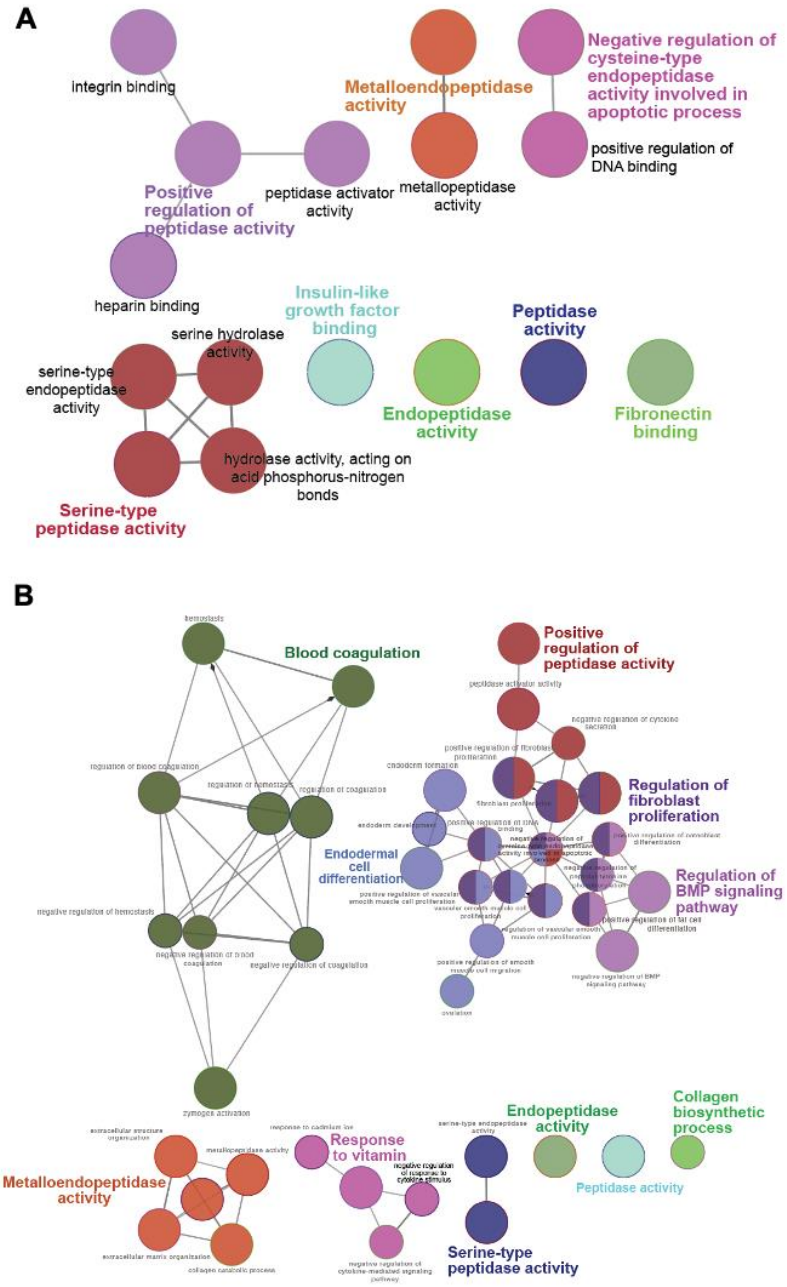

Figure 21: Cytoscape and ClueGO software organizes genes for the secreted proteins in the M2 transcriptome into defined groups by molecular function and biological process. ClueGO-Cytoscape groups of peptidases, as determined by genes for secreted peptidases, in the M2 transcriptome by molecular function (A) and by biological process (B). These images serve as the raw data for the pie charts in Figure 19.

Current work in the field supports a highly dynamic and nuanced role of macrophages in the development and progression of pulmonary fibrosis. Although profibrotic macrophages are known to secrete cytokines that are important for cell crosstalk, this study is the first to date to have considered the role of polarizing cytokines in the growth media as major contributors to

promoting profibrotic phenotypes in neighboring cells *in vitro* or used a systematic approach to determine whether fibroblast or alveolar epithelial cell responses were attributable to macrophages or polarization factors. In addition to providing a novel RNAseq dataset that can be interrogated by future researchers, the data in this paper provide further evidence that the profibrotic effects associated with M2 macrophages are more likely related to polarization cytokines than on other M2-secreted factors on lung structural cells, at least in these *in vitro* assays. While a limitation of this study is that it used polarized BMDMs rather than lung macrophages or moAMs which may have different transcriptomes and thus secretomes, our results support the concept that elevated IL-4 and IL-13 in lung fibrosis are critical features driving the phenotypes of macrophages, fibroblasts, and AECs. We also identify the fact that M2 macrophages secrete a protease or proteases that can give a false positive cleavage of the Caspase 3/7 Glo-substrate; thus future experiments should always test supernatant alone as a control in such experiments.

*Note: The contents of this chapter have already been published as a scientific journal article as:

Hult, E. M., Gurczynski, S. J. & Moore, B. B. M2 macrophages have unique transcriptomes but conditioned media does not promote profibrotic responses in lung fibroblasts or alveolar epithelial cells in vitro. *Am. J. Physiol. Lung Cell. Mol. Physiol.* **321**, L518–L532 (2021).

Chapter 3: Lyz2Cre-Mediated Deletion of HB-EGF in Myeloid and Lung Epithelial Cells Protects Against Lung Fibrosis

Abstract

Idiopathic pulmonary fibrosis (IPF) is a poorly understood, progressive, and often lethal lung disease with no known cure. In addition to alveolar epithelial cell (AEC) injury and excessive deposition of extracellular matrix proteins, chronic inflammation is a hallmark of IPF. There is evidence in the literature to support that the persistent inflammation seen in IPF primarily consists of monocytes and macrophages. Recent work demonstrates that monocyte-derived alveolar macrophages (moAMs) drive lung fibrosis, but further characterization of critical moAM cell attributes is necessary. Heparin-binding epidermal growth factor-like growth factor (HB-EGF) is an important EGFR (epidermal growth factor receptor) ligand that has essential roles in angiogenesis, wound healing, keratinocyte migration, and epithelial-mesenchymal transition. Past work in the lab has shown that HB-EGF is a primary marker of profibrotic M2 macrophages, and as such, we were interested to test its role as a major myeloid-derived profibrotic effector. This study seeks to characterize myeloid-derived HB-EGF and its primary mechanism of action in bleomycin-induced lung fibrosis using Hbegf$^{f/f}$;Lyz2Cre mice. Here, we show that IPF patients and fibrotic mice have increased expression of HB-EGF and that lung macrophages of fibrotic mice all express HB-EGF. We also show that Hbegf$^{f/f}$;Lyz2Cre mice are protected from bleomycin-induced fibrosis and that this protection is likely multifactorial, caused by genotypic differences in CCL2-dependent monocyte migration,

decreased fibroblast migration, and decreased contribution of HB-EGF from AEC sources when HB-EGF is removed under the Lyz2Cre promoter.

Introduction

The most common form of interstitial lung disease, idiopathic pulmonary fibrosis (IPF) is a progressive fibrotic lung disease with increasing incidence and high mortality[8,14,253]. Although the etiology of IPF remains incompletely understood, evidence in the field suggests that in IPF, perpetual injuries to the epithelium, resulting inflammation, accumulation of fibroblasts and increased deposition of extracellular matrix (ECM) proteins by activated myofibroblasts leads to stiffening of the lung, impaired gas exchange, and ultimately respiratory failure[10,13,85,254].

The dynamic role of innate immune cells in IPF pathogenesis has gained traction throughout the last ten years with evidence showing that both monocytes and macrophages are highly implicated in fibrosis[8,14,83,102,103,110,116]. Higher levels of circulating monocytes predict IPF disease progression[2,105,107] and in mice, depleting circulating monocytes (liposomal clodronate) or limiting their recruitment ($CCR2^{-/-}$ animals) to the lung results in ameliorated fibrosis[4,83,255]. It has been well-documented that inflammation triggers monocytes to travel to sites of injury and differentiate into inflammatory macrophages[256,257]. In the lung, bone marrow-derived monocytes recruited to the lung pass through an interstitial macrophage phenotype as they differentiate to monocyte-derived alveolar macrophages (moAMs)[6,7]. Recent work by Misharin et al. showed that genetic deletion of moAMs after their recruitment to the lung in mice results in protection from fibrosis[6]. Through the results of this work and others, moAMs are now considered to be the primary causal macrophage responsible for pulmonary fibrosis and there has been renewed energy to determine the role of moAMs in the lung and discover druggable targets against this cell type[7].

First isolated from macrophage supernatant and expressed by profibrotic M2-like macrophages[258,259], heparin-binding epidermal growth factor-like growth factor (HB-EGF) is one of four high-affinity binding ligands for epidermal growth factor receptor (EGFR)[149]. A critical molecular component in cell maintenance and repair, HB-EGF is also known for its role in wound healing: it is the predominant growth factor involved in epithelialization in skin wound healing, induces keratinocyte migration and invasiveness, and has essential roles in tissue healing, angiogenesis, proliferation, differentiation, and epithelial-mesenchymal transition[150,151,164,165,260].

However, the role of HB-EGF in pulmonary diseases is complex and data in the literature have attributed HB-EGF with both profibrotic and antifibrotic effects[145,151,164,208,261–263]. For example, evidence shows HB-EGF acting in a profibrotic manner in chronic obstructive pulmonary disease (COPD) patients: HB-EGF induces airway remodeling and epithelial mesenchymal transition (EMT) in human bronchial epithelial cells in COPD patients and its increased expression in sputum and lung tissue in COPD patients is positively correlated with disease severity[151,208]. Alternatively, HB-EGF acts in an antifibrotic manner in mouse models of pulmonary emphysema: HB-EGF promotes survival, increases body weight, attenuates lung injury, inflammatory cell, and cytokine infiltration, and prevents lung function decline[262].

No studies to date have examined the role of HB-EGF in IPF patients nor used the bleomycin mouse model to investigate HB-EGF as a primary focus. In this paper, we seek to understand the effects of HB-EGF in the lung using *ex vivo* techniques and conditional Hbegf$^{f/f}$;Lyz2Cre animals. Here, we show that expression of HB-EGF is increased in IPF patients and in fibrotic mice and that moAMs of fibrotic mice express HB-EGF. We also show that Hbegf$^{f/f}$;Lyz2Cre mice are protected from bleomycin-induced fibrosis and that this protection is

likely multifactorial, caused by genotypic differences in CCL2-dependent monocyte migration, decreased fibroblast migration, and decreased contribution of HB-EGF from epithelial cell (AEC) sources when HB-EGF is removed under the Lyz2Cre promoter.

Materials and Methods

IPF patient study

The data included in this paper are sub-analyses performed on data originally collected for the COMET clinical trial (clinicaltrials.gov, clinical trial ID no. NCT01071707). For detailed methods and full descriptions of the patient population, patient characteristics, sample preparation, and statistical analysis, please see reference ([264]).

In brief, the COMET study was an observational cohort study of well-defined IPF patients followed prospectively at 16-week intervals up to 80 weeks. Patients were diagnosed as having IPF based on characteristic computed tomography (CT) scans or usual interstitial pneumonia pathology confirmed by lung biopsy. Patients were allowed to stay on current treatments (and statistical analysis showed no differences between patients receiving treatments and those who did not; note this study was performed prior to FDA approval of current IPF medications). The combined endpoint was progression-free survival as determined by the time until any of the following: death, acute exacerbation of IPF, lung transplant, or relative decrease in forced vital capacity (FVC, liters) of ≥10% or DL_{CO} ($ml \cdot min^{-1} \cdot mmHg^{-1}$) of 15%. Sixty patients who had clinical follow up over the course of 80 weeks (518-645 days) were selected for plasma analysis for potential biomarkers. Peripheral blood was collected and plasma aliquots were sent to SomaLogics (Boulder, CO) for analysis on the SOMAscan panel (1129 analytes). SOMAmer analytes were reported in relative fluorescent units (RFU) and are directly proportional to the amount of protein in the original plasma sample. The ability of each of the

1129 continuous biomarkers to predict IPF progression status at 80 weeks was evaluated via ROC curves and a biomarker threshold was chosen to maximize the combined sensitivity plus specificity for each analyte[264]. For this report, sensitivity and specificity was determined for different thresholds of the measured biomarker, where high HB-EGF RFU values or high EGFR RFU values, respectively, were used to flag progression. The maximum sensitivity plus specificity of HB-EGF was achieved using a threshold of 810.2 RFU. Kaplan-Meier curves for groups above and below this threshold showed significantly worse progression for those below 810.2 RFU (logrank p=0.02, RMST p=0.03). The maximum sensitivity plus specificity of EGFR was achieved using a threshold of 34301.3 RFU. Kaplan-Meier curves for groups above and below this threshold showed significantly worse progression for those below 34301.3 RFU (logrank p=0.02, RMST p=0.02).

Animals and Housing

Six- to eight-week-old house-bred male and female Hbegf$^{f/f}$;Lyz2Cre mice (kindly provided by Dr. Howard Crawford, Henry Ford Health System, Detroit, MI[222,265]), were housed in specific pathogen-free conditions at the University of Michigan Animal Care Facility (Ann Arbor, MI). Male and female age-matched in-house bred Lyz2Cre^{+} (parent pair (B6.129P2-*Lyz2*$^{tm1(cre)Ifo}$/J strain: #004781) purchased from The Jackson Laboratory; Bar Harbor, ME) or in-house bred C57Bl/6J mice in some experiments were used as control animals and housed identically to the Hbegf$^{f/f}$;Lyz2Cre mice. All animal experiments were approved by the Institutional Animal Committee on Use and Care (IACUC) at the University of Michigan and were performed in accordance with the National Institutes of Health policies on the humane care and use of laboratory animals.

Bleomycin Administration

Mice were anesthetized with a mixture of ketamine and xylazine. Bleomycin (1U/kg) was administered to mice via oropharyngeal inoculation during which 50 µL of bleomycin (or saline control) was pipetted into the back of the throat while the tongue was pulled forward to allow the solution to be aspirated into the lungs. Mice were euthanized for downstream experiments on days 3, 7, or 21 post-administration via CO_2 asphyxiation.

Lung homogenate collection, bronchoalveolar lavage (BAL) and protein concentration assays

For lung homogenate studies, mouse lungs were perfused with PBS, then ancillary lobe removed and snap frozen in liquid nitrogen. The lobe was then homogenized in Trizol (ThermoFisher, Waltham, MA) for RNA extraction.

Bronchoalveolar lavage (BAL) fluid and BAL cells were collected as previously described[4]. In short, mouse tracheas were cannulated with tubing and were lavaged twice with 1ml of PBS/5 mM EDTA (Sigma-Aldrich, St. Louis, MO) for a total volume of 2 ml (recovery volume ~1.4-1.6 ml). To remove BAL cells, BAL fluid was spun at 1500 rpm and the supernatant was removed. Total protein content in BAL fluid was measured using a modification of the Bradford protein assay (Bio-Rad, Hercules, CA) according to the manufacturer's instructions. Concentration of CCL2 and albumin in the BAL fluid were measured via ELISAs according to the manufacturer's instructions (mouse CCL2/JE/MCP-1 DuoSet ELISA #DY479, R&D Systems, Minneapolis, MN; mouse Albumin ELISA (Kit #E99-134, Bethyl Laboratories, Inc., Montgomery, TX).

Total lung cell preparation, cell marker staining for flow cytometry, PrimeFlow staining, and tSNE analysis

Total lung cells were collected at days 3, 7, or 21 post-bleomycin administration as previously described[4]. Lungs were finely minced with scissors, then enzymatically digested at 37°C for 30 minutes in a solution containing Dulbecco's modified Eagle's medium (DMEM; Invitrogen Corp., Carlsbad, CA), 10% fetal calf serum (FCS), 1 mg/ml collagenase (Sigma), and 30 µg/mL DNAse. After incubation, the cell suspension was filtered through a 100 µM filter and centrifuged through a 20% Percoll (Sigma) gradient. Total lung cells were counted on a hemocytomer and cell viability was assessed by trypan blue exclusion.

After total lung cells were isolated, nonspecific Fc binding was blocked with a CD16/32 antibody (cat# 553142, BD Biosciences, San Jose, CA) while incubating on ice for 15 minutes, after which primary antibodies were added to cell samples for 30 minutes in the dark at 4ºC. For experiments requiring intracellular staining, cells were fixed and permeabilized in Fix/Perm buffer (eBioscience FoxP3/Transcription Factor Fixation/Permeabilization; Invitrogen, Carlsbad, CA) immediately after extracellular staining, then intracellular antibodies were added to the samples in the dark at room temperature for 30 minutes. After staining, cells were washed and fixed in 4% paraformaldehyde. Where applicable, fold change was calculated with normalized total cell numbers by setting the average of wild type and $Hbegf^{f/f}$;Lyz2Cre saline to one. Fold change samples were analyzed using an unpaired student t-test (2 group analysis). Total cell number were compared between samples using one-way ANOVA analysis with GraphPad Prism or Kruskal-Wallis test. The following antibodies were used: Zombie Violet (cat# 423113), Apotracker Green (cat# 427401), Ly6C-PE/Cy7 (cat# 128018), CD24-PerCP/Cy5.5 (cat# 101824), Ki67-PE (cat# 151209), CD11b-PE/Cy5 (cat# 101209), and CD64-PE (cat# 139303) from Biolegend (San Diego, CA), SiglecF-APC/Cy7 (cat# 565527), CD45-BV510 (cat# 563891), MHCII (I-A/I-E)-BV650 (cat# 563415), and Ly6G-APC (cat# 560599), from BD

Biosciences (San Diego, CA), and CD11c-PEefluor from Invitrogen (cat# 61-0114-82). See Figure 22 below for a representative flow gating scheme.

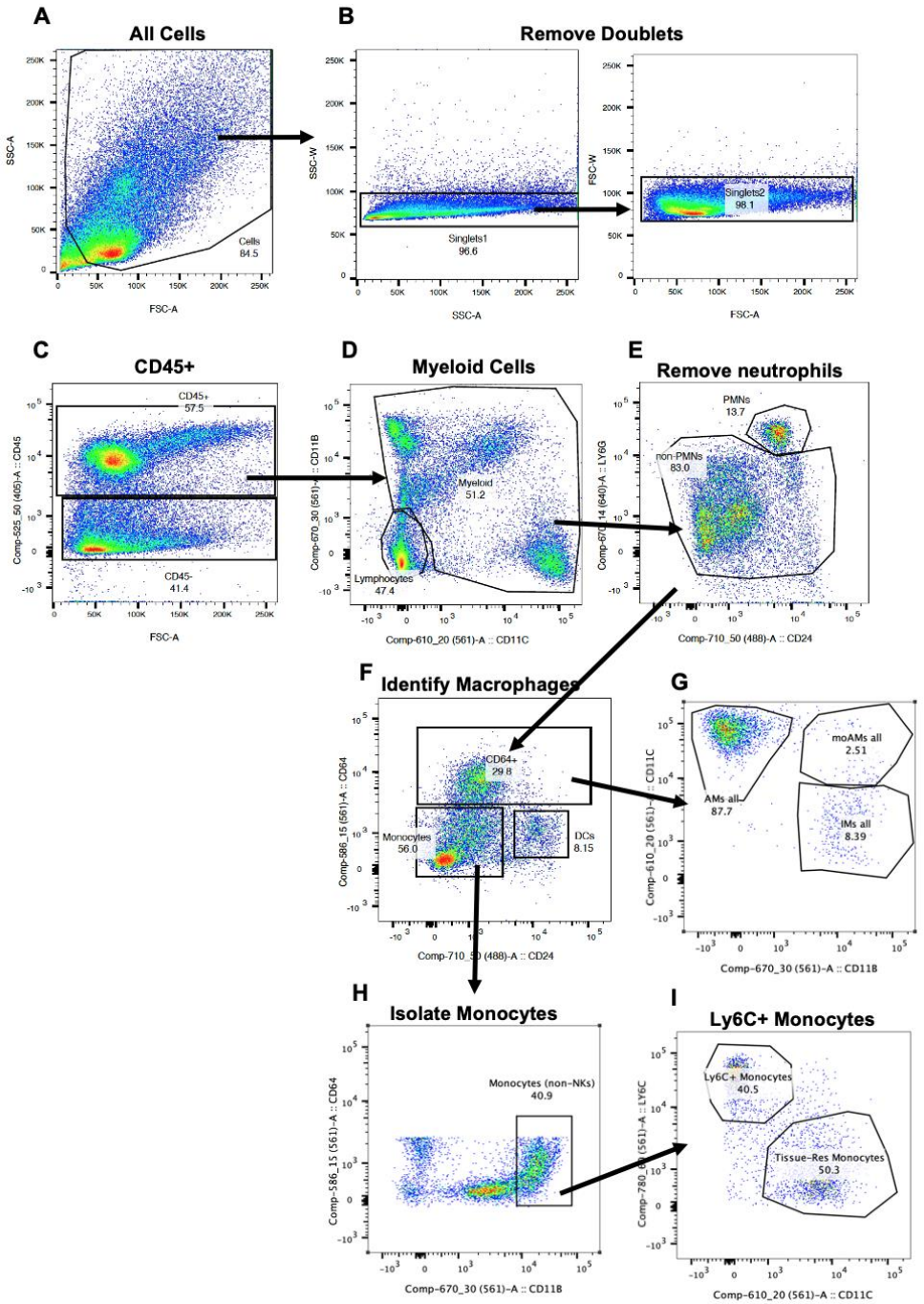

Figure 22: Representative flow gating of a d7 bleomycin-treated mouse. (A) all cells → (B) doublets removed → (C) $CD45^+$ cells → (D) myeloid cells ($CD11b^+CD11c^+$) → (E) removal of all $Ly6G^-$ cells (neutrophils) → (F) $CD64^+$ cells. From the $CD64^+$ cells, macrophage subsets can be identified (G): alveolar macrophages (AMs) ($CD11c^+CD11b^-SiglecF^{hi}$), monocyte-derived alveolar macrophages (moAMs) ($CD11c^+CD11b^+SiglecF^{int}$), and interstitial macrophages (IMs) ($CD11b^+CD11c^-SiglecF^{lo}$). Ly6C+ monocytes can also be identified ($CD64^{lo}CD11b^{hi}Ly6C^+$) (H, I). For PrimeFlow experiments, macrophages from (F) were gated to be HB-EGF^+ before looking at subsets (G).

For RNA PrimeFlow experiments, lung cells were isolated and stained with extracellular antibodies as described above. Downstream staining and procedures were done according to the manufacturer's instructions (https://www.thermofisher.com/us/en/home/life-science/cell-analysis/flow-cytometry/flow-cytometry-assays-reagents/rna-detection-flow-cytometry.html, ThermoFisher, Waltham, MA). The following PrimeFlow-specific intracellular probes were used: HB-EGF-AlexaFluor 647 (cat#VB1-15478-PF), ActB-AlexaFluor 750 (cat#VB6-12823-PF), and DapB-AlexaFluor 568 (cat#VF10-10409-PF). The following antibodies were used in PrimeFlow experiments: MHCII-BV421 (cat# 562564), CD45-BV510 (cat# 740140), SiglecF-BB515 (BD cat# 564514) from BD Biosciences and CD11c-PE/Dazzle (cat# 117348), CD11b-BV650 (cat# 101259), CD64-BV605 (cat# 139323), Ly6G-BV570 (cat# 127629), Ly6C-PE/Cy7 (cat# 128017), and Thy1.2-AF700 (cat# 105319) from Biolegend. All primeflow experiments were gated as described above ("flow gating scheme") through $CD64^+$ (all macrophages). Cells were then gated on HB-EGF and all $HB\text{-}EGF^+$ cells were labeled based on their CD11c, CD11b, and SiglecF expression (see Figure S1). *t*SNE was conducted in FlowJo v10.5 using a perplexity of 75.

Hydroxyproline Assays and Histology

Detailed descriptions of both hydroxyproline and histology assays can be found in ([4]). Briefly, for analysis of hydroxyproline content, lungs were perfused, and lung lobes removed. Lobes were homogenized in PBS and baked overnight with 12 N hydrochloric acid (HCl) at 110° C. Sample aliquots were assayed by subsequently adding a solution of chloramine T followed by Ehrlich's reagent prior to baking at 65°C for 15 min. Absorbance was measured at 550 nm, and the amount of hydroxyproline was determined against a standard curve composed of rat tail collagen (Sigma).

For histology, lungs were exsanguinated with PBS, then inflated with 1 ml of 10% neutral buffered formalin. The lungs were then removed and fixed overnight in formalin before being dehydrated in 70% ethanol. Lungs were processed using standard procedures and embedded in paraffin. Sections (3–5 μm) were cut, mounted on slides, and stained with H&E or Masson's trichrome blue for collagen deposition.

RT-qPCR

RNA for RT-qPCR experiments was obtained from isolated cells via Trizol (ThermoFisher) extraction following the manufacturer's protocol. The RNA concentration was normalized between samples to *GAPDH* or β-*actin* expression and qRT-PCR was performed on an ABI StepOnePlus real-time thermocycler (ThermoFisher) using a TaqMan® RNA-to-Ct™ 1-Step Kit (ThermoFisher) following the manufacturer's protocol. All primers and probes used in this study are listed in Table 1.

Table 2: Primers and Probes for Chapter 3

Gene	**Direction**	**Sequence**
GAPDH	Forward	5'-GGGCCACGCTAATCTCATTT-3'
	Reverse	5'-ATACGGCCAAATCCGTTCAC-3'
	Probe	5'-CTCCTCGAGCCTCGTCCCGT-3'
b-actin	Forward	5'-CCGTGAAAAGATGACCCAGATC-3'
	Reverse	5'-CACAGCCTGGATGGCTACGT-3'
	Probe	5'-TTTGAGACCTTCAACACCCCA-3'
Hbegf	Forward	5'-CGGTGATGCTGAAGCTCTTT-3'
	Reverse	5'-GCTGGTTTGTGGATCCAGTG-3'
	Probe	5'-ACGCGGACAACACTGCGGCC-3'
Collagen 1	Forward	5'-TGACTGGAAGAGCGGAGAGTACT-3'
	Reverse	5'-GGTCTGACCTGTCTCCATGTTG-3'
	Probe	5'-CTGCAACCTGGACGCCATCAAGG-3'
Collagen 3	Forward	5'-GGATCTGTCCTTTGCGATGAC-3'
	Reverse	5'-GCTGTGGGCATATTGCACAA-3'
	Probe	5'-TGCCCCAACCCAGAGATCCCATTT-3'

Fibronectin	Forward	5'-TCGAGCCCTGAGGATGGA-3'
	Reverse	5'-GTGCAAGGCAACCACACTGA-3'
	Probe	5'-CTGCAGGGCCTCAGGCCGG-3'
survivin	Forward	5'-GATCTGGCAGCTGTACCTCA-3'
	Reverse	5'-ATCAGGCTCGTTCTCGGTAG-3'
	Probe	5'-CTGGAGGACTGCGCCTGCAC-3'
XIAP	Forward	5'-ACCCTGCCATGTGTAGTGAA-3'
	Reverse	5'-TCTCTGGGGGTTAAATGAGC-3'
	Probe	5'-TGAAGTCATTTCAGAACTGGCCGG-3'
BCL2	Forward	5'-GGAGTGTGAGGACCCAATCT-3'
	Reverse	5'-CAACCACACCATCGATCTTC-3'
	Probe	5'-AGCCCCAGACCCCAACTCC-3'
Periostin	Forward	5'-GGGGTTGTCACTGTGAACTG-3'
	Reverse	5'-CGGCTGCTCTAAATGATGAA-3'
	Probe	5'-CGTGTCCTGACACAAATTGG-3'
VEGF	Forward	5'-CTTGCAGATGTGACAAGCCA-3'
	Reverse	5'-GAGAGGTCTGGTTCCCGAAA-3'
	Probe	5'-TGCAGCCTGGCTCACCGCCT-3'
CTGF	Forward	5'-GAGTGTGCACTGCCAAAGAT-3'
	Reverse	5'-GGCAAGTGCATTGGTATTTG-3'
	Probe	5'-CGCAGCGGTGAGTCCTTCCA-3'
PDGFa	Forward	5'-CGAAGTCAGATCCACAGCAT-3'
	Reverse	5'-GGGCTCTCAGACTTGTCTCC-3'
	Probe	5'-CCGGGACCTCCAGCGACTCT-3'
Cox2	Forward	5'-TGACCCCAAGGCTCAAAT-3'
	Reverse	5'-GAACCCAGGTCCTCGCTTATG-3'
	Probe	5'-TTTGCCCAGCACTTCACCCATCAG-3'
PGE synthase	Forward	5'-AACCTGGGCGAGTGGATCT-3'
	Reverse	5'-CTGTAAGTGGCTCCAAATGGG-3'
	Probe	5'-ACATGTGTGTTTCTTAGCCTTTTG-3'
CCL2	Forward	5'-GGCTCAGCCAGATGCAGTTAAC-3'
	Reverse	5'-CCTACTCATTGGGATCATCTTGCT-3'
	Probe	5'-CCCCACTCACCTGCTGCTACTCAT-3'
EGF	Forward	5'-CAACACTGAAGGTGGCTACG-3'
	Reverse	5'-GTGCGGTAGAGTCGAAACAG-3'
	Probe	5'-CCCGTCTCCTTCGTAGCCTTCTGAGC-3'
TGFa	Forward	5'-CTGAAGGGAAGGACTGCTTG-3'
	Reverse	5'-CCTGGCCAAATTCCTCCTCT-3'
	Probe	5'-CTGCCACTCTGAGACAGTGGTCTGA-3'

AREG	Forward	5'-GCGAGGATGACAAGGACCTA-3'
	Reverse	5'-TCGTTTCCAAAGGTGCACTG-3'
	Probe	5'-CCTCGCAGCTATTGGCATCGGCA-3'
EREG	Forward	5'-GTGCATCTACCTGGTGGACA-3'
	Reverse	5'-GAAGTGCTCACATCGCAGAC-3'
	Probe	5'-CAGTGTAGCCCACTTCACATCTGCAGA-3'
EPGN	Forward	5'-AGCAGTCTGCCTCTTGTTCA-3'
	Reverse	5'-TGTAGTCAGCTTCGGTGTTG-3'
	Probe	5'-TGCTTCTTCGCTCAGTGCTGCC-3'
BTC	Forward	5'-GCCCTGGGTCTTGCAATTCT-3'
	Reverse	5'-AGCTCCACAAAGAGAGCCAT-3'
	Probe	5'-TGTTCCCATCTGCTACCACACAGTGG-3'

Isolation of blood cells for flow cytometry

Blood was collected immediately after euthanasia with a 26G needle via cardiac puncture in the left ventricle and 3 µl of 0.5M EDTA was added to per 100 µl blood to prevent coagulation. Blood was then incubated with warmed red blood cell (RBC) lysis buffer for 5 minutes at room temperature, neutralized with warmed PBS, spun down and supernatant removed (process repeated twice) to remove RBCs. Cells were then counted on a hemocytometer in the presence of trypan blue, and aliquoted for flow staining.

Bone Marrow Transplantation (BMT)

BMT was performed as described previously[266,267]. In short, recipient mice were lethally irradiated with a total of 13 Gy (delivered in two 6.5 Gy doses spaced 3 hours apart) using a ^{137}Cesium irradiator. Whole bone marrow cells were isolated from donor mice injected into the tail vein of recipient mice at a concentration of 5 x10^6 cells/200 µl serum-free DMEM. After transplantation, mice were given acidified water (pH 3.3) for 3 weeks to limit infection during the immunosuppression period and switched to normal water for 2 more weeks. At the end of

this 5-week period, total numbers of hematopoietic cells in the lung are considered fully reconstituted,[268] and mice were treated with bleomycin as detailed above.

Type II alveolar epithelial cell isolation and apoptosis assay

Type II alveolar epithelial cells (AECs) were isolated using a whole lung dispase digestion after casting airways in low melt agarose as previously described[216]. In short, mouse tracheas were cannulated and filled with ~1.5 ml dispase (BD Biosciences) followed by ~1.5ml of 1% low-melting-point-agarose (ThermoFisher) to full inflation and promptly placed in cold PBS to solidify the agarose. After further digestion in dispase, lung lobes were minced in DMEM with 0.01% DNase and passed through 100-, 37-, and 25-um nylon mesh filters. Bone marrow-derived cells were removed by magnetic depletion using anti-CD32 and anti-CD45 antibodies (BD Pharmingen) and mesenchymal cells were removed by overnight adherence in a petri dish. Nonadherent AECs were then plated at 500,000 cells/well on 24-well plates coated with fibronectin (10µg/ml, cat# F2006, Sigma-Aldrich) for RNA extraction or at 50,000 cells/well on opaque 96-well plates for apoptosis assays. AEC apoptosis assays were performed as described previously[259]. Upon completion of the assay, CaspaseGlo3/7 (Roche, Indianapolis, IN) was added in a 1:1 dilution and activation of caspase-3/7 was measured according to the manufacturer's guidelines. Samples were analyzed using an M3 Microplate Luminometer and the value expressed in relative luminescence units compared with control AECs maintained in SFM alone.

Fibroblast isolation, proliferation, and migration assays

To isolate fibroblasts, lungs were perfused with sterile PBS, and lobes were extracted and minced with scissors. The lung mince was placed in a T175 tissue culture flask with ~30ml DMEM+10% FBS and cells were allowed to "grow out" of the lung mince for 14 days.

Fibroblast proliferation assays were completed as described previously[259]. In short, fibroblasts were plated at 10,000 cells/well in a 96-well plate in complete DMEM for 4hrs, followed by overnight treatment in SFM. 90 µl of rHB-EGF (25ng/ml, 50ng/ml; Sigma-Aldrich, cat# SRP6050) was placed on each well for 48 hours, followed by 10 µl of MTT solution that was allowed to incorporate for another 24 hours. Upon completion, the plate was read according to manufacturer's instruction (Sigma-Aldrich).

To investigate fibroblast migration using a scratch wound assay, fibroblasts were plated at 20,000 cells/well in clear bottomed 96-well plates (Essen Biosciences #4378, Ann Arbor, MI) overnight in DMEM+10% FBS. After fibroblast adherence, complete media was washed away and replaced with SFM overnight. The next day, a uniform wound gap in each well was created using the WoundMaker and starting media was replaced with SFM containing rHB-EGF (0ng/ml-100ng/ml). The plate was then placed into IncuCyte (Sartorius, Bohemia, NY) to acquire data and images every 4 hours for ~72 hours. Quantification was done using the Analysis module in the IncuCyte software.

Statistics

The GraphPad Prism software package (GraphPad Software, La Jolla, CA) was used for all murine studies' statistical analyses. All data were first put through outlier and normality tests. If normally distributed, differences between experimental groups were determined using one-way

ANOVA with a Tukey post-test (for comparing 3 or more groups) or an unpaired t-test (for comparing 2 groups). If non-normally distributed, data was analyzed by Kruskal-Wallis test and Dunn's multiple comparison post-test (for 3 or more groups). Differences were considered statistically significant when $p < 0.05$. All data are represented as mean +/- SEM. All experiments were repeated, at least, in duplicate with similar results unless noted in individual figure legend. Pertinent statistical information, i.e., n-values and p-values, are given in individual figure legends.

Results

Increased levels of HB-EGF are associated with increased IPF disease progression and fibrosis in mice

As HB-EGF has been shown to have both profibrotic and antifibrotic functions in different pulmonary diseases, we decided to begin our study by looking at the relative abundance of HB-EGF in IPF patients and in mouse models of fibrosis. The natural course of IPF can vary significantly between patients, and previous work has been done to identify relevant biomarkers of disease progression in IPF using unbiased proteomics. A study by Ashley et al. collected blood plasma from IPF patients enrolled in an observational trial (clinicaltrials.gov, COMET clinical trial ID no. NCT01071707) and used a slow off-rate modified aptamer (SOMAmer) array to determine an analyte index that could be used in clinical decision making in IPF[264]. Using this dataset, we examined the relative abundance of HB-EGF and its primary receptor, EGFR, in blood plasma of "slow-progressing" and "fast-progressing" cohorts of IPF patients. To do this analysis, a threshold for each biomarker was chosen to maximize sensitivity and specificity.

Interestingly, we noted that IPF individuals who have levels of EGFR and HB-EGF in plasma that are above the identified threshold have higher incidence of disease progression as defined by any of the following: acute exacerbations, a decline of 15% in diffusion capacity of the lung for carbon monoxide (DL_{CO}), or a 10% decline in forced vital capacity (FVC) (Figure 23A, 23B). Specifically, higher EGFR expression is correlated with more likely IPF progression (Logrank test, p= 0.02; RMST, p=0.03) and patients with above-threshold HB-EGF expression is also correlated with IPF disease progression (Logrank test, p= 0.02; RMST, p=0.02). These data highlight that IPF disease progression is associated with elevated expression of HB-EGF and its primary receptor.

To further investigate the role of HB-EGF in pulmonary fibrosis, we used the bleomycin mouse model. *HB-EGF* transcript was significantly upregulated 21 days post-bleomycin treatment in whole lung (Figure 23C) as well as in the bronchoalveolar lavage (BAL) cells (Figure 23D), a primarily macrophage population. Thus, increased levels of HB-EGF are also present in a bleomycin mouse model of experimental lung fibrosis. The data also suggest that HB-EGF produced by macrophages may be of particular importance in lung fibrosis.

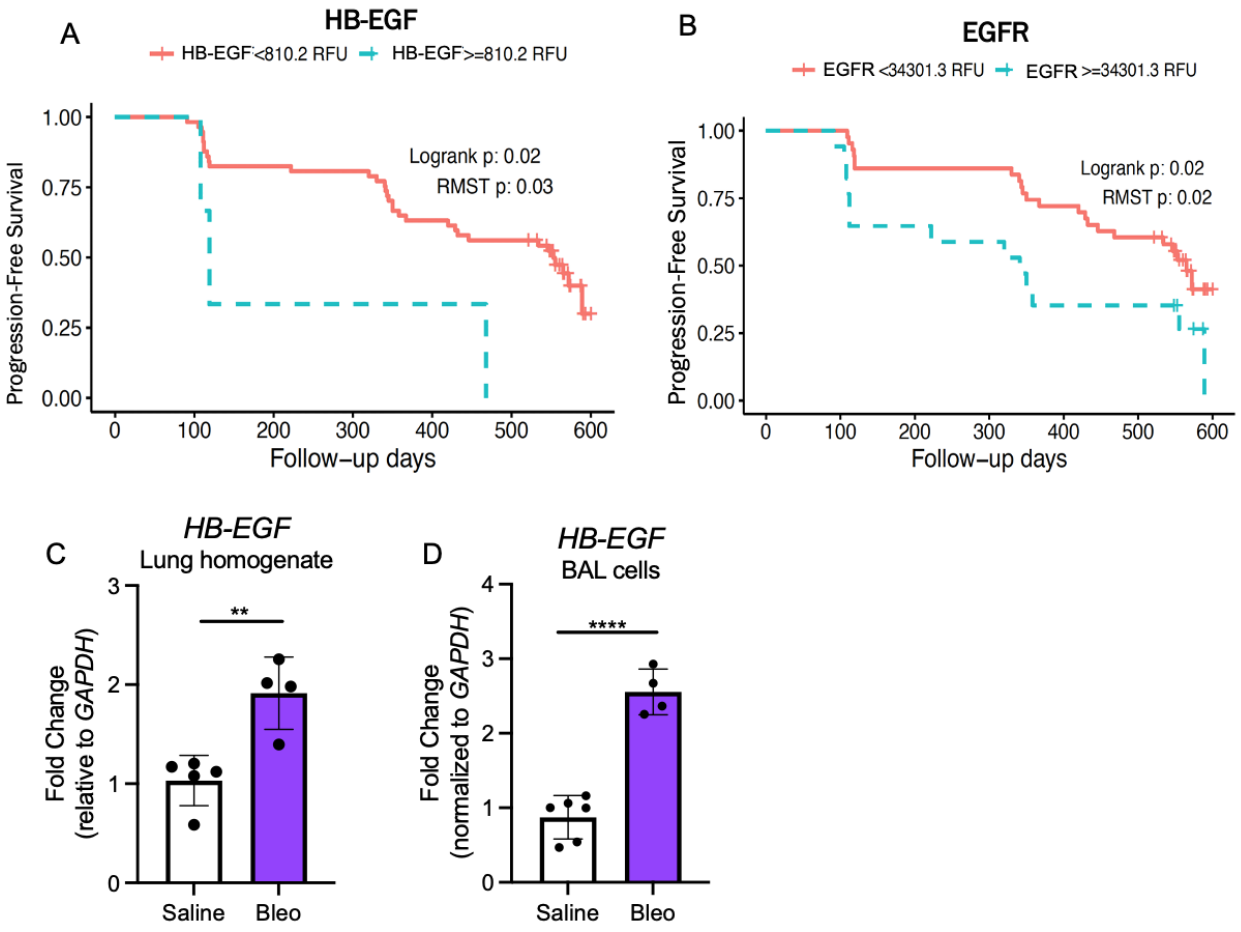

Figure 23: Increased levels of HB-EGF are associated with increased risk of IPF disease progression in humans and fibrosis in mice. IPF patients with faster disease progression have higher levels of (A) HB-EGF and (B) its receptor, EGFR, in their bloodstream and worsened survival compared to IPF patients with slower disease progression. Sensitivity and specificity was determined for different thresholds of the measured biomarker, where high HB-EGF RFU values or high EGFR RFU values, respectively, were used to flag progression. The maximum sensitivity plus specificity of HB-EGF was achieved using a threshold of 810.2 RFU. Kaplan-Meier curves for groups above and below this threshold showed significantly worse progression for those below 810.2 RFU (logrank p=0.02, RMST p=0.03). The maximum sensitivity plus specificity of EGFR was achieved using a threshold of 34301.3 RFU. Kaplan-Meier curves for groups above and below this threshold showed significantly worse progression for those below 34301.3 RFU (logrank p=0.02, RMST p=0.02). Orange lines indicate patients below threshold and blue lines indicate patients above the threshold for faster-progressing disease. Wild type mice treated with bleomycin-treated (bleo) mice have increased levels of HB-EGF mRNA expression in the lung homogenate (C) and in bronchoalveolar lavage (BAL) cells compared to saline-treated mice. Representative RT-qPCR data in C (2 experiments, n=4-6) and D (1 experiment, n=4-6). **: p<0.01, ****: p<0.0001.

Monocyte-derived alveolar macrophages (moAMs) express HB-EGF

The importance of the innate immune system in the development and progression of IPF and experimental lung fibrosis has been well-documented[8,83,102,103,110]. Recently, work by Misharin et al. showed that monocyte-derived alveolar macrophages (moAMs) are the prominent

and causal cell type responsible for driving lung fibrosis in mice[6]. Given the increased expression of HB-EGF in BAL cells after bleomycin treatment (Figure 23D), we wondered which type(s) of macrophages expressed HB-EGF. To do this, we turned to a form of flow cytometry.

Although antibodies for human HB-EGF are plentiful, there are no validated antibodies available to murine HB-EGF. Consequently, we decided to use RNA PrimeFlow (ThermoFisher), a technique that allows fluorophores to be conjugated to RNA transcripts rather than proteins, to measure HB-EGF mRNA expression in our samples. A benefit of RNA PrimeFlow is that it can be used alongside standard fluorophore-protein conjugates; thus, we used our standard myeloid flow antibody panel to identify lung macrophage populations and concurrently used specific RNA primer-probes to analyze HB-EGF, positive control β-actin (ActB), and negative bacterial control diaminopimelate-B (DapB) mRNA expression on day 21 post-saline or bleomycin instillation.

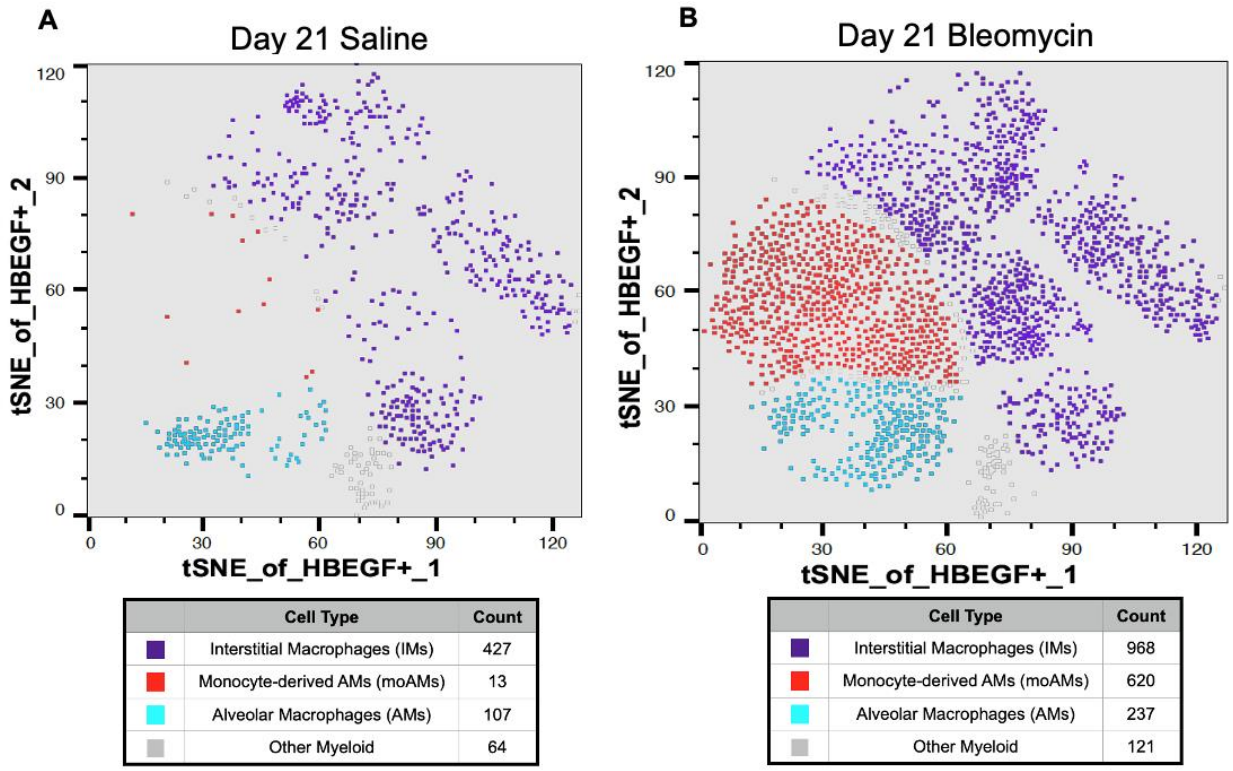

Figure 24: Monocyte-derived alveolar macrophages (moAMs) express HB-EGF. PrimeFlow RNA assays show the presence of HB-EGF^{+} alveolar macrophages (AMs) (CD11c^{+}SiglecF^{hi}), HB-EGF^{+} moAMs (CD11c^{+}CD11b^{+}SiglecF^{int}), and HB-EGF^{+} interstitial macrophages (IMs) (CD11b^{+}SiglecF^{lo}) in C57Bl/6J mice in control animals (A). Oral-pharyngeal administration of bleomycin induces an expansion of HB-EGF^{+} moAMs and interstitial macrophages (IMs) after 21 days (B) compared to mice treated with a saline control (A) in C57Bl/6J mice. tSNE data is representative of one experiment with three mice per group. All data representative of 3 experiments, n= 3.

As expected, lungs of both C57Bl/6J saline and bleomycin-treated animals contained alveolar macrophages (AMs, CD64^{+}CD11c^{+}SiglecF^{hi}), interstitial macrophages (IMs, CD64^{+}CD11b^{+}SiglecF^{lo}), and moAMs (CD64^{+}CD11c^{+}CD11b^{+}SiglecF^{int}) (Figure 24A, 24B). The total number of moAMs was much higher in bleomycin-treated mice, as has been demonstrated in other studies[6,7]. Interestingly, all three macrophage populations expressed HB-EGF at baseline in saline-treated mice, indicating that HB-EGF may be important in macrophage homeostasis. HB-EGF is also expressed in AMs, moAMs, and IMs 21 days post-bleomycin treatment. Given the vast influx of HB-EGF expressing moAMs to the fibrotic lung, it seems plausible that myeloid-derived HB-EGF may help promote lung fibrosis.

Hbegf$^{f/f}$;Lyz2Cre mice are protected from bleomycin-induced fibrosis despite similar levels of acute lung injury

As our data have shown that levels of HB-EGF increase in the fibrotic mouse lung (Figure 23C, 23D) and that HB-EGF is expressed by lung macrophages including moAMs after bleomycin (Figure 24B), we next wanted to look at the role of macrophage-specific HB-EGF in the context of fibrosis in Hbegf$^{f/f}$;Lyz2Cre mice[222,265]. This mouse has HB-EGF genetically removed through a Cre-lox system under the Lyz2 promoter and thus HB-EGF should be removed from all cells within the myeloid compartment including monocytes, macrophages, dendritic cells, and neutrophils.

Interestingly, Hbegf$^{f/f}$;Lyz2Cre mice were protected from bleomycin-induced fibrosis when compared to Lyz2Cre^{+} control mice. At day 21 post-treatment, Hbegf$^{f/f}$;Lyz2Cre mice showed significantly decreased amounts of hydroxyproline, a surrogate measure for collagen (Figure 25A), as well as decreased expression of profibrotic genes *collagen 1, collagen 3,* and *fibronectin* (Figure 25B). The Hbegf$^{f/f}$;Lyz2Cre mice also showed improved histology with less immune cell infiltration, less interstitial thickening, and less collagen deposition compared to Lyz2Cre^{+} control animals (Figure 25C).

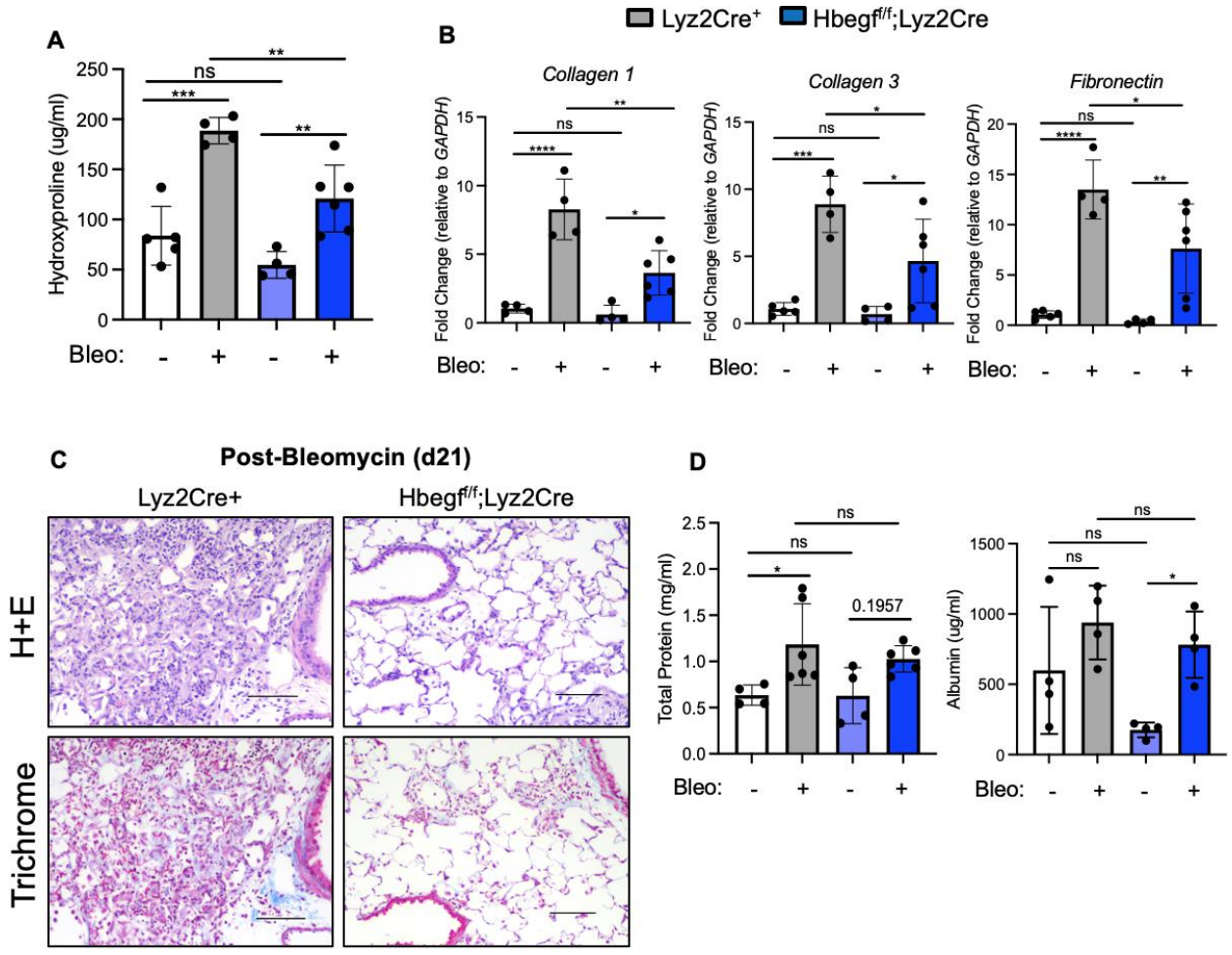

Figure 25: Hbegf$^{f/f}$;Lyz2Cre mice are protected from bleomycin-induced fibrosis despite similar levels of acute lung injury. Hbegf$^{f/f}$;Lyz2Cre mice have lower levels of hydroxyproline (A), decreased (B) expression of profibrotic genes (B) Collagen 1, Collagen 3, and Fibronectin, and improved lung histology (C) 21 days post-bleomycin treatment compared to Lyz2Cre^{+} control mice. Additionally, levels of total protein and albumin detected in the BAL fluid (BALF) is not different between Lyz2Cre^{+} and Hbegf$^{f/f}$;Lyz2Cre mice (D) three days post-bleomycin treatment, suggesting initial lung injury between genotypes is the same. n.s.: not significant, *: p<0.05, **: p<0.01, ***: p<0.001, ****: p<0.0001. Lines in (C) are 100 μm length. All data representative of 2-4 experiments, n=4-6.

Although the Hbegf$^{f/f}$;Lyz2Cre mice had decreased levels of key fibrosis markers at day 21, it is possible that these differences result from reduced lung injury rather than ameliorated fibrosis development/progression. To assess initial lung injury, we performed bronchoalveolar lavage (BAL) on mice at day 3 post-bleomycin and analyzed the BAL fluid (BALF) for total protein content. Our data showed that Hbegf$^{f/f}$;Lyz2Cre mice showed no difference in total protein (BCA assay) nor in albumin concentration, indicative of vascular leak, compared to

Lyz2Cre^{+} control animals (Figure 25D). Together, these data suggest that the protection from development of lung fibrosis in Hbegf$^{f/f}$;Lyz2Cre mice cannot be explained by reduced lung injury.

Hbegf$^{f/f}$;Lyz2Cre mice have decreased macrophage numbers during fibrosis initiation

To determine the mechanism of protection in the Hbegf$^{f/f}$;Lyz2Cre mice from fibrosis, we began by looking at overall levels of inflammation in these mice. As macrophages are particularly critical in fibrosis development and the Lyz2Cre promoter targets both monocytes and macrophages, we hypothesized that Hbegf$^{f/f}$;Lyz2Cre mice could be protected due to a reduction in lung macrophages or reduced inflammation.

In the bleomycin mouse model, peak inflammation and injury occurs on day 7 after bleomycin treatment. While flow analysis of day 7 lung cells showed no difference in total number of AMs after bleomycin, both moAMs and IMs had decreased numbers (Figure 26A) and decreased relative fold change between saline and bleomycin conditions by genotype (Figure 27A). As moAMs are thought to promote fibrosis, and infiltrating monocytes differentiate into moAMs via an IM-like phenotype, it is likely that a reduction in total numbers of moAMs contributes to protection of Hbegf$^{f/f}$;Lyz2Cre mice post-bleomycin.

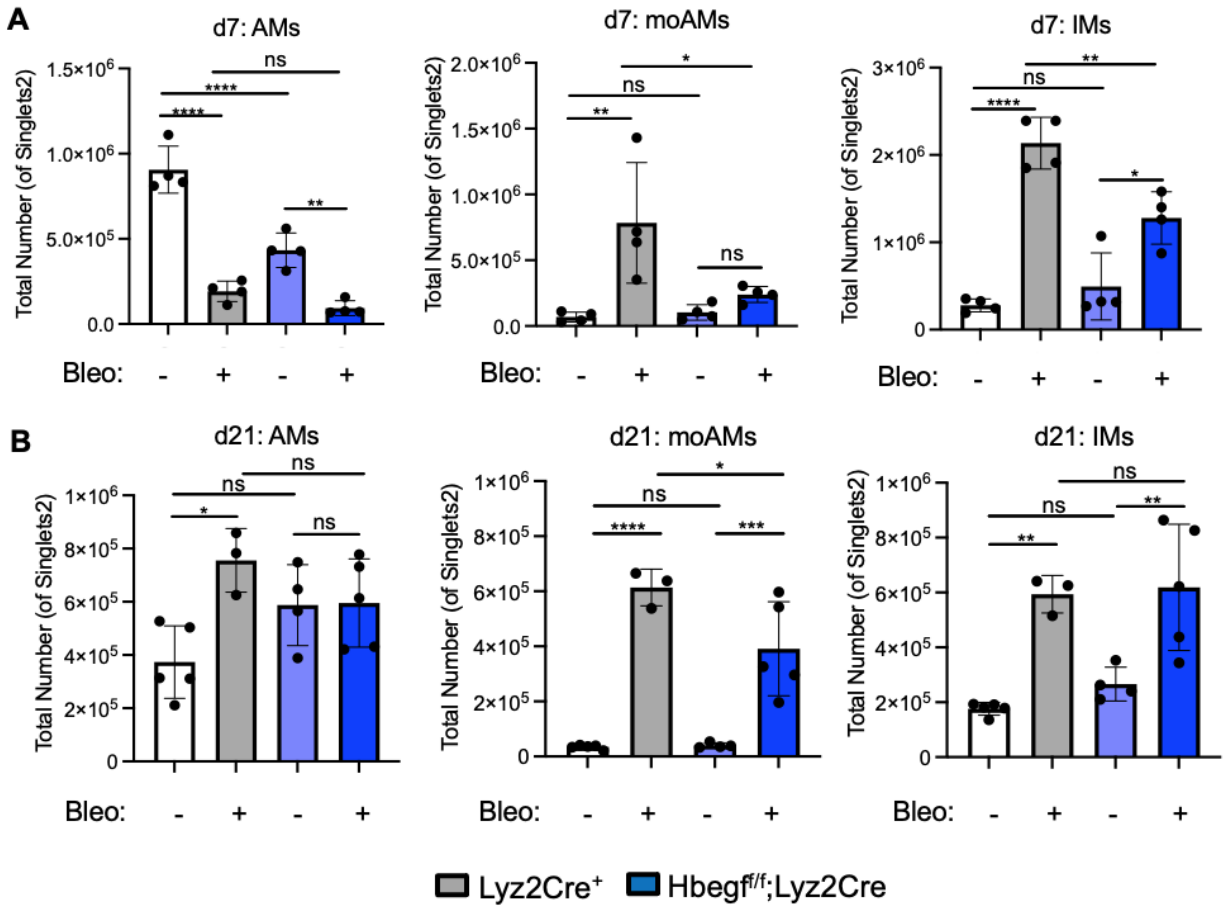

Figure 26: Hbegf$^{f/f}$;Lyz2Cre mice have decreased macrophage numbers during fibrosis initiation. (A) Hbegf$^{f/f}$;Lyz2Cre number at day 7 post-bleomycin. (B) Hbegf$^{f/f}$;Lyz2Cre mice also have lower levels of moAMs 21 days post-bleomycin treatment by total cell number. n.s.: not significant, *: p<0.05, **: p<0.01, ***: p<0.001, ****: p<0.0001. All data representative of 3-5 experiments, n=4-6.

At day 21, AMs and IMs were not statistically different after bleomycin between Hbegf$^{f/f}$;Lyz2Cre mice and Lyz2Cre^{+} controls, a change from day 7 patterns (Figure 26B**,** Figure 27B). MoAMs remained lower in Hbegf$^{f/f}$;Lyz2Cre mice compared to Lyz2Cre^{+} mice controls at days 7 and 21 by total number (Figure 26B) and by relative fold change (Figure 27B). These results suggest fewer moAMs are present during peak inflammation (day 7) in Hbegf$^{f/f}$;Lyz2Cre mice and that this difference persists during the fibroproliferative stage.

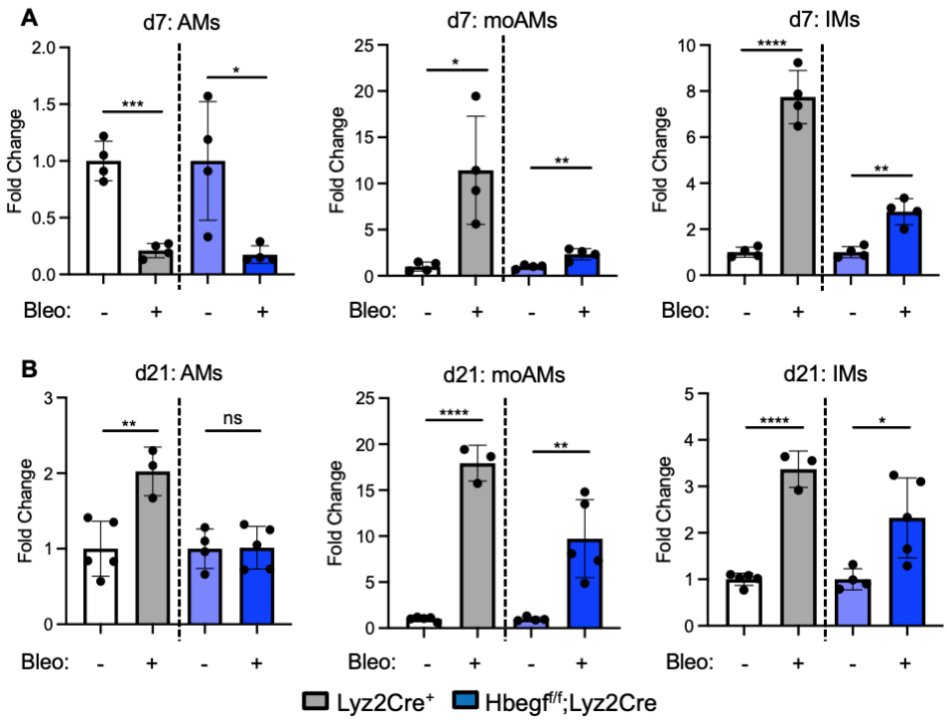

Figure 27: Hbegf$^{f/f}$;Lyz2Cre mice also show decreased macrophage numbers during fibrosis initiation by fold change. (A) Hbegf$^{f/f}$;Lyz2Cre mice have lower levels of moAMs and IMs 7 days post-bleomycin treatment as determined by relative fold change (B) Hbegf$^{f/f}$;Lyz2Cre mice also have lower levels of moAMs 21 days post-bleomycin treatment by relative fold change. Data in Figure 27A correspond to data in Figure 26A; data in Figure 27B correspond to data in Figure 26B. t-tests performed comparing treatments within a single genotype. n.s.: not significant, *: p<0.05, **: p<0.01, ***: p<0.001, ****: p<0.0001. All data representative of 3-5 experiments, n=4-6.

Protection in Hbegf$^{f/f}$;Lyz2Cre mice correlates with impaired macrophage migration and decreased CCL2 expression

Next, we wanted to determine why Hbegf$^{f/f}$;Lyz2Cre mice have fewer moAMs at day 7 during fibrosis development. Decreased numbers of moAMs could be the result of several phenomena: decreased moAM proliferation, increased moAM apoptosis, decreased moAM migration, or a combination of these. The relative changes in Ki67 staining for AMs, IMs, moAMs, or Ly6C^{+} monocytes at day 7 was similar between Lyz2Cre^{+} and Hbegf$^{f/f}$;Lyz2Cre animals (Figure 28A, 28B), likely ruling out proliferative defects. Similarly, there were no statistical differences between Hbegf$^{f/f}$;Lyz2Cre and control mice in total numbers of dead

moAMs or moAMs in early or late apoptosis (Figure 28C) ruling out increased apoptosis of these cells in Hbegf$^{f/f}$;Lyz2Cre mice.

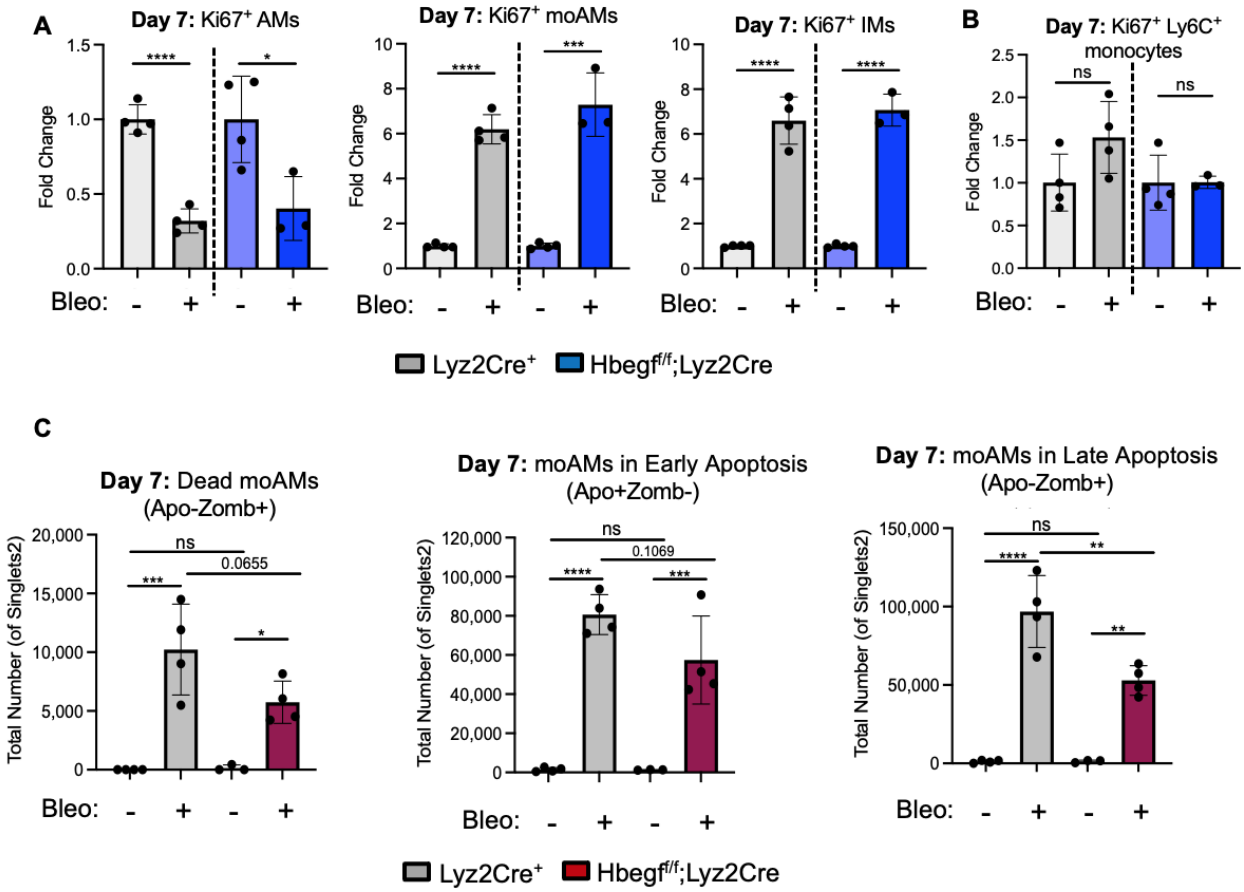

Figure 28: Protection of Hbegf$^{f/f}$;Lyz2Cre mice from bleomycin-induced fibrosis is not caused by decreased proliferation in moAMs (A) or Ly6C+ monocytes (B) or increased moAM apoptosis (C). Data in panels (A-B) representative of two experiments (n=3-4) using t-tests to compare treatments within a single genotype, data in panel (C) shows a single experiment (n=3-4) using ANOVA comparisons. n.s.: not significant, *: p<0.05, **: p<0.01, ***: p<0.001, ****: p<0.0001.

As moAMs arise from inflammatory (Ly6C$^+$) monocytes, we tested our migration hypothesis by measuring the total number of monocytes in the lung of wild type and Hbegf$^{f/f}$;Lyz2Cre mice. We found that Hbegf$^{f/f}$;Lyz2Cre mice have fewer Ly6C$^+$ monocytes at day 7 compared to controls (p=0.054; Figure 29A), but that there are no differences in Ly6C$^+$ monocytes in blood (Figure 29B). These data indicate that there are no differences in hematopoietic cell production or in ability to differentiate into monocytes at baseline in the Hbegf$^{f/f}$;Lyz2Cre mice. Additionally, the data imply that monocytes in Hbegf$^{f/f}$;Lyz2Cre mice

can circulate in the blood with the same efficiency as they do in wild type animals and thus, that the difference between total Ly6C$^+$ monocyte numbers seen in Figure 29A is based on recruitment to the lung.

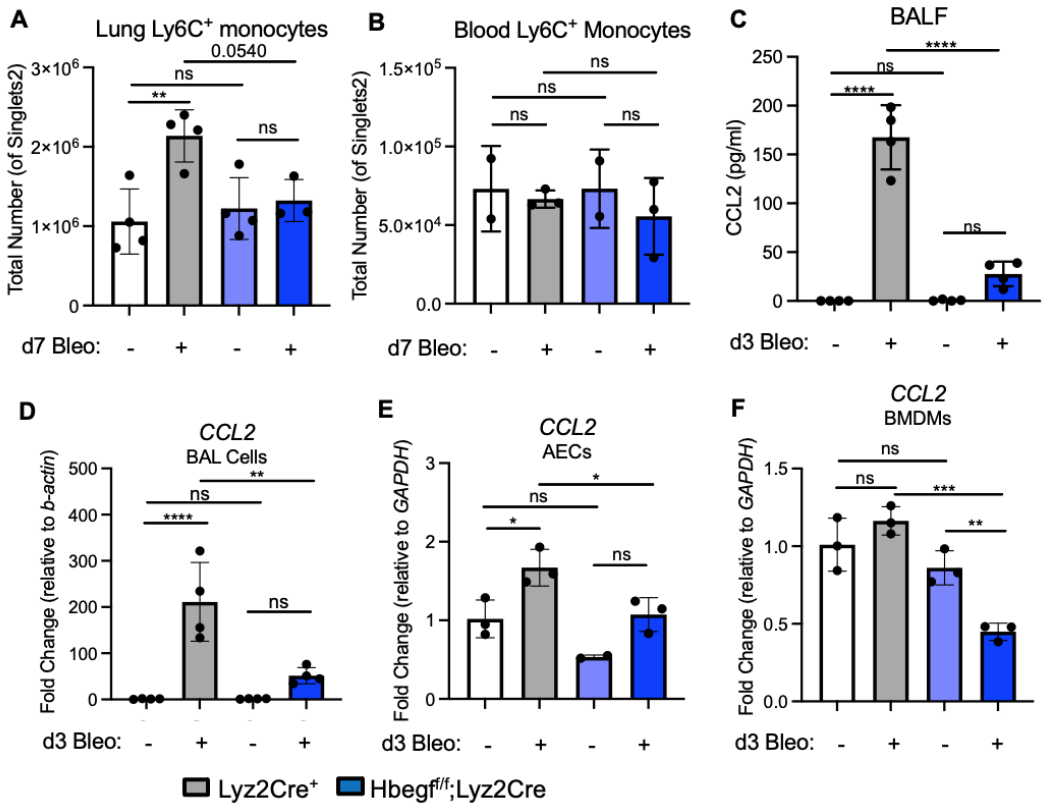

Figure 29: Protection in Hbegf$^{f/f}$;Lyz2Cre mice correlates with impaired macrophage migration and decreased CCL2 expression. Hbegf$^{f/f}$;Lyz2Cre mice have decreased numbers of Ly6C$^+$ monocytes in the lungs compared to wild type mice 7 days post-bleomycin treatment (A), but no difference in total Ly6C$^+$ monocytes in the blood at the same time point (B). Hbegf$^{f/f}$;Lyz2Cre mice have lower levels of CCL2 in their BALF (C), in BAL cells (D), in AECs (E), and in BMDMs (F) 3 days post-bleomycin compared to Lyz2Cre$^+$ controls. n.s.: not significant, *: p<0.05, **: p<0.01, ***: p<0.001, ****: p<0.0001. Data in (A), (C), (D), and (E) are representative data from 2-3 experiments with n=2-5, and data in (B) and (F) are representative of 1 experiment, n=2-3.

To determine which chemokine(s) could be responsible for decreased monocyte recruitment, we performed a multi-gene qPCR array and re-examined hits with a fold change greater than 2 (data not shown). A top hit was CCL2 (C-C Motif Chemokine Ligand 2), also known as MCP-1 or JE in the mouse. A potent chemokine known for its ability to chemoattract monocytes as well as a variety of other immune cells, elevated levels of CCL2 have also been linked to ARDS, COPD, and animal models of fibrosis and human IPF[4,269–271].

To investigate the role of CCL2, we took BAL fluid from Lyz2Cre^{+} control and Hbegf$^{f/f}$;Lyz2Cre mice 3 days after bleomycin treatment. ELISA data showed that while CCL2 is greatly increased after bleomycin in control mice, levels of CCL2 are greatly diminished in Hbegf$^{f/f}$;Lyz2Cre mice (Figure 29C). Additionally, CCL2 mRNA expression is dramatically decreased in the BAL cells (Figure 29D), in AECs (Figure 29E), and in BMDMs (Figure 29F) of Hbegf$^{f/f}$;Lyz2Cre mice 3 days post-bleomycin treatment. Given the differences in CCL2 production between genotypes, we wanted to see if the addition of recombinant mouse (r)HB-EGF could stimulate lung cells to produce CCL2 directly. We did not see any induction of CCL2 mRNA expression in AECs, BMDMs, or fibroblasts treated with rHB-EGF over a 24-hour period (Figure 30), nor an increase in CCL2 mRNA expression in AECs treated with rHB-EGF after removal from a day 3 bleomycin-treated mouse (Figure 30). Together, these data suggest that HB-EGF alone cannot prime CCL2 expression in these cell types and that bleomycin injury may not be enough to prime CCL2 expression even with HB-EGF addition.

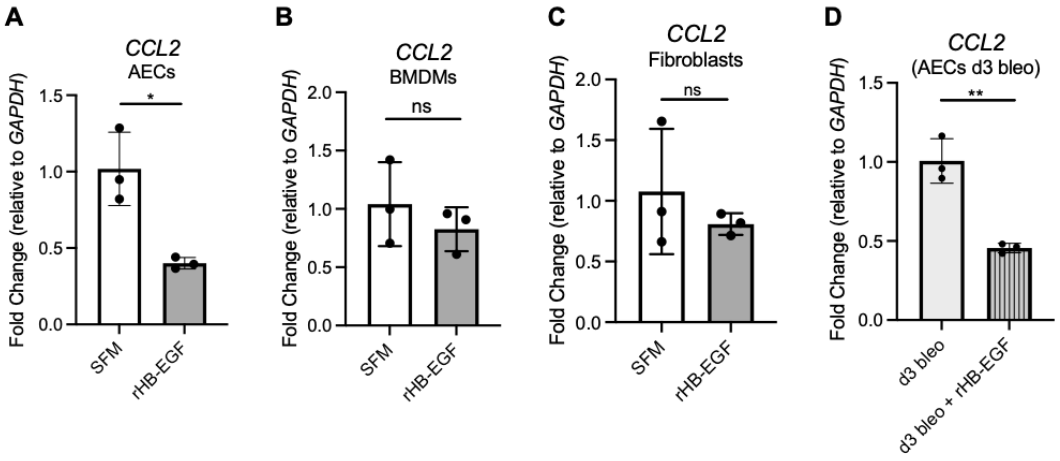

Figure 30: rHB-EGF (50ng/ml) treatment for 24hrs on AECs (A), BMDMs (B), or primary lung fibroblasts (C) does not cause an increase in CCL2 expression as measured by qPCR. Additionally, the combination of bleomycin (day 3) treatment followed by rHB-EGF (50ng/ml) administration (24hr) does not increase CCL2 expression (D). n.s.: not significant, *: $p<0.05$, **: $p<0.01$, ***: $p<0.001$, ****: $p<0.0001$.

Lyz2Cre deletes HB-EGF in AECs which may also contribute to protection from fibrosis

While the Lyz2Cre mouse was originally designed to target macrophages and granulocytes[272], multiple studies have confirmed that Lyz2Cre^{+} removes floxed genes from both the myeloid lineage as well as from AECs[273–276]. Work by Desai et al. and by McCubbrey et al. provide strong evidence that Lyz2Cre hits mature AT2s, accounting for approximately 25% of all AECs in the lung[274,275]. We sought to verify these findings in our own mice by isolating AECs from Lyz2Cre^{+} and Hbegf$^{f/f}$;Lyz2Cre mice 21 days after bleomycin treatment. Although bleomycin decreases *HB-EGF* expression in AECs from control mice, levels of *HB-EGF* in Hbegf$^{f/f}$;Lyz2Cre AECs are similarly low in both saline and bleomycin-treated animals, indicating removal of HB-EGF from this cell compartment (Figure 31A). Interestingly, it appears that removal of HB-EGF from AECs in Hbegf$^{f/f}$;Lyz2Cre mice did not promote compensation in any other ligands of the ErbB pathway, as there are no striking differences in EGFR ligand expression after bleomycin between the genotypes at peak fibrosis 21 days post-bleomycin (Figure 32).

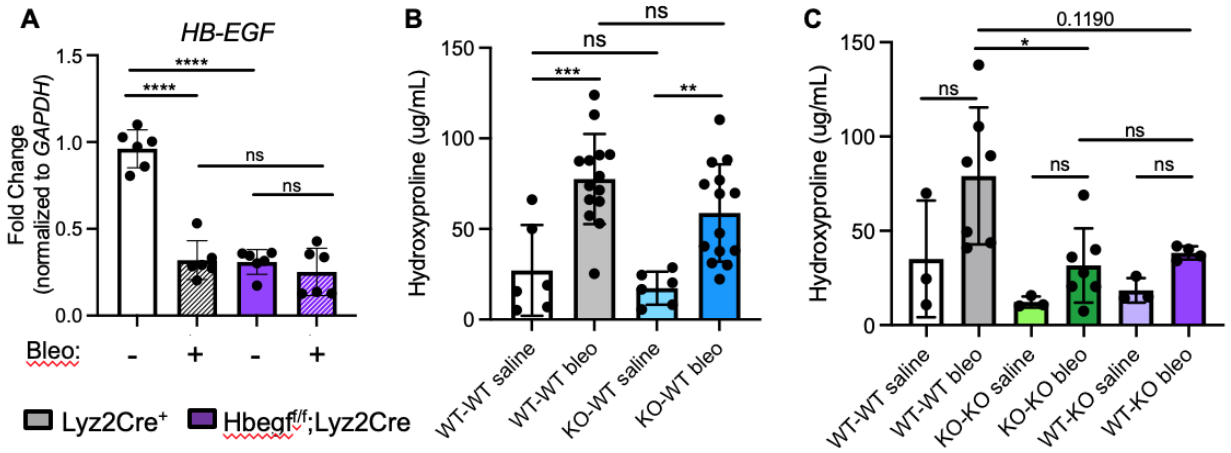

Figure 31: Lyz2Cre deletes HB-EGF in AECs which may also contribute to protection from fibrosis. (A) AECs from Hbegf$^{f/f}$;Lyz2Cre mice have highly decreased levels of HB-EGF at baseline (saline treatment) as well as 21 days post-bleomycin treatment. Representative data of two experiments, n=6. (B) Lethally-irradiated C57Bl/6J mice reconstituted with Hbegf$^{f/f}$;Lyz2Cre bone marrow showed no difference in overall hydroxyproline content compared to lethally-irradiated C57Bl/6J mice reconstituted with C57Bl/6J bone marrow. Representative of three experiments, n=3-7. (C) Lethally-irradiated Hbegf$^{f/f}$;Lyz2Cre mice reconstituted with C57Bl/6J bone marrow showed no difference in overall hydroxyproline compared to Hbegf$^{f/f}$;Lyz2Cre mice reconstituted with Hbegf$^{f/f}$;Lyz2Cre bone marrow, implying HB-EGF derived from the epithelium is more important in fibrosis

protection than immune cell-derived HB-EGF. Representative of one experiment, n=3-7. n.s.: not significant, *: p<0.05, **: p<0.01, ***: p<0.001, ****: p<0.0001.

Since HB-EGF is removed in both myeloid cells and in AECs in our Hbegf$^{f/f}$;Lyz2Cre mouse, we were interested to determine which cellular compartment was primarily responsible for protection against bleomycin-induced fibrosis. To test, we designed a bone marrow transplant experiment where C57Bl/6J mice were lethally irradiated using ^{137}Cesium irradiator (13 Gy, split dose) and given bone marrow from either C57Bl/6J mice or Hbegf$^{f/f}$;Lyz2Cre donor mice via tail vein injection. After allowing enough time for full immune system reconstitution (5 weeks), we then challenged these mice to a standard dose of bleomycin for 21 days. At day 21, hydroxyproline assay demonstrated that bleomycin-treated C57Bl/6J mice receiving C57Bl/6J bone marrow ("WT-WT bleo") have significantly increased levels of hydroxyproline compared to WT-WT saline mice (Figure 31B). However, C57Bl/6J mice that received Hbegf$^{f/f}$;Lyz2Cre bone marrow ("KO-WT") also had high levels of hydroxyproline 21 days after bleomycin and these levels were not different from those in the WT-WT bleo mice (Figure 31B). Since the KO-WT mice were not protected from fibrosis, and these mice have WT AECs but a Hbegf$^{f/f}$;Lyz2Cre immune system, it implies that the protection that we noted in Figure 25 in the Hbegf$^{f/f}$;Lyz2Cre mice is likely provided at least in part by HB-EGF removal from AECs. To confirm this updated hypothesis, we again used a bone marrow transplant experiment, this time lethally irradiating Hbegf$^{f/f}$;Lyz2Cre recipient mice and giving bone marrow from either C57Bl/6J donor mice ("WT-KO") or Hbegf$^{f/f}$;Lyz2Cre donor mice ("KO-KO"). We also repeated our WT-WT bone marrow transplant alongside these treatment groups as a control.

At day 21 post-bleomycin, hydroxyproline levels of KO-KO bleo mice were significantly decreased compared to WT-WT bleo mice (Figure 31C). This is expected, as the KO-KO bleo mice are essentially Hbegf$^{f/f}$;Lyz2Cre mice since HB-EGF is removed from both the immune cell

and AEC compartments. Although differences in day 21 hydroxyproline between WT-WT bleo and WT-KO bleo were close, but did not reach statistical significance (p=0.1190), intriguingly there was no difference in hydroxyproline levels between KO-KO bleo and WT-KO bleo mice (Figure 31C). Together, these data suggest that the removal of HB-EGF from AECs in Hbegf$^{f/f}$;Lyz2Cre mice is almost certainly the more important source of HB-EGF and the likely more prominent cause of protection in Hbegf$^{f/f}$;Lyz2Cre mice from bleomycin-induced fibrosis.

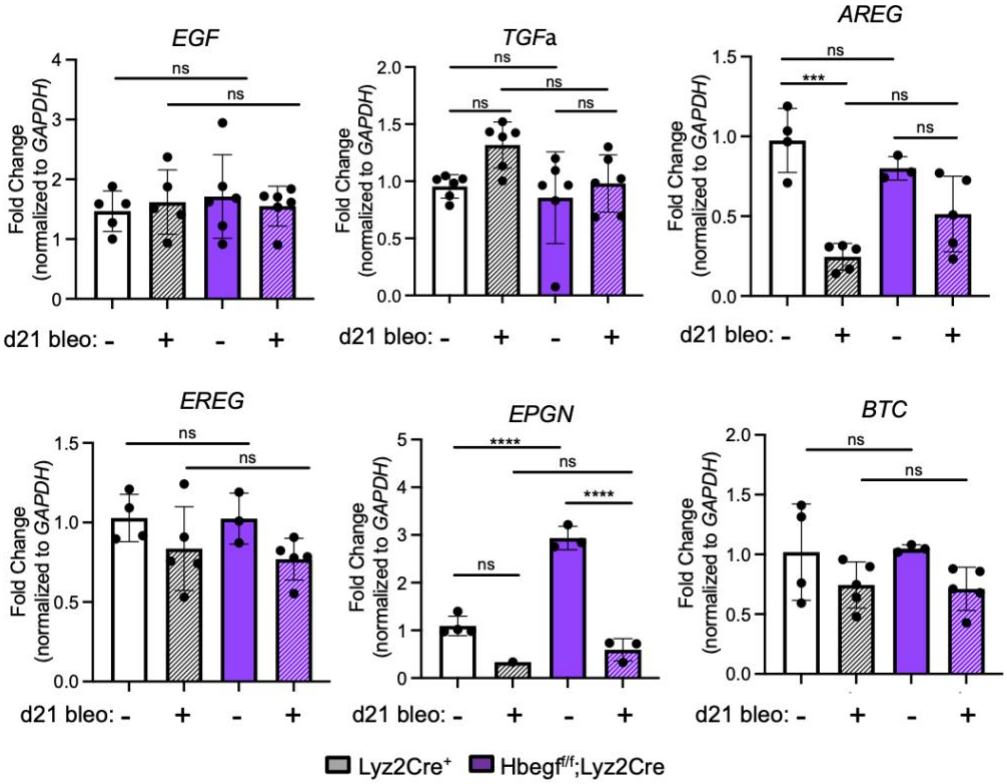

Figure 32: Removal of HB-EGF from AECs does not alter expression of other EGFR ligands 21 days post-bleomycin (EGF: epidermal growth factor, TGFa: transforming growth factor-alpha, AREG: amphiregulin, EREG: epiregulin, EPGN: epigen, BTC: betacellulin). n.s.: not significant, *: p<0.05, **: p<0.01, ***: p<0.001, ****: p<0.0001.

rHB-EGF does not induce a profibrotic response in AECs

As the data show that HB-EGF is removed from both myeloid cells and AECs in the Hbegf$^{f/f}$;Lyz2Cre mice and that AEC-derived HB-EGF may be particularly potent in affecting nearby structural cells like AECs and fibroblasts, we next wanted to know if rHB-EGF is sufficient to induce profibrotic changes in AECs. Interestingly, rHB-EGF does not promote

increased expression of key profibrotic genes as *periostin, PDGFa,* and *VEGF* all had decreased expression with HB-EGF treatment compared to SFM alone and *CTGF* had no change in expression (Figure 33A).

A key characteristic of pulmonary fibrosis is increased AEC apoptosis. If a reagent does not promote profibrotic changes in gene expression in AECs, it could still act in a profibrotic manner by inducing heightened AEC apoptosis. Surprisingly, the addition of rHB-EGF to AECs did not cause a change in anti-apoptotic genes *BCL2, XIAP,* or *survivin* (Figure 33B), nor did it increase caspase 3/7 activation like positive control TGF-β (4ng/ml) in an apoptosis assay (Figure 33C). Our data show that rHB-EGF does not directly induce these profibrotic effects in AECs.

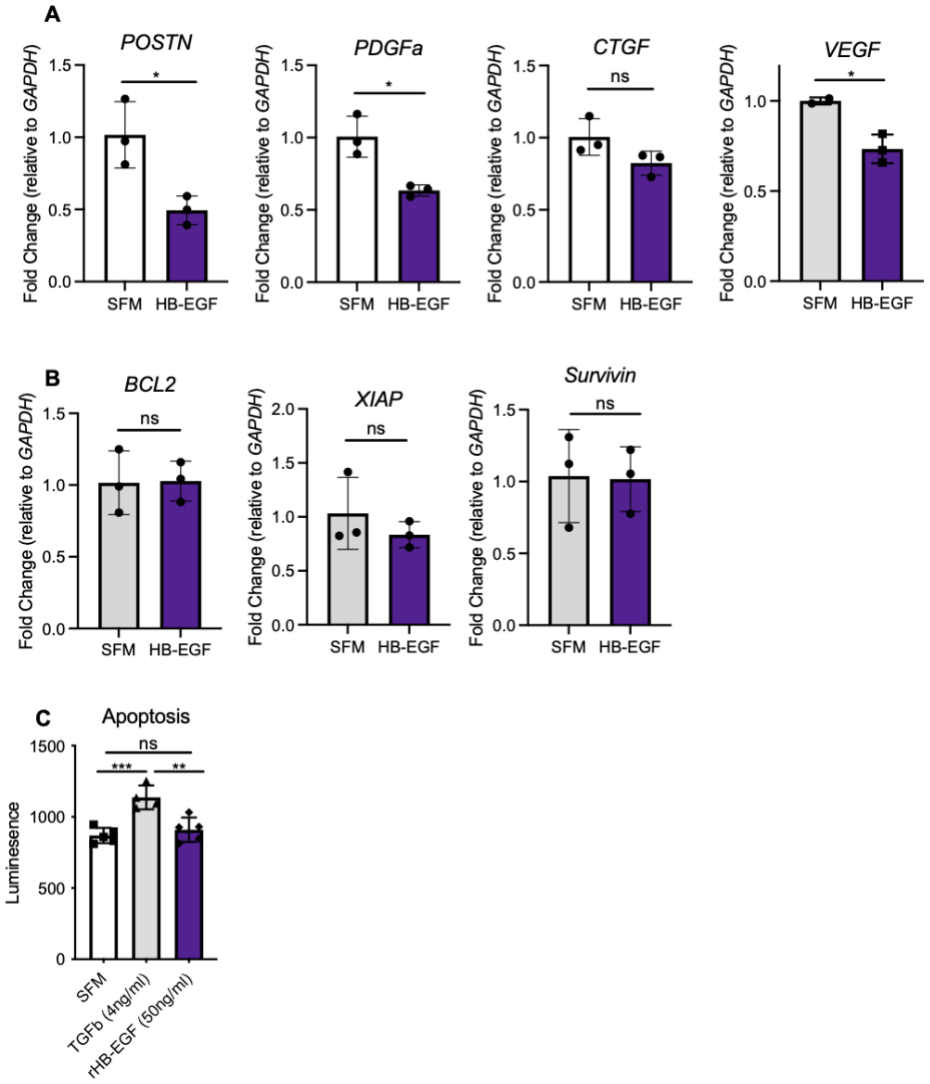

Figure 33: rHB-EGF does not induce a profibrotic response in AECs. (A) Primary lung fibroblasts treated with rHB-EGF (50ng/ml) do not show increases in expression of profibrotic genes periostin, PDGFa, CTGF, or VEGF or alterations in anti-apoptotic gene expression (B) BCL2, XIAP, or survivin. (C) rHB-EGF (50ng/ml) does not induce AEC apoptosis compared to positive control TGFb (4n/gml) as measured via caspase-glo 3/7 assay. Representative data shown of experiments repeated at least three times, n=3-5. *: $p<0.05$, **: $p<0.01$. Data in (C) are representative of at least three experiments, n=5 per group.

rHB-EGF induces fibroblast migration with little impact on proliferation or matrix gene expression

Fibroblasts are structural cells in the lung that exist near AECs and macrophages. Located adjacent to the basement membrane in the lung interstitium, fibroblasts produce extracellular matrix (ECM) proteins that help maintain lung architecture during homeostasis. In IPF, repeated injuries to the epithelium often leads to AEC death. To help seal the wound caused by dying

AECs and to reestablish barrier function, nearby fibroblasts become activated and subsequently proliferate and migrate to fill the wound site. These cells will also produce ECM proteins, including *collagen 1, collagen 3,* and *fibronectin*[5,85]. While in normal wound healing these processes resolve over time, in IPF, fibroblast migration and ECM production occurs to an excessive degree.

Although fibroblasts do not express Lyz2 and thus HB-EGF is not removed from these cells in the Hbegf$^{f/f}$;Lyz2Cre mice, fibroblasts do express EGFR and can respond to HB-EGF secreted by other cell types. Additionally, the location of fibroblasts and their ability to become activated into a profibrotic state made them be of interest to us. To determine if rHB-EGF prompts a profibrotic response in fibroblasts *in vitro,* we measured fibroblast proliferation, ECM production, and migration in Lyz2Cre^{+} fibroblasts. rHB-EGF did not induce fibroblast proliferation as measured by MTT assay (Figure 34A) or flow cytometry (data not shown). Similarly, addition of rHB-EGF did not cause an increase in expression of profibrotic genes *collagen 1, collagen 3,* or *fibronectin* compared to SFM controls after 24 hours (Figure 34B).

To measure fibroblast migration, we performed a scratch assay where primary lung fibroblasts were grown to confluence, evenly scratched with a WoundMaker device, then treated with concentrations of rHB-EGF (3.125ng/ml-100ng/ml) and ability of the fibroblasts to migrate and close the wound were measured over time. As fibroblasts showed no increased proliferation in response to rHB-EGF (Figure 34A) and all cells were treated with rHB-EGF in SFM, we consider the scratch wound assay to be an accurate measure of migration. Intriguingly, rHB-EGF induced a dramatic wound closure migration response where migration is increased in a dose-dependent fashion (Figures 34C, 34D). Beginning at just 12 hours post-scratch, all fibroblasts treated with at least 6.25ng/ml of rHB-EGF had closed the wound significantly more than SFM-

treated fibroblasts, and this difference persisted throughout the 68-hour experiment when fibroblasts treated with 100ng/ml of rHB-EGF had fully closed the scratch wound.

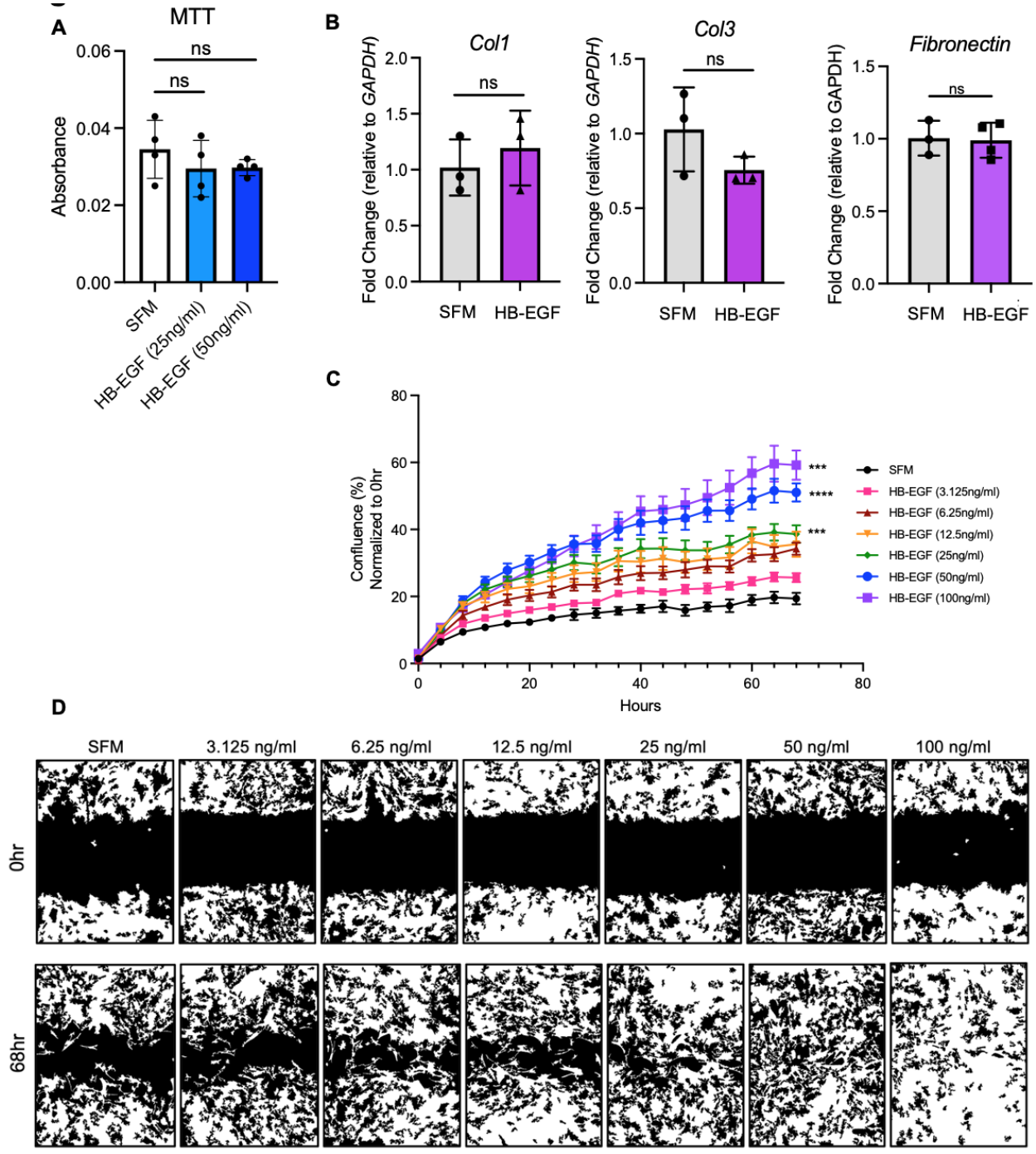

Figure 34: rHB-EGF induces fibroblast migration with little impact on proliferation or matrix gene expression. (A) Fibroblasts treated with rHB-EGF (25ng/ml, 50ng/ml) do not have increased proliferation as measured by MTT. (B) qPCR fold change of key profibrotic genes collagen1, collagen3, and fibronectin is not induced in fibroblasts after rHB-EGF (50ng/ml) administration. (C, D) rHB-EGF promotes fibroblast migration. Representative data shown of at least three experiments, n=3-6. In (C), all doses of HB-EGF from 6.25ng/ml-100ng/ml are significantly different from SFM control starting at 12 hours. p-values are given for HB-EGF

(25ng/ml), HB-EGF (50ng/ml), and HB-EGF (100ng/ml) and represent differences between treatment group and SFM at final timepoint (68hr). n.s.: not significant, ***: p<0.001, ****: p<0.0001.

Discussion

Although the role of HB-EGF has been previously described in other fibrosis models[151,208,262], there is no work to date directly examining its role in IPF or in a murine model of bleomycin-induced fibrosis. EGFR and EGFR signaling may be important in IPF progression, as patients with increased risk of an IPF disease-promoting event had higher levels of both EGFR and HB-EGF via subgroup analysis (Figure 23). These data align with previous work in the field showing that lung fibrosis patients have heightened expression of EGFR[102] and that overexpression of TGFα (a different EGFR ligand) can promote pulmonary fibrosis in murine models[161]. Our data showing HB-EGF expression in myeloid and epithelial cells in fibrosis are also supported in the single cell RNAseq data made publicly available through the IPF Cell Atlas[104,277–281] (http://www.ipfcellatlas.com/) and UCSC Cell Browser – NU Pulmonary[7,104,282] (https://www.nupulmonary.org/resources/) websites. These resources allow for gene expression comparison between IPF vs. donor patients and saline vs. bleomycin-treated mice.

HB-EGF expression was robustly increased in our bleomycin-treated mice (Figure 23). Interestingly, both lung homogenate and BAL cells showed this HB-EGF increase at days 14 and 21 post-bleomycin, but neither population had increased HB-EGF expression at days 3 or 7 (data not shown). There are two possibilities for this. First, this could imply that while HB-EGF is expressed at homeostasis in macrophages and in the lung, differences in HB-EGF expression may not arise until fibrosis development (days 10-21) rather than during initial injury (days 0-3). Alternatively, increased HB-EGF expression in the lung homogenate at day 21 could be caused by an influx of HB-EGF-producing cells to the lung after lung injury and during the inflammatory stage (days 3-7). Previous studies report that $Ly6C^+$ monocytes migrate to sites of

tissue injury and differentiate into macrophages upon arrival[256,257], and in the lungs, monocytes transit through an IM phenotypic stage during their transition to moAMs[6,7]. While all macrophage subtypes express HB-EGF at baseline (Figure 24), there are twice as many HB-EGF-expressing IMs and 47-times as many HB-EGF-expressing moAMs in the lung at day 21 post-bleomycin treatment compared to saline lungs (Figure 24). Together, these data suggest that overall levels of HB-EGF in the fibrotic mouse lung are higher due to increased number of HB-EGF^{+} moAMs and HB-EGF^{+} IMs.

We further probed the role of HB-EGF+ macrophages using Hbegf$^{f/f}$;Lyz2Cre mice in bleomycin-based fibrosis studies. Hbegf$^{f/f}$;Lyz2Cre mice were protected from fibrosis as measured by decreased hydroxyproline content, decreased profibrotic gene expression, and improved histology compared to Lyz2Cre^{+} animals (Figure 25). While our dose of bleomycin (1U/kg) causes < 25% mortality in wild type mice, Hbegf$^{f/f}$;Lyz2Cre mice had decreased mortality and higher body weight at 21 days compared to wild type mice (data not shown), further supporting the protection phenotype. Interestingly, total levels of hydroxyproline and profibrotic gene expression in bleomycin-treated Hbegf$^{f/f}$;Lyz2Cre mice was always higher than levels in saline-treated Hbegf$^{f/f}$;Lyz2Cre mice, indicating some degree of fibroproliferation even in the presence of reduced HB-EGF expression.

Given the importance of moAMs in fibrosis development and the protection phenotype of the Hbegf$^{f/f}$;Lyz2Cre mice, it is unsurprising that Hbegf$^{f/f}$;Lyz2Cre mice have fewer moAMs present during the inflammatory stage of fibrosis development (Figure 26, Figure 27). Hbegf$^{f/f}$;Lyz2Cre mice routinely had lower numbers of moAMs at both day 7 and day 21 compared to Lyz2Cre^{+} mice. Considering these moAM differences at day 21, however, it is interesting that total numbers of IMs are the not different between genotypes at the same time

point. This could be caused by impaired IM-moAM differentiation in Hbegf$^{f/f}$;Lyz2Cre mice, but if true, one might have predicted increased IM populations accumulating in the Hbegf$^{f/f}$;Lyz2Cre mice which we do not see. It could also relate to the difficulty of accurately identifying the heterogenous populations of recruited and inflammatory cells with dynamic changes in cell surface marker expression[13,14,110]. It is also interesting to note that total numbers of neutrophils are decreased at day 7 post-bleomycin in Hbegf$^{f/f}$;Lyz2Cre mice (Figure 35). Neutrophils produce neutrophil elastase (NE), which promotes fibroblast migration and myofibroblast differentiation *in vitro*[283]. A lack of neutrophils in these mice during peak inflammation is consistent with a decreased fibrosis phenotype and it is possible that decreases in moAMs and neutrophils together contribute to protection of Hbegf$^{f/f}$;Lyz2Cre mice.

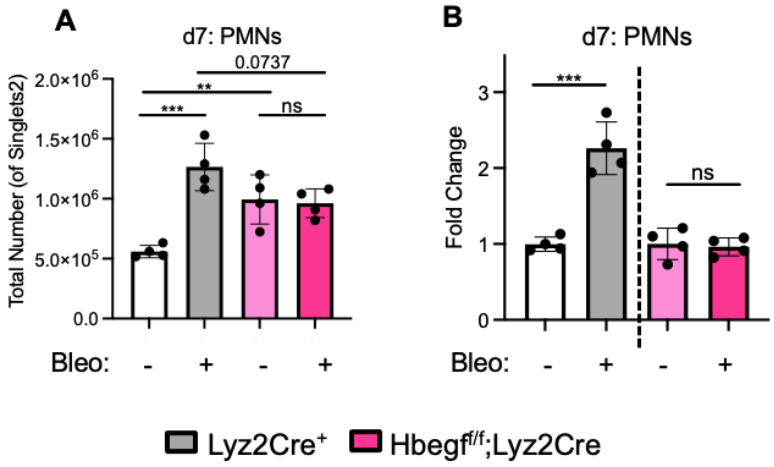

Figure 35: Hbegf$^{f/f}$;Lyz2Cre mice also show decreased neutrophil (PMN) numbers during fibrosis initiation. Hbegf$^{f/f}$;Lyz2Cre mice have lower levels of PMNs 7 days post-bleomycin treatment as determined by total number (A) and relative fold change (B). Data in Figure 35A/B correspond to data in Figure 26A and Figure 27A. ANOVA statistics in (A), in (B) t-tests performed comparing treatments within a single genotype. n.s.: not significant, *: p<0.05, **: p<0.01, ***: p<0.001, ****: p<0.0001. All data representative of 2-5 experiments, n=4-6.

Our data show that the decreased numbers of moAMs in Hbegf$^{f/f}$;Lyz2Cre mice at day 7 are the result of decreased monocyte migration (Figure 29, Figure 28). As such, we add further evidence to the current theory that depleting monocytes reduces fibrosis severity[4,83,110]. In addition, our evidence suggests lower levels of monocyte migration to the lung is caused by

decreased amounts of CCL2 in the BALF, BAL cells, and AECs of Hbegf$^{f/f}$;Lyz2Cre mice during initial lung injury (Figure 29). BMDMs of mice also have decreased levels of CCL2, suggesting that bleomycin induces a systemic effect that is likely regulated by a soluble factor (Figure 29). CCL2 binds its receptor, CCR2, found predominantly on monocytes[4]. CCL2 is present in increased levels in IPF patients and is associated with increased lung injury scores in patients with acute respiratory distress syndrome (ARDS)[284,285]. While rHB-EGF alone does not induce CCL2 expression in macrophages, fibroblasts, or AECs (Figure 30), it is possible that rHB-EGF requires a second stimulus such as LPS, cytokines (IL4, IL13), or bleomycin injury, although preliminary experiments with such secondary signals have not been supportive (Figure 30D, data not shown) suggesting that the full induction of CCL2 may be regulated by the complex injured lung milieu. HB-EGF is biologically active in both a soluble (sHB-EGF) and membrane-bound (pro-HB-EGF) form. It is also possible that CCL2 induction requires pro-HB-EGF for juxtacrine signaling, rather than paracrine or autocrine signaling alone. More likely, however, is that since monocytes and macrophages can recruit themselves to sites of injury, reduced numbers of both cell types could relate to the presence of fewer moAMs in the lung that produce CCL2.

While our evidence that Hbegf$^{f/f}$;Lyz2Cre mice are protected is robust (Figure 25), it is equally apparent that the protection is not an exclusively macrophage or immune cell phenotype. While our first bone marrow transplant (BMT) results show that wild type mice who received Hbegf$^{f/f}$;Lyz2Cre bone marrow had indistinguishable levels of fibrosis compared to wild type mice who received wild type bone marrow (Figure 31), supporting the conclusion that Lyz2Cre effectively removes HB-EGF from AT2s and that the epithelium plays a contributing role in fibrosis protection in Hbegf$^{f/f}$;Lyz2Cre mice, the results of our second BMT more conclusively

point to AEC-derived HB-EGF as a prominent reason for protection in Hbegf$^{f/f}$;Lyz2Cre animals. Another possibility is that the threshold level of HB-EGF in the lung is more critical than the cellular source. Future experiments will be needed to address this more fully. Although various sources provide evidence that Lyz2Cre targets the alveolar epithelium, the consensus is that the target gene is only removed in 25% of AECs and that this specifically corresponds with AT2s[275,286]. AT2s are the surfactant-producing stem cell of the epithelium that differentiate into AT1s to fill in gaps after injury[12,15,21], and as such, Lyz2Cre-based removal of HB-EGF from AT2s should persist in daughter AT1 cells. As single-cell RNA sequencing data from Riemondy et al. has shown that HB-EGF is expressed in AT1s[287], it is likely that HB-EGF is removed from both AT1s and AT2s in Hbegf$^{f/f}$;Lyz2Cre mice though this cannot be quantified due to a lack of anti-mouse HB-EGF antibody.

Regardless of the cell source, our results indicate that there should be lower thresholds of HB-EGF present in the lung of Hbegf$^{f/f}$;Lyz2Cre mice. We chose to look next at soluble HB-EGF to see if its increased presence would induce profibrotic changes on AECs and fibroblasts. Interestingly, rHB-EGF addition to AECs did not increase levels of profibrotic gene expression, decrease levels of anti-apoptotic gene expression, or increase apoptosis (Figure 33), all expected hallmarks of a profibrotic gene response. In addition, previous work suggested that HB-EGF regulates AT2 proliferation *in vivo* and thus it could be expected that HB-EGF would promote epithelial repair and improve fibrotic outcome[275]. However, Hbegf$^{f/f}$;Lyz2Cre mice are protected; thus, it does not appear that loss of HB-EGF in the Lyz2Cre^{+} AECs limited lung repair. Although rHB-EGF does not induce profibrotic changes in AECs, it is possible HB-EGF acts differently on fibroblasts. While rHB-EGF did not increase proliferation or expression of profibrotic genes in fibroblasts, rHB-EGF did dramatically increase migration in a scratch wound assay (Figure

34). HB-EGF is also known to increase keratinocyte migration rather than proliferation[150]. Taken together, the role of HB-EGF is multidimensional.

This study has several caveats. First, this study was conducted in a murine model of fibrosis. Although the bleomycin model is the best characterized and most widely used animal model of pulmonary fibrosis, it does not fully recapitulate all of the phenotypes seen in IPF patients[48,71].

A second caveat is the technical limitations of the Lyz2Cre system and the lack of an appropriate inducible system. The conditional Lyz2Cre Cre-loxP system was chosen for this study because of its ability to remove HB-EGF from all macrophage populations (AMs, IMs, moAMs) with nearly 100% efficiency[286]. We chose Lyz2Cre over other Cre-loxP systems we deemed less appropriate: Csf1r-Cre targets all leukocytes in addition to macrophages and inducible Cre-loxP systems CX_3CR1-ERCre and CD78-rtTA do not target every lung macrophage population (no resident AMs)[286]. Like most Cre systems, however, Lyz2Cre also depletes off-target cell types. Previous work by McCubbrey et al. and Desai et al. have shown that Lyz2Cre targets 25% of alveolar epithelial cells, specifically the AT2 subtype[273,275,276,286]. Our data confirm this finding (Figure 31). As such, we are unable to fully rectify the role that AEC-specific HB-EGF has in this mouse model, although the data from our bone marrow transplant experiment demonstrate that HB-EGF-derived from AECs is critical to the protection of the $Hbegf^{f/f}$;Lyz2Cre animals from bleomycin-induced fibrosis (Figure 31).

In addition to AT2s, Lyz2Cre targets other innate immune cells including neutrophils (100%), $Ly6C^+$ monocytes (68%), dendritic cells (DCs) (50%), and eosinophils (< 20%)[286]. Although recent work has shown that all subtypes of peripheral blood dendritic cells are severely depleted in IPF patients, the role of DCs in fibrosis is not fully understood[288]. Neutrophils, by

contrast, may have an important role in fibrosis. Use of the NE-specific inhibitor, Sivelestat, has been shown to be protective in a bleomycin mouse model[289,290]. Studies have also shown that IPF patients with neutrophilia experience reduced survival[291]. However, the limited number of neutrophils present in lung tissue of IPF patients make it challenging to confidently assign them a precise function in IPF[291]. It is possible that there may be a role for neutrophil-derived HB-EGF, either in function or in total quantity, that we are unable to address in this study. Additionally, we were unable to determine if the protection in the Hbegf$^{f/f}$;Lyz2Cre mice is simply a threshold effect. Finally, HB-EGF likely acts in profibrotic ways on certain cell types (e.g., fibroblasts) but in an antifibrotic manner for others (e.g., AECs). Ideally, the eventual availability of validated murine HB-EGF antibodies (e.g., ELISA kits) and murine HB-EGF inhibitors will allow this to be a more feasible future research direction.

Overall, we demonstrated that HB-EGF is expressed in IPF patients as well as in all populations of lung macrophages (AMs, IMs, moAMs) in fibrotic mice. We also showed that Hbegf$^{f/f}$;Lyz2Cre mice are protected from bleomycin-induced fibrosis and that this protection is multifactorial, caused by genotypic differences in CCL2-dependent monocyte migration, decreased fibroblast migration, and decreased contribution of HB-EGF from AEC sources when HB-EGF is removed under the Lyz2Cre promoter. Together, the data from this study provide evidence that HB-EGF is heavily involved in the development of pulmonary fibrosis and highlights the need to continue study of the intersection between macrophage dynamics, cellular crosstalk, and specific growth factors in homeostatic and fibrotic disease states.

Chapter 4: Discussion

Bringing It All Together

Although IPF was formerly thought to be an exclusively epithelial-mesenchymal cell disease, work over the last two decades have once again shown that innate immune cells also have a central role in IPF development and progression. The recent impetus to study immune cells in IPF was most noticeably prompted by the results of the 2012 PANTHER clinical trials, in which IPF patients given a combination of immunosuppressants had worse clinical outcomes than the placebo group, implying a distinct role for immune cells[3,292]. Since then, research has shown that macrophages are involved at all stages of the wound repair response[293] and that the severity of IPF disease progression can be linked to increases in monocyte and macrophage numbers[4,8,255,294,14,83,102,103,106,107,110,116].

Interestingly, the removal of macrophages at different time points can have helpful or harmful effects in fibrosis development and progression. On one hand, studies have shown that depleting macrophages early after injury greatly dampens the inflammatory response and leads to less fibrotic injury[4,83,255,295]. Conversely, macrophage removal can also promote worsened fibrosis, as macrophage depletion can result in decreased wound debridement and less efficient tissue repair and regeneration[296]. Since macrophages can promote either a profibrotic or an antifibrotic environment, it follows that in addition to variations in timing, the key to one path over the other is caused by crucial differences in (a) the presence of certain soluble mediators and/or (b) in macrophage-structural cell crosstalk and resulting downstream signaling.

Significance of Chapter 2

While both M1-like and M2-like macrophages are known to be present in the bleomycin mouse lung at different times during fibrosis development, M2-like macrophages have long been associated with a profibrotic phenotype[82,138,297–299]. The scar formation characteristic of pulmonary fibrosis has been shown to be directly linked to the appearance of M2-like macrophages[8] and macrophages in IPF patients also show increased expression for M2 markers like CD206[103]. Depletion of M2-like macrophages has been associated with a reduced fibrotic phenotype in mouse models[14], and pirfenidone, one of 2 FDA-approved drugs for IPF, exerts anti-fibrotic property in part by suppressing TGF-β expression associated with M2 polarization[1].

One reason that M2 macrophages are problematic in fibrosis is their secretion of soluble profibrotic factors. Macrophages are an important source of chemokines, matrix metalloproteinases, and other inflammatory mediators that drive the initial cell response following injury[83,300]. Macrophage production of soluble factors promotes the recruitment of fibroblasts, differentiation into myofibroblasts, and increases fibroblast contractility and ECM production[301]. Macrophages also crosstalk with the epithelium and regulate components of AEC activation[302]. M2 macrophages in particular have been described to secrete key profibrotic proteins. For example, M2 macrophages produce CCL18, which is elevated in the BAL and AMs of ILD patients and is known to drive collagen production from human fibroblasts[139,303]. Increased levels of CCL18 also correlate with increased fibrosis severity in IPF[139]. Additionally, M2 macrophages produce TGF-β1, which stimulates collagen production in myofibroblasts and enhances expression of tissue inhibitors of metalloproteinases (TIMPs) that block degradation of ECM proteins[122].

Given the importance of M2 macrophages in fibrosis and the widespread use of the M1/M2 dichotomy *in vitro*, we sought to characterize the transcriptomes of BMDM-derived M1 and M2 macrophages to better understand their overall function as mediators of fibrosis. We discovered that M1-like and M2-like BMDMs have different gene expression profiles based on RNAseq analyses. Most notably, gene clusters with highest enrichment scores in M1s were related to inflammation, while clusters with highest enrichment scores in M2s were related to cell processing. Interestingly, M2-like BMDMs have a higher number of genes encoding for secreted proteins, indicative of the importance of M2-derived soluble mediators may play in fibrosis development and progression.

While M2 supernatant increased fibroblast migration, proliferation, and profibrotic gene expression compared to fibroblasts treated with M1 supernatant, all these effects could be attributed to the lingering presence of IL-4 and IL-13, which was required to polarize the BMDMs to an M2 phenotype. This same phenomenon was noted in the increased expression of profibrotic genes in AECs, as statistical differences between AECs given M2 supernatant and those given IL-4+IL-13 controls were indistinguishable. In our study, we saw initial evidence that M2 supernatant could induce AEC apoptosis separate from an IL-4+IL-13 effect. However, further experimentation showed that this result was actually a false positive, caused by the presence of an aspartic acid protease that functioned as a caspase-3/7 "lookalike" and cleaved our luminescent substrate indicative of an apoptosis readout. While additional analysis of the M2 transcriptome showed an increased number of genes with molecular functions related to protease binding, collagen binding, integrin binding, and growth factor/growth factor receptor binding compared to the M1 transcriptome, further study will need to be done to verify these findings in

the secretome, quantify their presence in macrophage supernatant, and translate these findings to an *in vivo* model.

Significance of Chapter 3

In addition to the presence of macrophage-derived soluble mediators that can prompt a fibrosis response, alterations in macrophage-structural cell crosstalk and the resulting changes to downstream signaling in multiple cell types can also promote a fibrotic phenotype. The importance of crosstalk between macrophages and structural cells of the lung has become more well-studied, especially as scientists have learned that communication signals extend in both directions. For example, research has shown that injured lung epithelial cells produce and secrete many cytokines. Some of these promote recruitment of fibrocytes and inflammatory cells to the lung to help with the injury response[304,305], while others including TGF-β, PDGF, CTGF, and EGF promote migration, proliferation, and activation of nearby fibroblasts[85]. Macrophages, in turn, are known to be involved in AEC activation[3] and the expansion of neighboring parenchymal and stromal cells in areas of injury[83]. Recent work has also shown that macrophages have fibroblast-stimulating properties, so much so that circulating monocytes in IPF patients appear pre-programmed for this prior to entering the lung[306].

Evidence in the literature also shows that aberrant signaling in key cell maintenance pathways can lead to fibrosis. EGFR is a receptor tyrosine kinase with key downstream effector pathways that regulate a wide variety of cellular functions, including MEK/ERK, PI3K/AKT, STAT, and mTOR[141–144]. EGFR signaling is particularly important in the lung, as proper EGFR signaling is critical for controlled cell turnover and tissue repair, mucus production, and alveolar homeostasis[141,176]. EGFR mutations are present in a large percentage of lung cancer patients and

thus a significant amount of research has been done trying to develop effective anti-EGFR therapeutics[176].

In addition to cancer, EGFR dysfunction is highly associated with lung fibrosis and hypersecretory diseases like COPD, asthma, and cystic fibrosis[202–204]. Although heightened expression of EGFR in lung fibrosis patients is well established[205], published work describing the effects of EGFR antagonism is contradictory. For example, murine studies have shown that EGFR ligand overexpression can promote pulmonary fibrosis[161], but EGFR antagonism using the EGFR-TKI *gefitinib* has been shown both to worsen and to protect against pulmonary fibrosis in other animal work[197,210]. These discrepancies are likely the consequence of differential cell-specific effects of ligands or of receptor actions or the timing of their administration.

HB-EGF is one of four high-affinity ligands for EGFR and is highly expressed in M2 macrophages[149,259]. As HB-EGF has a known role in the wound healing response but conflicting functions in mouse models of interstitial lung disease, we chose to further investigate the role of HB-EGF in pulmonary fibrosis. In our work, we first validated the importance of HB-EGF in IPF patients by measuring levels of HB-EGF and EGFR in IPF patient plasma using SOMAmer technology. We demonstrated that faster-progressing IPF patients had both higher levels of EGFR (Logrank test, p=0.02; RMST, p=0.03) and of HB-EGF (Logrank test, p=0.02; RMST, p=0.02). Additionally, we confirmed that mRNA levels of HB-EGF are increased in the lungs of bleomycin-treated mice: *HB-EGF* expression was higher both in lung homogenates and in BAL cells in fibrotic mice compared to saline control mice.

As *HB-EGF* was increased in moAMs of fibrotic lungs, we acquired a mouse model that had HB-EGF removed from the myeloid compartment (Hbegf$^{f/f}$;Lyz2Cre mice). Interestingly, Hbegf$^{f/f}$;Lyz2Cre mice are protected from bleomycin-induced fibrosis as evidenced by lower

levels of hydroxyproline, profibrotic gene expression, and improved histology. Hbegf$^{f/f}$;Lyz2Cre mice also show no difference in initial lung injury compared to wild type controls, indicating that protection from the development of lung fibrosis in Hbegf$^{f/f}$;Lyz2Cre mice cannot be explained by reduced lung injury.

Further investigation of these Hbegf$^{f/f}$;Lyz2Cre mice yielded interesting results. Hbegf$^{f/f}$;Lyz2Cre mice have lower total numbers of moAMs at day 7 and day 21 post-bleomycin compared to control animals, indicating a likely mechanism of protection. This difference in cell number is likely attributed to genotypic differences in CCL2-dependent monocyte migration. Importantly, bone marrow transplant studies showed that having an Hbegf$^{f/f}$;Lyz2Cre immune system was not sufficient to confer protection from fibrosis, but the removal of HB-EGF from an AEC source prevents an overall increase in hydroxyproline typical to levels seen in WT mice. As such, we conclude that the protection seen in Hbegf$^{f/f}$;Lyz2Cre mice is likely multifactorial, caused by genotypic differences in CCL2-dependent monocyte migration, decreased fibroblast migration, and decreased contribution of HB-EGF from AEC sources when HB-EGF is removed under the Lyz2Cre promoter.

Study Caveats

A primary caveat of this body of work is the use of a mouse model to study pulmonary fibrosis rather than samples derived from IPF patients. Although patient samples would be the most relevant option, acquiring these samples on a routine basis is challenging. Furthermore, acquiring samples of only fibrotic patients would restrict our research to questions investigating fibrosis progression, not fibrosis development. Many animal models of pulmonary fibrosis exist, each with their own benefits and drawbacks[307]. Bleomycin is the most widely used murine model

of fibrotic lung disease and is the gold standard for testing anti-fibrotic therapies in mice, primarily because of the large body of research that has been conducted in this mouse model[48,71]. We chose to use bleomycin for our animal studies primarily for this reason. However, it should be noted that the histopathology of single-dose oropharyngeal bleomycin administration does not fully recapitulate the features of UIP seen in humans (e.g., fibrotic foci are rare)[81]. Additionally, mice treated with bleomycin show eventual resolution of the disease course (~ day 35), which is not seen in IPF patients[75–80]. Despite these drawbacks, we feel the use of single-dose bleomycin was appropriate for our studies given our research questions.

A second caveat of this project is the use of a Cre-Lox transgenic mouse. In this system, mice containing a gene of interest flanked by two LoxP sites are crossed with mice that have a Cre recombinase transgene under the control of a tissue-specific promoter. Offspring should have the gene of interest deleted ubiquitously in cells expressing the specific Cre promoter. Although Cre-Lox technology has been used successfully in mice since 1998[308], certain promoter regions allow for more robust expression of Cre protein. Consequently, some Cre strains show off-target effects and delete the gene of interest from cells that do not express the tissue-specific promoter[309]. Additionally, some Cre lines demonstrate off-target effects by having Cre activity in the germline, which results in recombination of the floxed allele that is independent of the regulatory Cre-driving element and leads to sex-specific effects[310]. As noted below, Hbegf$^{f/f}$;Lyz2Cre mice deleted gene expression in both myeloid and epithelial cell types consistent with expression of the Lyz2 promoter in these cells. Furthermore, the possibility of off-target germline activation of the Cre in female mice is worrisome and could lead to sex-specific differences in transgene expression. To guard against this, future crosses are being generated with Cre always expressed in the male line.

The Lyz2Cre promoter does target multiple cell populations[273–276]. McCubbrey *et al*. used fluorescent reporter lines to investigate off-target effects of several well-known "macrophage" Cre driver lines, including Csf1r-Cre, Lyz2Cre, CX_3CR1-ERCre and CD68-rtTA[274]. They saw that Lyz2Cre targets all macrophage populations (AMs, IMs, moAMs) with nearly 100% efficiency and $Ly6C^+$ monocytes with approximately 70% efficiency[274]: beneficial statistics for our macrophage-based studies. However, Lyz2Cre also targets < 20% of eosinophils, ~50% of dendritic cells (DCs), and ~100% of neutrophils. Furthermore, other studies have shown that Lyz2Cre targets 25% of all AECs and that these AECs specifically correspond to AT2s[274,275].

While peripheral blood DCs are known to be depleted in IPF patients, the specific role of DCs in fibrosis is not well understood[288]. HB-EGF is deleted in approximately half of the DCs in our mouse model. We do not have a strong hypothesis as to what effects this removal could have on fibrosis development in general. By contrast, HB-EGF removal from essentially all neutrophils could have a major impact on our fibrosis phenotype in the $Hbegf^{f/f}$;Lyz2Cre mice. Though challenging to study lung neutrophils in IPF patients due to reduced need for bronchoscopy for diagnosis, an increased neutrophil count is associated with worsened fibrosis[2,311,312]. Specifically, neutrophils have been described to participate in regulation of ECM remodeling and formation of PMN extracellular traps, both of which may have profibrotic effects[291]. Additionally, mice deficient in the neutrophil product, neutrophil elastase (NE), are protected from fibrosis and even inhibiting NE dampens the fibrosis response in mice[291]. It is possible that there may be a role for neutrophil-derived HB-EGF, either in function or in total quantity, that we are unable to address in this study. The most problematic aspect of the Lyz2Cre, of course, is its propensity to target AT2s. As it is well-known that AT2s differentiate into AT1s and that this process is significantly upregulated after AT1 injury, deletion of HB-

EGF from AT2s under the Lyz2Cre promoter might effectively remove HB-EGF from many AECs in Hbegf$^{f/f}$;Lyz2Cre mice after bleomycin administration. Consequently, we are unable to fully rectify the role that AEC-specific HB-EGF has in this mouse model, nor can we rectify the role of macrophage-specific HB-EGF in this mouse model. Future studies, described below, will be needed to further advance these questions.

Though not a caveat, one serious limitation in this work is the lack of validated murine HB-EGF antibodies. Although HB-EGF is well-studied in the cancer field and as such there are many human antibodies for this protein, none exist for the mouse. This makes some experiments highly challenging; there is no direct way to measure levels of HB-EGF secreted from various cell types or measure total HB-EGF protein in the lung. As such, we have been unable to determine if HB-EGF is required to be present at a certain threshold in the lung to induce an overall profibrotic lung phenotype or rather, if the cell source of HB-EGF is more important.

Future Directions

Next Steps for Chapter 2 Studies

Throughout this dissertation work, we have placed a large emphasis on the role of soluble factors derived from profibrotic M2 macrophages. One future direction that would continue in the exploration of soluble M2 factors would be to identity the "lookalike" protease in M2 supernatant that caused a false positive for caspase-3/7 cleavage. To determine which aspartic acid protease is responsible, we could systematically target a variety of proteases made in BMDMs using siRNAs. By comparing which siRNA causes M2 supernatant luminescence to drop to levels equal to the heat-denatured control supernatant, we could determine our protease of interest.

However, it would also be interesting to next consider the role of juxtacrine signaling in macrophages and neighboring cell types. This would allow us to further interrogate how M2 macrophages act in a profibrotic manner on multiple cell types and what the relative contribution of juxtacrine signaling versus paracrine or autocrine signaling might be. For example, we noted in our M2 study that M2 supernatant does not induce robust AEC apoptosis, despite ample evidence in the literature that AECs apoptose in the fibrotic lung. While our results demonstrate that soluble factors from M2 polarized BMDMs cannot induce AEC apoptosis alone, it is very likely that cells adjacent to AECs are primed by injury cytokines present in the lung milieu, and that these primed adjacent cells then undergo a juxtacrine signaling response to the AECs that prompts AEC apoptosis.

To investigate questions like these, we would want to use a co-culture system and plate M2 macrophages with AECs or M2 macrophages with fibroblasts to allow cell-cell contact. Though less straightforward than supernatant alone studies, we could use a variety of techniques to repeat assays that examine AEC apoptosis (flow cytometry), AEC profibrotic gene expression (anti-CD45 bead sort), fibroblast migration (irradiated macrophages and/or fluorescent labeling by cell type), and fibroblast proliferation (flow cytometry). To distinguish macrophages from AECs or fibroblasts, we could perform the assays using flow cytometry and gate out $CD45^+$ cells (macrophages) or we could use anti-CD45 magnetic beads to separate out macrophages, leaving only AECs or fibroblasts behind in the flow-through for downstream analysis.

As BMDM-derived M2 macrophages cultured *in vitro* can be criticized for having less relevance to *in vivo* disease phenotypes, we could also consider using a more relevant macrophage subtype for these juxtacrine signaling experiments. This could include performing BALs followed by adherence purification to examine a primarily AM population, performing

collagenase digests with bead-sorting and/or adherence purification to look at AMs or IMs, or even FACS-sorting out moAMs to look at the most physiologically relevant macrophage cell type in the lung. By treating mice with bleomycin instead of relying on a reductionist M1-M2 polarization scheme *in vitro,* it would also allow us to better recapitulate macrophage phenotypes during the fibrotic response for these assays. By better understanding the functional responses that occur because of juxtacrine signaling, these studies would offer the potential to lead to possible therapeutic strategies in the future.

Next Steps for Chapter 3 Studies

In addition to expanding overall knowledge in M2 macrophage dynamics, this body of work also highlights the importance of macrophages in the establishment of fibrosis. Data from the literature show that different macrophage populations play distinct and non-redundant roles in tissue repair, fibrosis development, and regeneration[313–315]. As macrophages themselves are a highly heterogenous population[102], it follows that there needs to be ample understanding of the various roles of each type of macrophage in the field. Our work supports data by Misharin (2017) and Joshi (2020) that moAMs have a critical role in fibrosis development[6,7]. Despite these studies, there is still not much collective evidence describing moAMs and their various functional properties. As a next step, we plan to focus specifically on moAM signaling and maintenance pathways through several approaches.

While Hbegf$^{f/f}$;Lyz2Cre mice are protected from bleomycin-induced pulmonary fibrosis, the Lyz2Cre promoter targets both the alveolar epithelium as well as a number of immune cells[286]. To elucidate the importance of HB-EGF in moAMs specifically, we could consider creating a mouse with HB-EGF deleted from only moAMs, which would allow us to determine if

HB-EGF-specific moAM deletion was sufficient to protect mice from fibrosis and assist in additional experiments to identify the role of HB-EGF in moAM maintenance and homeostasis. Unfortunately, it would be highly challenging to generate this mouse, as there is no targetable moAM-specific Cre driver at present. To investigate the role of HB-EGF in moAMs, therefore, we could consider FACS-sorting moAMs from wild type mice and performing tail vein injections to provide these moAMs in a mouse lacking HB-EGF^{+} macrophages (e.g., Hbegf$^{f/f}$;Lyz2Cre or Hbegf$^{f/f}$;Csf1rCre mice) and comparing results to mice that receive tail vein injections of HB-EGF^{-} macrophages (from Hbegf$^{f/f}$;Lyz2Cre or Hbegf$^{f/f}$;Csf1rCre mice, e.g.). Although this technique would not be able to identify how the removal of HB-EGF effects downstream pathways in a loss-of-function system, it would show how the presence of HB-EGF can influence moAMs specifically in a gain-of-function style.

Since moAMs derive from Ly6C^{+} monocytes circulating in the bloodstream, it is also possible that HB-EGF is involved in differentiation of Ly6C^{+} monocytes into moAMs and/or that HB-EGF is required for homing of Ly6C^{+} monocytes to the lung after injury. This could be through extravasation and/or through regulation of important chemokine signaling. Our work identified that Hbegf$^{f/f}$;Lyz2Cre mice have less CCL2 present in BALF three days post-bleomycin and that AECs and BAL cells make less CCL2 transcript at the same time compared to wild type animals. We tested HB-EGF for direct ability to induce CCL2 mRNA, but results were negative in macrophages, AECs, and fibroblasts. Future experiments could explore inhibition of HB-EGF signaling (via EGFR inhibition with Erlotinib) on CCL2 production in these cells to see its effects on downstream targets or attempt to study co-regulation pathways with other CCL2-inducing signals. Additionally, work by Joshi has demonstrated that MCSF signaling is required for maintenance and persistence of moAMs in the lung, and a study by

Schneider et al. showed that differentiation of recruited monocytes and their engraftment into the alveolar niche is dependent on GMCSF[111,316]. While our preliminary work did not support an effect of HB-EGF bolstering MCSF expression or increased downstream MCSF signaling pathways, it is possible that all three growth factors, separately or in combination, have a necessary role in moAM recruitment, establishment, and persistence that may or may not be related to CCL2 production.

In addition to considering moAM-specific HB-EGF removal, we should also conclusively determine the role of HB-EGF in AECs. To do this, we could consider obtaining a mouse that allows for either AT2-specific (SPC-Cre) or AT1-specific (Aqp5-Cre-IRES-DsRed) removal of HB-EGF[309,317]. An AT1-specific deletion of HB-EGF would be beneficial: as AT1s are the cell type that undergo extensive apoptosis in the fibrotic lung, removing HB-EGF from these cells would target the majority of cells in the epithelium and conclusively show if HB-EGF makes AT1s prone to injury. An AT2-specific deletion of HB-EGF could also be a good choice: AT2s differentiate into AT1s after injury, which would allow both AT2s and many AT1s to have HB-EGF removed after bleomycin treatment and during fibrosis development and progression. We could also mine scRNAseq databases to compare overall levels of HB-EGF mRNA expression in AT1s, AT2s, and transitional AECs at homeostasis and after bleomycin before committing to a specific mouse model. To determine which cell source of HB-EGF is more critical in protection and/or resolution of the injury phenotype, we could perform lung leak assays (e.g. total protein, Albumin ELISAs) at day 3 post-bleomycin and a hydroxyproline assay to look at fibrosis severity at day 21 post-bleomycin in both of these AEC-specific mouse models. We could also further investigate the role of CCL2 in these AECs, as it is possible that loss of HB-EGF in AECs changes downstream HB-EGF signaling that alters normal activation

of CCL2 in injured AECs. Since evidence shows that EGFR signaling may regulate AEC repair *in vivo* and *in vitro*[15], this is a plausible mechanistic explanation in Hbegf$^{f/f}$;Lyz2Cre mice.

Intriguingly, our studies show that wild type mice express lower levels of HB-EGF mRNA in AECs after bleomycin treatment, which could indicate that decreased levels of HB-EGF in AECs may promote a fibrotic phenotype. However, this is contradictory to the results in our second BMT experiment in which the data showed that protection in Hbegf$^{f/f}$;Lyz2Cre mice is almost certainly enabled by a (partial) removal of HB-EGF in AECs. One explanation could be that the process of ATII cell isolation, which takes several days, may artificially lower HB-EGF mRNA expression. It is also possible that HB-EGF is regulated post-transcriptionally and these changes cannot be detected in qPCR analysis. Since there is no murine HB-EGF antibody, use of mice with an AT1- or AT2-specific HB-EGF deletion could offer a route to understanding these differences through a third experimental technique.

The most interesting future direction for this body of work is also the most technically challenging: elucidating the role of membrane-bound HB-EGF (proHB-EGF) compared to soluble (s)HB-EGF. HB-EGF is initially synthesized as a membrane-bound growth factor (proHB-EGF). In a process termed ectodomain shedding, proHB-EGF is cleaved by one of several proteases, resulting in a soluble component (sHB-EGF) and an intracellular carboxy-terminal HB-EGF domain (HB-EGF C)[318]. Both proHB-EGF and sHB-EGF are known to be biologically active, and since evidence exists showing that proHB-EGF-dependent signaling cannot always be replicated by sHB-EGF, it suggests that the two forms of HB-EGF have different functions, or at least promote different downstream events, from each other[319]. ProHB-EGF is known to stimulate DNA synthesis, enhance intercellular adhesion, and regulate cell survival, sometimes with the help of cognate receptors or accessory proteins in the cell

membrane[319]. Additionally, proHB-EGF has been shown to have growth inhibitory activity, while sHB-EGF stimulates growth and keratinocyte migration and invasiveness[318,320].

That said, differing functions between proHB-EGF and sHB-EGF are hard to elucidate and may vary by organ; for example, proHB-EGF inhibits growth and apoptosis in a kidney cell line but induces mitogenic activity in EP170.1 cells[320]. Additionally, proHB-EGF and sHB-EGF may have different roles during homeostasis versus wound healing. A study by Singh et al. demonstrated that juxtacrine signaling via proHB-EGF was vital for maintaining normal epithelial structures in kidney cells, but pathological disruption of cell-cell junction induced cleavage of proHB-EGF into sHB-EGF, which then promoted proliferation, migration, and dedifferentiation[168]. Understanding the nuances of proHB-EGF and sHB-EGF is further complicated since HB-EGF C is biologically active, able to help initiate DNA replication and enhancing anti-apoptotic effects when binding to BCL-2 cofactor BAG1 after translocating to the nucleus[318,321].

To further complicate the situation, both proHB-EGF and sHB-EGF can bind to ErbB family receptors EGFR and HER4. Differences in downstream signaling pathways exist based on receptor-binding differences: while HB-EGF is not a mitogen in HER4-expressing cells, HB-EGF can stimulate both chemotaxis and proliferation in cells expressing EGFR[322]. Furthermore, sHB-EGF, along with other GPCR agonists, can cause EGFR transactivation[323,324].

Despite these challenges, understanding how proHB-EGF and sHB-EGF function in different cell sources in the lung during homeostasis or after injury is a critical next step. Like our future directions in the M1/M2 macrophage study, we could begin by examining the roles of proHB-EGF signaling *in vitro* with coculture studies and comparing experimental results to cells that only received supernatant (and thus, only sHB-EGF) during each assay. To be even more

precise, we could generate a mouse that is unable to cleave proHB-EGF in a specific cell type using one of the Cre-lox models outlined above for all myeloid cells (Lyz2Cre), for only moAMs, for AT2s (SPC-Cre), or for AT1s (Aqp5-Cre-IRES-DsRed). Data in the literature show that ADAM17 is the preferential sheddase for proHB-EGF and in cases where ADAM17 has been removed, ADAM10 can sufficiently recapitulate the sheddase function[318]. As whole-body ADAM10$^{-/-}$ and ADAM17$^{-/-}$ are embryonic lethal and perinatal lethal, respectively[318], use of a cell-specific ADAM10$^{-/-}$ADAM17$^{-/-}$ mouse would allow us to investigate effects of proHB-EGF without interference from sHB-EGF in an *in vivo* model. We could use ADAM10$^{-/-}$ADAM17$^{-/-}$;Lyz2Cre mice to test if proHB-EGF promotes or protects against pulmonary fibrosis. There are two primary hypotheses that are possible. In the first, it could be that proHB-EGF is protective while sHB-EGF is pathogenic. In this scenario, Hbegf$^{f/f}$;Lyz2Cre mice are protected from fibrosis since the pathogenic sHB-EGF is removed from macrophages. Although we know that Hbegf$^{f/f}$;Lyz2Cre mice are protected, rHB-EGF did not induce a robust profibrotic response in fibroblasts or in AECs *in vitro*. It could be that sHB-EGF is actually profibrotic, but we were unable to see a robust *in vitro* phenotype because we did not measure the correct fibrotic outcomes in fibroblasts and AECs and/or we did not look in the correct cell type (e.g., endothelial cells). ADAM10$^{-/-}$ADAM17$^{-/-}$;Lyz2Cre mice, then, should be protected in this scenario since there is an inability of macrophages to cleave proHB-EGF into sHB-EGF.

A second hypothesis could be that proHB-EGF is pathogenic and sHB-EGF, as our *in vitro* data showed, is relatively unimportant in disease pathogenesis. In this scenario, Hbegf$^{f/f}$;Lyz2Cre mice would be protected, as both forms of HB-EGF are removed, but ADAM10$^{-/-}$ADAM17$^{-/-}$;Lyz2Cre mice would develop fibrosis. Assuming that there is no proHB-EGF cleavage compensation by MMP3 or MMP7[318], lack of protection in ADAM10$^{-/-}$ADAM17^{-}

$^{/-}$;Lyz2Cre mice would support the concept that proHB-EGF is profibrotic and sHB-EGF is a less important factor in fibrosis development. However, it is highly unlikely that proHB-EGF and sHB-EGF act in a ubiquitous manner across all cell types. Rather, proHB-EGF may be pathologic for certain cell types (e.g., AECs) while sHB-EGF may be for others (e.g., fibroblasts). The two could also have preferential expression and activation based on the specific tissue and/or the inflammatory state, as is the case in the kidney and pancreas[168,169]. Additionally, we must consider the role of HB-EGF C, which when translocated to the nucleus post-ectodomain shedding, could influence propensity for apoptosis. Although this will be a complicated mechanism to fully unravel, a good next step would be to put different cell types in coculture with macrophages and perform assays similarly to what we have done with rHB-EGF. Ideally, putting all of these data together side-by-side will yield insights into the pathologic versus protective nature of proHB-EGF and sHB-EGF.

Concluding Remarks

IPF is a highly debilitating and deadly disease. With the use of a mouse model and various *in vitro* assays, we have been able to investigate factors that may regulate establishment of a profibrotic environment and the overall development of fibrosis. A primary goal of this work was to help close the gap in understanding of the intersection of macrophage dynamics, cellular crosstalk, and the role of specific growth factors in the development and progression of pulmonary fibrosis. We hope that this work may help lead to new therapeutic interventions for patients suffering from this devastating disease.

Bibliography

1. Richeldi, L., Collard, H. R. & Jones, M. G. Idiopathic pulmonary fibrosis. *The Lancet* vol. 389 1941–1952 (2017).
2. Scott, M. K. D. *et al.* Increased monocyte count as a cellular biomarker for poor outcomes in fibrotic diseases: a retrospective, multicentre cohort study. *Lancet Respir. Med.* **7**, 497–508 (2019).
3. Desai, O., Winkler, J., Minasyan, M. & Herzog, E. L. The role of immune and inflammatory cells in idiopathic pulmonary fibrosis. *Frontiers in Medicine* vol. 5 (2018).
4. Moore, B. B. *et al.* Protection from Pulmonary Fibrosis in the Absence of CCR2 Signaling. *J. Immunol.* **167**, 4368–4377 (2001).
5. Moore, B. B. *et al.* Animal models of fibrotic lung disease. *American Journal of Respiratory Cell and Molecular Biology* vol. 49 167–179 (2013).
6. Misharin, A. V. *et al.* Monocyte-derived alveolar macrophages drive lung fibrosis and persist in the lung over the life span. *J. Exp. Med.* **214**, 2387–2404 (2017).
7. Joshi, N. *et al.* A spatially restricted fibrotic niche in pulmonary fibrosis is sustained by M-CSF/M-CSFR signalling in monocyte-derived alveolar macrophages. *Eur. Respir. J.* **55**, (2020).
8. Byrne, A. J., Mathie, S. A., Gregory, L. G. & Lloyd, C. M. Pulmonary macrophages: Key players in the innate defence of the airways. *Thorax* vol. 70 1189–1196 (2015).
9. Pardo, A. Role of Epithelial Cells in Idiopathic Pulmonary Fibrosis From Innocent Targets to Serial Killers. doi:10.1513/pats.200601-003TK.
10. Ryu, C., Homer, R. J. & Herzog, E. L. The airway in idiopathic pulmonary fibrosis: Protecting the lung or promoting disease? *American Journal of Respiratory and Critical Care Medicine* vol. 193 1080–1082 (2016).
11. Robbie, H., Daccord, C., Chua, F. & Devaraj, A. Evaluating disease severity in idiopathic pulmonary fibrosis. *European Respiratory Review* vol. 26 (2017).
12. Parimon, T., Yao, C., Stripp, B. R., Noble, P. W. & Chen, P. Alveolar epithelial type II cells as drivers of lung fibrosis in idiopathic pulmonary fibrosis. *Int. J. Mol. Sci.* **21**, (2020).

13. Zhang, L. *et al.* Macrophages: Friend or foe in idiopathic pulmonary fibrosis? *Respiratory Research* vol. 19 (2018).

14. Byrne, A. J., Maher, T. M. & Lloyd, C. M. Pulmonary Macrophages: A New Therapeutic Pathway in Fibrosing Lung Disease? *Trends in Molecular Medicine* vol. 22 303–316 (2016).

15. Selman, M. & Pardo, A. Role of epithelial cells in idiopathic pulmonary fibrosis: From innocent targets to serial killers. *Proceedings of the American Thoracic Society* vol. 3 364–372 (2006).

16. About IPF | Idiopathic Pulmonary Fibrosis (IPF) Treatment. http://www.manageipf.com/about-ipf.

17. Glassberg, M. K. Overview of idiopathic pulmonary fibrosis, evidence-based guidelines, and recent developments in the treatment landscape. *Am. J. Manag. Care* **25**, S195–S203 (2019).

18. Raghu, G. *et al.* Idiopathic pulmonary fibrosis in US Medicare beneficiaries aged 65 years and older: Incidence, prevalence, and survival, 2001-11. *Lancet Respir. Med.* **2**, 566–572 (2014).

19. Esposito, D. B. *et al.* Idiopathic pulmonary fibrosis in United States automated claims incidence, prevalence, and algorithm validation. *Am. J. Respir. Crit. Care Med.* **192**, 1200–1207 (2015).

20. Lederer, D. J. & Martinez, F. J. Idiopathic Pulmonary Fibrosis. *New England Journal of Medicine* vol. 378 1811–1823 (2018).

21. Wolters, P. J. *et al.* Time for a change: is idiopathic pulmonary fibrosis still idiopathic and only fibrotic? *The Lancet Respiratory Medicine* vol. 6 154–160 (2018).

22. Raghu, G., Weycker, D., Edelsberg, J., Bradford, W. Z. & Oster, G. Incidence and prevalence of idiopathic pulmonary fibrosis. *Am. J. Respir. Crit. Care Med.* **174**, 810–816 (2006).

23. Raghu, G. *et al.* Diagnosis of idiopathic pulmonary fibrosis An Official ATS/ERS/JRS/ALAT Clinical practice guideline. *Am. J. Respir. Crit. Care Med.* **198**, e44–e68 (2018).

24. Naikawadi, R. P. *et al.* Telomere dysfunction in alveolar epithelial cells causes lung remodeling and fibrosis. *JCI Insight* **1**, (2016).

25. Kropski, J. A. *et al.* Extensive phenotyping of individuals at risk for familial interstitial pneumonia reveals clues to the pathogenesis of interstitial lung disease. *Am. J. Respir. Crit. Care Med.* **191**, 417–426 (2015).

26. Ley, B. *et al.* The MUC5B promoter polymorphism and telomere length in patients with chronic hypersensitivity pneumonitis: an observational cohort-control study. *Lancet Respir. Med.* **5**, 639–647 (2017).

27. Alder, J. K. *et al.* Short telomeres are a risk factor for idiopathic pulmonary fibrosis. *Proc. Natl. Acad. Sci. U. S. A.* **105**, 13051–13056 (2008).

28. Ballester, Milara & Cortijo. Mucins as a New Frontier in Pulmonary Fibrosis. *J. Clin. Med.* **8**, 1447 (2019).

29. Zhang, Y. *et al.* Histopathological and molecular analysis of idiopathic pulmonary fibrosis lungs from patients treated with pirfenidone or nintedanib. *Histopathology* **74**, 341–349 (2019).

30. Ohshimo, S. *et al.* Significance of bronchoalveolar lavage for the diagnosis of idiopathic pulmonary fibrosis. *Am. J. Respir. Crit. Care Med.* **179**, 1043–1047 (2009).

31. Collard, H. R. *et al.* Acute exacerbation of idiopathic pulmonary fibrosis an international working group report. *American Journal of Respiratory and Critical Care Medicine* vol. 194 265–275 (2016).

32. Valapour, M. *et al.* OPTN/SRTR 2016 Annual Data Report: Lung. *Am. J. Transplant.* **18**, 363–433 (2018).

33. Misharin, A. V. & Scott Budinger, G. R. Targeting the myofibroblast in pulmonary fibrosis. *American Journal of Respiratory and Critical Care Medicine* vol. 198 834–835 (2018).

34. Karimi-Shah, B. A. & Chowdhury, B. A. Forced vital capacity in idiopathic pulmonary fibrosis - FDA review of pirfenidone and nintedanib. *N. Engl. J. Med.* **372**, 1189–1191 (2015).

35. Noble, P. W. *et al.* Pirfenidone in patients with idiopathic pulmonary fibrosis (CAPACITY): Two randomised trials. *Lancet* **377**, 1760–1769 (2011).

36. King, T. E. *et al.* A phase 3 trial of pirfenidone in patients with idiopathic pulmonary fibrosis. *N. Engl. J. Med.* **370**, 2083–2092 (2014).

37. Richeldi, L. *et al.* Efficacy and safety of nintedanib in idiopathic pulmonary fibrosis. *N. Engl. J. Med.* **370**, 2071–2082 (2014).

38. Richeldi, L. *et al.* Efficacy of a tyrosine kinase inhibitor in idiopathic pulmonary fibrosis. *N. Engl. J. Med.* **365**, 1079–1087 (2011).

39. Azuma, A. *et al.* Double-blind, placebo-controlled trial of pirfenidone in patients with idiopathic pulmonary fibrosis. *Am. J. Respir. Crit. Care Med.* **171**, 1040–1047 (2005).

40. Corte, T. *et al.* Safety, tolerability and appropriate use of nintedanib in idiopathic pulmonary fibrosis. *Respir. Res.* **16**, (2015).

41. Costabel, U. *et al.* Efficacy of nintedanib in idiopathic pulmonary fibrosis across prespecified subgroups in INPULSIS. *Am. J. Respir. Crit. Care Med.* **193**, 178–185 (2016).

42. Woodcock, H. V, Molyneaux, P. L. & Maher, T. M. Reducing lung function decline in patients with idiopathic pulmonary fibrosis: potential of nintedanib. *Drug Des. Devel. Ther.* **7**, 503–10 (2013).

43. Olsson, A. K., Dimberg, A., Kreuger, J. & Claesson-Welsh, L. VEGF receptor signalling - In control of vascular function. *Nature Reviews Molecular Cell Biology* vol. 7 359–371 (2006).

44. Lee, B. S., Margolin, S. B. & Nowak, R. A. Pirfenidone: A novel pharmacological agent that inhibits leiomyoma cell proliferation and collagen production. *J. Clin. Endocrinol. Metab.* **83**, 219–223 (1998).

45. Schaefer, C. J., Ruhrmund, D. W., Pan, L., Seiwert, S. D. & Kossen, K. Antifibrotic activities of pirfenidone in animal models. *European Respiratory Review* vol. 20 85–97 (2011).

46. Ley, B. *et al.* Pirfenidone reduces respiratory-related hospitalizations in idiopathic pulmonary fibrosis. *Am. J. Respir. Crit. Care Med.* **196**, 756–761 (2017).

47. Roberts, S. N. *et al.* A novel model for human interstitial lung disease: Hapten-driven lung fibrosis in rodents. *J. Pathol.* **176**, 309–318 (1995).

48. Moore, B. B. & Hogaboam, C. M. Murine models of pulmonary fibrosis. *American Journal of Physiology - Lung Cellular and Molecular Physiology* vol. 294 L152-60 (2008).

49. Moore, B. B. *et al.* The role of CCL12 in the recruitment of fibrocytes and lung fibrosis. *Am. J. Respir. Cell Mol. Biol.* **35**, 175–181 (2006).

50. Chan, J. Y. W. *et al.* Regulation of TLR4 in silica-induced inflammation: An underlying mechanism of silicosis. *Int. J. Med. Sci.* **15**, 986–991 (2018).

51. Davis, G. S., Leslie, K. O. & Hemenway, D. R. Silicosis in mice: effects of dose, time, and genetic strain. *J. Environ. Pathol. Toxicol. Oncol.* **17**, 81–97 (1998).

52. Kishimoto, T. *et al.* Clinical, radiological, and pathological investigation of asbestosis. *Int. J. Environ. Res. Public Health* **8**, 899–912 (2011).

53. Roggli, V. L. *et al.* Pathology of asbestosis - An update of the diagnostic criteria report of

the asbestosis committee of the college of american pathologists and pulmonary pathology society. *Arch. Pathol. Lab. Med.* **134**, 462–480 (2010).

54. De Volder, M. F. L., Tawfick, S. H., Baughman, R. H. & Hart, A. J. Carbon nanotubes: Present and future commercial applications. *Science* vol. 339 535–539 (2013).

55. Frank, E. A., Carreira, V. S., Birch, M. E. & Yadav, J. S. Carbon Nanotube and Asbestos Exposures Induce Overlapping but Distinct Profiles of Lung Pathology in Non-Swiss Albino CF-1 Mice. *Toxicol. Pathol.* **44**, 211–225 (2016).

56. Sime, P. J., Xing, Z., Graham, F. L., Csaky, K. G. & Gauldie, J. Adenovector-mediated gene transfer of active transforming growth factor- β1 induces prolonged severe fibrosis in rat lung. *J. Clin. Invest.* **100**, 768–776 (1997).

57. Chun, G. L., Kang, H. R., Homer, R. J., Chupp, G. & Elias, J. A. Transgenic modeling of transforming growth factor-β1: Role of apoptosis in fibrosis and alveolar remodeling. in *Proceedings of the American Thoracic Society* vol. 3 418–423 (2006).

58. Sureshbabu, A. *et al.* Conditional overexpression of TGFβ1 promotes pulmonary inflammation, apoptosis and mortality via TGFβR2 in the developing mouse lung. *Respir. Res.* **16**, (2015).

59. Hardie, W. D. *et al.* Genomic profile of matrix and vasculature remodeling in TGF-α-induced pulmonary fibrosis. *Am. J. Respir. Cell Mol. Biol.* **37**, 309–321 (2007).

60. Madala, S. K. *et al.* Inhibition of the αvβ6 integrin leads to limited alteration of TGF-α-induced pulmonary fibrosis. *Am. J. Physiol. - Lung Cell. Mol. Physiol.* **306**, L726-35 (2014).

61. Fujita, M. *et al.* Overexpression of Tumor Necrosis Factor-α Diminishes Pulmonary Fibrosis Induced by Bleomycin or Transforming Growth Factor-β. *Am. J. Respir. Cell Mol. Biol.* **29**, 669–676 (2003).

62. Sime, P. J. *et al.* Transfer of tumor necrosis factor-α to rat lung induces severe pulmonary inflammation and patchy interstitial fibrogenesis with induction of transforming growth factor-β1 and myofibroblasts. *Am. J. Pathol.* **153**, 825–832 (1998).

63. Kolb, M., Margetts, P. J., Anthony, D. C., Pitossi, F. & Gauldie, J. Transient expression of IL-1β induces acute lung injury and chronic repair leading to pulmonary fibrosis. *J. Clin. Invest.* **107**, 1529–1536 (2001).

64. Chun Geun Lee *et al.* Interleukin-13 induces tissue fibrosis by selectively stimulating and activating transforming growth factor β1. *J. Exp. Med.* **194**, 809–821 (2001).

65. Murray, L. A. *et al.* Targeting interleukin-13 with tralokinumab attenuates lung fibrosis and epithelial damage in a humanized SCID idiopathic pulmonary fibrosis model. *Am. J.*

Respir. Cell Mol. Biol. **50**, 985–994 (2014).

66. Sisson, T. H. *et al.* Targeted injury of type II alveolar epithelial cells induces pulmonary fibrosis. *Am. J. Respir. Crit. Care Med.* **181**, 254–263 (2010).

67. Beach, T. A., Groves, A. M., Williams, J. P. & Finkelstein, J. N. Modeling radiation-induced lung injury: lessons learned from whole thorax irradiation. *International Journal of Radiation Biology* vol. 96 129–144 (2020).

68. Torres-González, E. *et al.* Role of endoplasmic reticulum stress in age-related susceptibility to lung fibrosis. *Am. J. Respir. Cell Mol. Biol.* **46**, 748–756 (2012).

69. Habiel, D. M., Espindola, M. S., Coelho, A. L. & Hogaboam, C. M. Modeling Idiopathic Pulmonary Fibrosis in Humanized Severe Combined Immunodeficient Mice. *Am. J. Pathol.* **188**, 891–903 (2018).

70. Pierce, E. M. *et al.* Therapeutic targeting of CC ligand 21 or CC chemokine receptor 7 abrogates pulmonary fibrosis induced by the adoptive transfer of human pulmonary fibroblasts to immunodeficient mice. *Am. J. Pathol.* **170**, 1152–1164 (2007).

71. Degryse, A. L. & Lawson, W. E. Progress toward improving animal models for idiopathic pulmonary fibrosis. in *American Journal of the Medical Sciences* vol. 341 444–449 (2011).

72. Moeller, A., Ask, K., Warburton, D., Gauldie, J. & Kolb, M. The bleomycin animal model: A useful tool to investigate treatment options for idiopathic pulmonary fibrosis? *International Journal of Biochemistry and Cell Biology* vol. 40 362–382 (2008).

73. Muggia, F. M., Louie, A. C. & Sikic, B. I. Pulmonary toxicity of antitumor agents. *Cancer Treat. Rev.* **10**, 221–243 (1983).

74. Peng, R. *et al.* Bleomycin Induces Molecular Changes Directly Relevant to Idiopathic Pulmonary Fibrosis: A Model for 'Active' Disease. *PLoS One* **8**, (2013).

75. Goldstein, R. H., Lucey, E. C., Franzblau, C. & Snider, G. L. Failure of mechanical properties to parallel changes in lung connective tissue composition in bleomycin-induced pulmonary fibrosis in hamsters. *Am. Rev. Respir. Dis.* **120**, 67–73 (1979).

76. Lawson, W. E. *et al.* Increased and prolonged pulmonary fibrosis in surfactant protein C-deficient mice following intratracheal bleomycin. *Am. J. Pathol.* **167**, 1267–1277 (2005).

77. Starcher, B. C., Kuhn, C. & Overton, J. E. Increased elastin and collagen content in the lungs of hamsters receiving an intratracheal injection of bleomycin. *Am. Rev. Respir. Dis.* **117**, 299–305 (1978).

78. Thrall, R. S., McCormick, J. R., Jack, R. M., McReynolds, R. A. & Ward, P. A.

Bleomycin-induced pulmonary fibrosis in the rat. Inhibition by indomethacin. *Am. J. Pathol.* **95**, 117–130 (1979).

79. Gharaee-Kermani, M., Hatano, K., Nozaki, Y. & Phan, S. H. Gender-based differences in bleomycin-induced pulmonary fibrosis. *Am. J. Pathol.* **166**, 1593–1606 (2005).

80. Phan, S. H. *et al.* A comparative study of pulmonary fibrosis induced by bleomycin and an O2 metabolite producing enzyme system. *Chest* **83**, 44S-45S (1983).

81. Jenkins, R. G. *et al.* An official American thoracic society workshop report: Use of animal models for the preclinical assessment of potential therapies for pulmonary fibrosis. *Am. J. Respir. Cell Mol. Biol.* **56**, 667–679 (2017).

82. Misharin, A. V., Morales-Nebreda, L., Mutlu, G. M., Budinger, G. R. S. & Perlman, H. Flow cytometric analysis of macrophages and dendritic cell subsets in the mouse lung. *Am. J. Respir. Cell Mol. Biol.* **49**, 503–510 (2013).

83. Wynn, T. A. & Vannella, K. M. Review Macrophages in Tissue Repair, Regeneration, and Fibrosis. doi:10.1016/j.immuni.2016.02.015.

84. Zhou, Y. *et al.* Chitinase 3-like 1 suppresses injury and promotes fibroproliferative responses in mammalian lung fibrosis. *Sci. Transl. Med.* **6**, 240ra76 (2014).

85. Moore, M. W. & Herzog, E. L. Regulation and Relevance of Myofibroblast Responses in Idiopathic Pulmonary Fibrosis. *Current Pathobiology Reports* vol. 1 199–208 (2013).

86. Klingberg, F., Hinz, B. & White, E. S. The myofibroblast matrix: Implications for tissue repair andfibrosis. *Journal of Pathology* vol. 229 298–309 (2013).

87. Hinz, B. *et al.* Recent developments in myofibroblast biology: Paradigms for connective tissue remodeling. *American Journal of Pathology* vol. 180 1340–1355 (2012).

88. Cory, G. Scratch-wound assay. *Methods Mol. Biol.* **769**, 25–30 (2011).

89. Barbas-Filho, J. V. *et al.* Evidence of type II pneumocyte apoptosis in the pathogenesis of idiopathic pulmonary fibrosis (IFP)/usual interstitial pneumonia (UIP). *J. Clin. Pathol.* **54**, 132–138 (2001).

90. Plataki, M. *et al.* Expression of apoptotic and antiapoptotic markers in epithelial cells in idiopathic pulmonary fibrosis. *Chest* **127**, 266–274 (2005).

91. Maeyama, T. *et al.* Upregulation of Fas-signalling molecules in lung epithelial cells from patients with idiopathic pulmonary fibrosis. *Eur. Respir. J.* **17**, 180–189 (2001).

92. Kuwano, K. *et al.* The involvement of Fas-Fas ligand pathway in fibrosing lung diseases. *Am. J. Respir. Cell Mol. Biol.* **20**, 53–60 (1999).

93. Hagimoto, N., Kuwano, K., Nomoto, Y., Kunitake, R. & Hara, N. Apoptosis and Expression of Fas/Fas Ligand mRNA in Bleomycin-induced Pulmonary Fibrosis in Mice. *Am. J. Respir. Cell Mol. Biol.* **16**, 91–101 (1997).

94. Korfei, M. *et al.* Epithelial endoplasmic reticulum stress and apoptosis in sporadic idiopathic pulmonary fibrosis. *Am. J. Respir. Crit. Care Med.* **178**, 838–846 (2008).

95. Lawson, W. E. *et al.* Endoplasmic reticulum stress in alveolar epithelial cells is prominent in IPF: Association with altered surfactant protein processing and herpesvirus infection. *Am. J. Physiol. - Lung Cell. Mol. Physiol.* **294**, L1119-26 (2008).

96. Lawson, W. E. *et al.* Endoplasmic reticulum stress enhances fibrotic remodeling in the lungs. *Proc. Natl. Acad. Sci. U. S. A.* **108**, 10562–10567 (2011).

97. Piantadosi, C. A. & Suliman, H. B. Mitochondrial Dysfunction in Lung Pathogenesis. *Annu. Rev. Physiol.* **79**, 495–515 (2017).

98. Mora, A. L., Bueno, M. & Rojas, M. Mitochondria in the spotlight of aging and idiopathic pulmonary fibrosis. *Journal of Clinical Investigation* vol. 127 405–414 (2017).

99. Kropski, J. A. & Blackwell, T. S. Endoplasmic reticulum stress in the pathogenesis of fibrotic disease. *Journal of Clinical Investigation* vol. 128 64–73 (2018).

100. Yao, C. *et al.* Senescence of Alveolar Stem Cells Drives Progressive Pulmonary Fibrosis. *SSRN Electron. J.* (2019) doi:10.2139/ssrn.3438364.

101. Selman, M. & Pardo, A. The leading role of epithelial cells in the pathogenesis of idiopathic pulmonary fibrosis. *Cell. Signal.* **66**, (2020).

102. Braga, T. T., Agudelo, J. S. H. & Camara, N. O. S. Macrophages during the fibrotic process: M2 as friend and foe. *Frontiers in Immunology* vol. 6 (2015).

103. Misharin, A. V., Budinger, G. R. S. & Perlman, H. The lung macrophage: A jack of all trades. *American Journal of Respiratory and Critical Care Medicine* vol. 184 497–498 (2011).

104. Reyfman, P. A. *et al.* Single-cell transcriptomic analysis of human lung provides insights into the pathobiology of pulmonary fibrosis. *Am. J. Respir. Crit. Care Med.* **199**, 1517–1536 (2019).

105. Moore, B. B. *et al.* Inflammatory leukocyte phenotypes correlate with disease progression in idiopathic pulmonary fibrosis. *Front. Med.* **1**, (2014).

106. Scott, M. K. D. *et al.* Increased monocyte count as a cellular biomarker for poor outcomes in fibrotic diseases: a retrospective, multicentre cohort study. *Lancet. Respir. Med.* **7**, 497–508 (2019).

107. Kreuter, M. *et al.* Monocyte Count as a Prognostic Biomarker in Patients with Idiopathic Pulmonary Fibrosis. *Am. J. Respir. Crit. Care Med.* **204**, 74–81 (2021).

108. Stockmann, C. *et al.* Loss of myeloid cell-derived vascular endothelial growth factor accelerates fibrosis. *Proc. Natl. Acad. Sci. U. S. A.* **107**, 4329–34 (2010).

109. Barratt, S. L. *et al.* Differential expression of VEGF-Axxx isoforms is critical for development of pulmonary fibrosis. *Am. J. Respir. Crit. Care Med.* **196**, 479–493 (2017).

110. Koch, C. M., Stephen, F. C., Misharin, A. V. & Ridge, K. M. Lung interstitial macrophages: Establishing identity and uncovering heterogeneity. *American Journal of Respiratory Cell and Molecular Biology* vol. 57 7–9 (2017).

111. Guilliams, M. *et al.* Alveolar macrophages develop from fetal monocytes that differentiate into long-lived cells in the first week of life via GM-CSF. *J. Exp. Med.* **210**, 1977–1992 (2013).

112. Hashimoto, D. *et al.* Tissue-resident macrophages self-maintain locally throughout adult life with minimal contribution from circulating monocytes. *Immunity* **38**, 792–804 (2013).

113. Landsman, L., Varol, C. & Jung, S. Distinct Differentiation Potential of Blood Monocyte Subsets in the Lung. *J. Immunol.* **178**, 2000–2007 (2007).

114. Landsman, L. & Jung, S. Lung Macrophages Serve as Obligatory Intermediate between Blood Monocytes and Alveolar Macrophages. *J. Immunol.* **179**, 3488–3494 (2007).

115. Ji, W. J. *et al.* Temporal and spatial characterization of mononuclear phagocytes in circulating, lung alveolar and interstitial compartments in a mouse model of bleomycin-induced pulmonary injury. *J. Immunol. Methods* **403**, 7–16 (2014).

116. Joshi, N., Walter, J. M. & Misharin, A. V. Alveolar Macrophages. (2018) doi:10.1016/j.cellimm.2018.01.005.

117. Maus, U. A. *et al.* Resident alveolar macrophages are replaced by recruited monocytes in response to endotoxin-induced lung inflammation. *Am. J. Respir. Cell Mol. Biol.* **35**, 227–35 (2006).

118. Galli, S. J., Borregaard, N. & Wynn, T. A. Phenotypic and functional plasticity of cells of innate immunity: Macrophages, mast cells and neutrophils. *Nature Immunology* vol. 12 1035–1044 (2011).

119. Davies, L. C., Jenkins, S. J., Allen, J. E. & Taylor, P. R. Tissue-resident macrophages. *Nature Immunology* vol. 14 986–995 (2013).

120. Watanabe, S., Alexander, M., Misharin, A. V. & Budinger, G. R. S. The role of macrophages in the resolution of inflammation. *Journal of Clinical Investigation* vol. 129

2619–2628 (2019).

121. McCubbrey, A. L. *et al.* Selective and inducible targeting of CD11b+ mononuclear phagocytes in the murine lung with hCD68-rtTA transgenic systems. *Am. J. Physiol. - Lung Cell. Mol. Physiol.* **311**, L87–L100 (2016).

122. Ruytinx, P., Proost, P., Van Damme, J. & Struyf, S. Chemokine-induced macrophage polarization in inflammatory conditions. *Frontiers in Immunology* vol. 9 (2018).

123. West, A. P. *et al.* TLR signalling augments macrophage bactericidal activity through mitochondrial ROS. *Nature* **472**, 476–480 (2011).

124. Mosser, D. M. & Edwards, J. P. Exploring the full spectrum of macrophage activation. *Nature Reviews Immunology* vol. 8 958–969 (2008).

125. Raes, G. *et al.* FIZZ1 and Ym as tools to discriminate between differentially activated macrophages. in *Developmental Immunology* vol. 9 151–159 (Hindawi Limited, 2002).

126. Hesketh, M., Sahin, K. B., West, Z. E. & Murray, R. Z. Macrophage phenotypes regulate scar formation and chronic wound healing. *International Journal of Molecular Sciences* vol. 18 (2017).

127. Ginhoux, F. & Guilliams, M. Tissue-Resident Macrophage Ontogeny and Homeostasis. *Immunity* vol. 44 439–449 (2016).

128. Gautiar, E. L. *et al.* Gene-expression profiles and transcriptional regulatory pathways that underlie the identity and diversity of mouse tissue macrophages. *Nat. Immunol.* **13**, 1118–1128 (2012).

129. Homer, R. J., Elias, J. A., Lee, C. G. & Herzog, E. Modern concepts on the role of inflammation in pulmonary fibrosis. *Archives of Pathology and Laboratory Medicine* vol. 135 780–788 (2011).

130. Sivakumar, P., Ntolios, P., Jenkins, G. & Laurent, G. Into the matrix: Targeting fibroblasts in pulmonary fibrosis. *Curr. Opin. Pulm. Med.* **18**, 462–469 (2012).

131. Gordon, S. & Martinez, F. O. Review Alternative Activation of Macrophages: Mechanism and Functions. *Immunity* **32**, 593–604.

132. Rauh, M. J. *et al.* SHIP represses the generation of alternatively activated macrophages. *Immunity* **23**, 361–374 (2005).

133. Hesse, M. *et al.* Differential Regulation of Nitric Oxide Synthase-2 and Arginase-1 by Type 1/Type 2 Cytokines In Vivo: Granulomatous Pathology Is Shaped by the Pattern of l-Arginine Metabolism. *J. Immunol.* **167**, 6533–6544 (2001).

134. Van Dyken, S. J. & Locksley, R. M. Interleukin-4- and Interleukin-13-Mediated

Alternatively Activated Macrophages: Roles in Homeostasis and Disease. *Annu. Rev. Immunol.* **31**, 317–343 (2013).

135. Roberts, A. B. *et al.* Transforming growth factor type β: Rapid induction of fibrosis and angiogenesis in vivo and stimulation of collagen formation in vitro. *Proc. Natl. Acad. Sci. U. S. A.* **83**, 4167–4171 (1986).

136. Sunderkotter, C., Steinbrink, K., Goebeler, M., Bhardwaj, R. & Sorg, C. Macrophages and angiogenesis. *Journal of Leukocyte Biology* vol. 55 410–422 (1994).

137. Atamas, S. P. *et al.* Pulmonary and Activation-Regulated Chemokine Stimulates Collagen Production in Lung Fibroblasts. *Am. J. Respir. Cell Mol. Biol.* **29**, 743–749 (2003).

138. Prasse, A. *et al.* A vicious circle of alveolar macrophages and fibroblasts perpetuates pulmonary fibrosis via CCL18. *Am. J. Respir. Crit. Care Med.* **173**, 781–792 (2006).

139. Prasse, A. *et al.* Serum CC-chemokine ligand 18 concentration predicts outcome in idiopathic pulmonary fibrosis. *Am. J. Respir. Crit. Care Med.* **179**, 717–723 (2009).

140. Inomata, M. *et al.* Pirfenidone inhibits fibrocyte accumulation in the lungs in bleomycin-induced murine pulmonary fibrosis. *Respir. Res.* **15**, 16 (2014).

141. Vallath, S., Hynds, R. E., Succony, L., Janes, S. M. & Giangreco, A. Targeting EGFR signalling in chronic lung disease: therapeutic challenges and opportunities. *Eur. Respir. J.* **44**, 513–22 (2014).

142. Higashiyama, S. *et al.* Membrane-anchored growth factors, the epidermal growth factor family: beyond receptor ligands. *Cancer Sci.* **99**, 214–20 (2008).

143. Zhang, H. *et al.* ErbB receptors: From oncogenes to targeted cancer therapies. *Journal of Clinical Investigation* vol. 117 2051–2058 (2007).

144. Jorissen, R. N. *et al.* Epidermal growth factor receptor: Mechanisms of activation and signalling. *Experimental Cell Research* vol. 284 31–53 (2003).

145. Venkataraman, T. & Frieman, M. B. The role of epidermal growth factor receptor (EGFR) signaling in SARS coronavirus-induced pulmonary fibrosis. *Antiviral Res.* **143**, 142–150 (2017).

146. Roskoski, R. The ErbB/HER family of protein-tyrosine kinases and cancer. *Pharmacological Research* vol. 79 34–74 (2014).

147. Zeng, F. & Harris, R. C. Epidermal growth factor, from gene organization to bedside. *Seminars in Cell and Developmental Biology* vol. 28 2–11 (2014).

148. Riese, D. J. & Cullum, R. L. Epiregulin: Roles in normal physiology and cancer. *Seminars in Cell and Developmental Biology* vol. 28 49–56 (2014).

149. Singh, B., Carpenter, G. & Coffey, R. J. EGF receptor ligands: Recent advances [version 1; referees: 3 approved]. *F1000Research* vol. 5 (2016).

150. Taylor, S. R., Markesbery, M. G. & Harding, P. A. Heparin-binding epidermal growth factor-like growth factor (HB-EGF) and proteolytic processing by a disintegrin and metalloproteinases (ADAM): A regulator of several pathways. *Seminars in Cell and Developmental Biology* vol. 28 22–30 (2014).

151. Eapen, M. S. *et al.* Heparin-binding epidermal growth factor (HB-EGF) drives EMT in patients with COPD: implications for disease pathogenesis and novel therapies. *Laboratory Investigation* vol. 99 150–157 (2019).

152. Liu, T. C., Jin, X., Wang, Y. & Wang, K. Role of epidermal growth factor receptor in lung cancer and targeted therapies. *American Journal of Cancer Research* vol. 7 187–202 (2017).

153. Roepstorff, K. *et al.* Differential effects of EGFR ligands on endocytic sorting of the receptor. *Traffic* **10**, 1115–27 (2009).

154. Singh, B. & Coffey, R. J. From wavy hair to naked proteins: The role of transforming growth factor alpha in health and disease. *Seminars in Cell and Developmental Biology* vol. 28 12–21 (2014).

155. Berasain, C. & Avila, M. A. Amphiregulin. *Seminars in Cell and Developmental Biology* vol. 28 31–41 (2014).

156. Wilson, K. J., Gilmore, J. L., Foley, J., Lemmon, M. A. & Riese, D. J. Functional selectivity of EGF family peptide growth factors: Implications for cancer. *Pharmacology and Therapeutics* vol. 122 1–8 (2009).

157. Knudsen, S. L. J., Wai Mac, A. S., Henriksen, L., Van Deurs, B. & Grøvdal, L. M. EGFR signaling patterns are regulated by its different ligands. *Growth Factors* **32**, 155–163 (2014).

158. Ronan, T. *et al.* Different Epidermal Growth Factor Receptor (EGFR) agonists produce unique signatures for the recruitment of downstream signaling proteins. *J. Biol. Chem.* **291**, 5528–5540 (2016).

159. Barrientos, S., Stojadinovic, O., Golinko, M. S., Brem, H. & Tomic-Canic, M. Growth factors and cytokines in wound healing. *Wound Repair and Regeneration* vol. 16 585–601 (2008).

160. Madtes, D. K., Elston, A. L., Hackman, R. C., Dunn, A. R. & Clark, J. G. *Transforming Growth Factor-Deficiency Reduces Pulmonary Fibrosis in Transgenic Mice*. *Am. J. Respir. Cell Mol. Biol* vol. 20 www.atsjournals.org (1999).

161. Hardie, W. D. *et al.* Conditional expression of transforming growth factor-α in adult mouse lung causes pulmonary fibrosis. *Am. J. Physiol. - Lung Cell. Mol. Physiol.* **286**, (2004).

162. Madtes, D. K. *et al.* Elevated transforming growth factor-α levels in bronchoalveolar lavage fluid of patients with acute respiratory distress syndrome. *Am. J. Respir. Crit. Care Med.* **158**, 424–430 (1998).

163. Dahlhoff, M., Wolf, E. & Schneider, M. R. The ABC of BTC: Structural properties and biological roles of betacellulin. *Seminars in Cell and Developmental Biology* vol. 28 42–48 (2014).

164. Hirabayashi, M. *et al.* Possible pro-inflammatory role of heparin-binding epidermal growth factor-like growth factor in the active phase of systemic sclerosis. *J. Dermatol.* **45**, 182–188 (2018).

165. Shirakata, Y. *et al.* Heparin-binding EGF-like growth factor accelerates keratinocyte migration and skin wound healing. *J. Cell Sci.* **118**, 2363–70 (2005).

166. Singh, A. B., Tsukada, T., Zent, R. & Harris, R. C. Membrane-associated HB-EGF modulates HGF-induced cellular responses in MDCK cells. *J. Cell Sci.* **117**, 1365–1379 (2004).

167. Singh, A. B. & Harris, R. C. Autocrine, paracrine and juxtacrine signaling by EGFR ligands. *Cell. Signal.* **17**, 1183–93 (2005).

168. Singh, A. B., Sugimoto, K., Dhawan, P. & Harris, R. C. Juxtacrine activation of EGFR regulates claudin expression and increases transepithelial resistance. *Am. J. Physiol. Cell Physiol.* **293**, C1660-8 (2007).

169. Ray, K. C. *et al.* Transmembrane and soluble isoforms of heparin-binding epidermal growth factor-like growth factor regulate distinct processes in the pancreas. *Gastroenterology* **137**, 1785–94 (2009).

170. Miyoshi, E., Higashiyama, S., Nakagawa, T., Hayashi, N. & Taniguchi, N. Membrane-anchored heparin-binding epidermal growth factor-like growth factor acts as a tumor survival factor in a hepatoma cell line. *J. Biol. Chem.* **272**, 14349–55 (1997).

171. Val, S., Belade, E., George, I., Boczkowski, J. & Baeza-Squiban, A. Fine PM induce airway MUC5AC expression through the autocrine effect of amphiregulin. *Arch. Toxicol.* **86**, 1851–1859 (2012).

172. de Boer, W. I. *et al.* Expression of epidermal growth factors and their receptors in the bronchial epithelium of subjects with chronic obstructive pulmonary disease. *Am. J. Clin. Pathol.* **125**, 184–92 (2006).

173. Zhou, Y. *et al.* Amphiregulin, an epidermal growth factor receptor ligand, plays an essential role in the pathogenesis of transforming growth factor-β-induced pulmonary fibrosis. *J. Biol. Chem.* **287**, 41991–42000 (2012).

174. Califano, D. *et al.* IFN-γ increases susceptibility to influenza A infection through suppression of group II innate lymphoid cells. *Mucosal Immunol.* **11**, 209–219 (2018).

175. Schneider, M. R. & Yarden, Y. Structure and function of epigen, the last EGFR ligand. *Seminars in Cell and Developmental Biology* vol. 28 57–61 (2014).

176. Yotsumoto, F. *et al.* HB-EGF Is a Promising Therapeutic Target for Lung Cancer with Secondary Mutation of EGFRT790M. *Anticancer Res.* **37**, 3825–3831 (2017).

177. Schneider, M. R. & Wolf, E. The epidermal growth factor receptor ligands at a glance. *Journal of Cellular Physiology* vol. 218 460–466 (2009).

178. Bethune, G., Bethune, D., Ridgway, N. & Xu, Z. Epidermal growth factor receptor (EGFR) in lung cancer: An overview and update. *Journal of Thoracic Disease* vol. 2 48–51 (2010).

179. Mishima, K. *et al.* Heparin-binding epidermal growth factor-like growth factor stimulates mitogenic signaling and is highly expressed in human malignant gliomas. *Acta Neuropathol.* **96**, 322–328 (1998).

180. De Vos, J. *et al.* Identifying intercellular signaling genes expressed in malignant plasma cells by using complementary DNA arrays. *Blood* **98**, 771–80 (2001).

181. Sato, S., Drake, A. W., Tsuji, I. & Fan, J. A Potent Anti-HB-EGF Monoclonal Antibody Inhibits Cancer Cell Proliferation and Multiple Angiogenic Activities of HB-EGF. *PLoS One* **7**, e51964 (2012).

182. Regales, L. *et al.* Dual targeting of EGFR can overcome a major drug resistance mutation in mouse models of EGFR mutant lung cancer. *J. Clin. Invest.* **119**, 3000–3010 (2009).

183. Hanna, N. *et al.* Phase II trial of cetuximab in patients with previously treated non-small-cell lung cancer. *J. Clin. Oncol.* **24**, 5253–5258 (2006).

184. Kato, T. & Nishio, K. Clinical aspects of epidermal growth factor receptor inhibitors: Benefit and risk. *Respirology* vol. 11 693–698 (2006).

185. Shepherd, F. A. *et al.* Erlotinib in previously treated non-small-cell lung cancer. *N. Engl. J. Med.* **353**, 123–32 (2005).

186. Syrigos, K. N., Saif, M. W., Karapanagiotou, E. M., Oikonomopoulos, G. & De Marinis, F. The need for third-line treatment in non-small cell lung cancer: An overview of new options. *Anticancer Research* vol. 31 649–659 (2011).

187. Pérez-Soler, R. *et al.* Determinants of tumor response and survival with erlotinib in patients with non--small-cell lung cancer. *J. Clin. Oncol.* **22**, 3238–47 (2004).

188. Langer, C. J. Emerging role of epidermal growth factor receptor inhibition in therapy for advanced malignancy: focus on NSCLC. *Int. J. Radiat. Oncol. Biol. Phys.* **58**, 991–1002 (2004).

189. Kris, M. G. *et al.* Efficacy of gefitinib, an inhibitor of the epidermal growth factor receptor tyrosine kinase, in symptomatic patients with non-small cell lung cancer: a randomized trial. *JAMA* **290**, 2149–58 (2003).

190. Giaccone, G. The role of gefitinib in lung cancer treatment. in *Clinical Cancer Research* vol. 10 4233s-4237s (American Association for Cancer Research, 2004).

191. Kobayashi, S. *et al.* EGFR mutation and resistance of non-small-cell lung cancer to gefitinib. *N. Engl. J. Med.* **352**, 786–792 (2005).

192. Kobayashi, S. *et al.* An alternative inhibitor overcomes resistance caused by a mutation of the epidermal growth factor receptor. *Cancer Res.* **65**, 7096–7101 (2005).

193. Yamaoka, T. *et al.* Blockade of EGFR activation promotes TNF-induced lung epithelial cell apoptosis and pulmonary injury. *Int. J. Mol. Sci.* **20**, (2019).

194. Ding, P. N. *et al.* Risk of Treatment-Related Toxicities from EGFR Tyrosine Kinase Inhibitors: A Meta-analysis of Clinical Trials of Gefitinib, Erlotinib, and Afatinib in Advanced EGFR-Mutated Non-Small Cell Lung Cancer. *J. Thorac. Oncol.* **12**, 633–643 (2017).

195. Camus, P., Kudoh, S. & Ebina, M. Interstitial lung disease associated with drug therapy. *Br. J. Cancer* **91 Suppl 2**, S18-23 (2004).

196. Saito, S., Lasky, J. A., Hagiwara, K. & Kondoh, Y. Ethnic differences in idiopathic pulmonary fibrosis: The Japanese perspective. *Respir. Investig.* **56**, 375–383 (2018).

197. Ishii, Y., Fujimoto, S. & Fukuda, T. Gefitinib prevents bleomycin-induced lung fibrosis in mice. *Am. J. Respir. Crit. Care Med.* **174**, 550–6 (2006).

198. Inoue, A. *et al.* Severe acute interstitial pneumonia and gefitinib. *Lancet* **361**, 137–139 (2003).

199. Aviram, G., Yu, E., Tai, P. & Lefcoe, M. S. Computed tomography to assess pulmonary injury associated with concurrent chemo-radiotherapy for inoperable non-small cell lung cancer. *Can. Assoc. Radiol. J.* **52**, 385–91 (2001).

200. Merad, M., Le Cesne, A., Baldeyrou, P., Mesurolle, B. & Le Chevalier, T. Docetaxel and interstitial pulmonary injury. *Ann. Oncol. Off. J. Eur. Soc. Med. Oncol.* **8**, 191–4 (1997).

201. Cleverley, J. R., Screaton, N. J., Hiorns, M. P., Flint, J. D. A. & Müller, N. L. Drug-induced lung disease: High-resolution CT and histological findings. *Clin. Radiol.* **57**, 292–299 (2002).

202. Sharma, S. V., Bell, D. W., Settleman, J. & Haber, D. A. Epidermal growth factor receptor mutations in lung cancer. *Nature Reviews Cancer* vol. 7 169–181 (2007).

203. Burgel, P. R. & Nadel, J. A. Epidermal growth factor receptor-mediated innate immune responses and their roles in airway diseases. *European Respiratory Journal* vol. 32 1068–1081 (2008).

204. Lai, H. Y. & Rogers, D. F. Mucus hypersecretion in asthma: Intracellular signalling pathways as targets for pharmacotherapy. *Current Opinion in Allergy and Clinical Immunology* vol. 10 67–76 (2010).

205. Tzouvelekis, A. *et al.* Increased expression of epidermal growth factor receptor (EGF-R) in patients with different forms of lung fibrosis. *Biomed Res. Int.* **2013**, 654354 (2013).

206. Shochet, G. E., Brook, E., Eyal, O., Edelstein, E. & Shitrit, D. Epidermal growth factor receptor paracrine upregulation in idiopathic pulmonary fibrosis fibroblasts is blocked by nintedanib. *Am. J. Physiol. - Lung Cell. Mol. Physiol.* **316**, L1025–L1034 (2019).

207. Grimminger, F., Günther, A. & Vancheri, C. The role of tyrosine kinases in the pathogenesis of idiopathic pulmonary fibrosis. *European Respiratory Journal* vol. 45 1426–1433 (2015).

208. Lai, T. *et al.* Heparin-binding epidermal growth factor contributes to COPD disease severity by modulating airway fibrosis and pulmonary epithelial-mesenchymal transition. *Lab. Invest.* **98**, 1159–1169 (2018).

209. Madtes, D. K., Busby, H. K., Strandjord, T. P. & Clark, J. G. Expression of transforming growth factor-alpha and epidermal growth factor receptor is increased following bleomycin-induced lung injury in rats. *Am. J. Respir. Cell Mol. Biol.* **11**, 540–551 (1994).

210. Suzuki, H., Aoshiba, K., Yokohori, N. & Nagai, A. Epidermal growth factor receptor tyrosine kinase inhibition augments a murine model of pulmonary fibrosis. *Cancer Res.* **63**, 5054–9 (2003).

211. Hardie, W. D. *et al.* EGF receptor tyrosine kinase inhibitors diminish transforming growth factor-α-induced pulmonary fibrosis. *Am. J. Physiol. - Lung Cell. Mol. Physiol.* **294**, L1217-25 (2008).

212. Adachi, K. *et al.* Effects of erlotinib on lung injury induced by intratracheal administration of bleomycin (BLM) in rats. *J. Toxicol. Sci.* **35**, 503–514 (2010).

213. Holt, D. J., Chamberlain, L. M. & Grainger, D. W. Cell-cell signaling in co-cultures of

macrophages and fibroblasts. *Biomaterials* **31**, 9382–9394 (2010).

214. Ishii, M. *et al.* Epigenetic regulation of the alternatively activated macrophage phenotype. *Blood* **114**, 3244–3254 (2009).

215. Sun, L. *et al.* Loss of myeloid-specific protein phosphatase 2A enhances lung injury and fibrosis and results in IL-10-dependent sensitization of epithelial cell apoptosis. *Am. J. Physiol. - Lung Cell. Mol. Physiol.* **316**, L1035–L1048 (2019).

216. Bauman, K. A. *et al.* The antifibrotic effects of plasminogen activation occur via prostaglandin E2 synthesis in humans and mice. *J. Clin. Invest.* **120**, 1950–1960 (2010).

217. Liang, Q. *et al.* Lycorine ameliorates bleomycin-induced pulmonary fibrosis via inhibiting NLRP3 inflammasome activation and pyroptosis. *Pharmacol. Res.* **158**, (2020).

218. Gharib, S. A. *et al.* MMP28 promotes macrophage polarization toward M2 cells and augments pulmonary fibrosis. *J. Leukoc. Biol.* **95**, 9–18 (2014).

219. Bhatia, D. *et al.* Mitophagy-dependent macrophage reprogramming protects against kidney fibrosis. *JCI Insight* **4**, (2019).

220. Schyns, J. *et al.* Non-classical tissue monocytes and two functionally distinct populations of interstitial macrophages populate the mouse lung. *Nat. Commun.* **10**, (2019).

221. Nair, M. G., Cochrane, D. W. & Allen, J. E. Macrophages in chronic type 2 inflammation have a novel phenotype characterized by the abundant expression of Ym1 and Fizz1 that can be partly replicated in vitro. *Immunol. Lett.* **85**, 173–180 (2003).

222. Wen, H. J. *et al.* Myeloid Cell-Derived HB-EGF Drives Tissue Recovery After Pancreatitis. *CMGH* **8**, 173–192 (2019).

223. Kendall, R. T. & Feghali-Bostwick, C. A. Fibroblasts in fibrosis: Novel roles and mediators. *Frontiers in Pharmacology* vol. 5 MAY (2014).

224. Maher, T. M. *et al.* Diminished prostaglandin E2 contributes to the apoptosis paradox in idiopathic pulmonary fibrosis. *Am. J. Respir. Crit. Care Med.* **182**, 73–82 (2010).

225. Nho, R. S., Peterson, M., Hergert, P. & Henke, C. A. FoxO3a (Forkhead Box O3a) Deficiency Protects Idiopathic Pulmonary Fibrosis (IPF) Fibroblasts from Type I Polymerized Collagen Matrix-Induced Apoptosis via Caveolin-1 (cav-1) and Fas. *PLoS One* **8**, (2013).

226. Bozyk, P. D. & Moore, B. B. Prostaglandin E 2 and the pathogenesis of pulmonary fibrosis. *American Journal of Respiratory Cell and Molecular Biology* vol. 45 445–452 (2011).

227. Vancheri, C., Mastruzzo, C., Sortino, M. A. & Crimi, N. The lung as a privileged site for

the beneficial actions of PGE2. *Trends in Immunology* vol. 25 40–46 (2004).

228. Sgalla, G. *et al.* Idiopathic pulmonary fibrosis: Pathogenesis and management. *Respiratory Research* vol. 19 (2018).

229. Kim, S. J. *et al.* Mitochondrial 8-oxoguanine DNA glycosylase mitigates alveolar epithelial cell PINK1 deficiency, mitochondrial DNA damage, apoptosis, and lung fibrosis. *Am. J. Physiol. Lung Cell. Mol. Physiol.* **318**, L1084–L1096 (2020).

230. Akram, K. M., Lomas, N. J., Forsyth, N. R. & Spiteri, M. A. Alveolar epithelial cells in idiopathic pulmonary fibrosis display upregulation of TRAIL, DR4 and DR5 expression with simultaneous preferential over-expression of pro-apoptotic marker p53. *Int. J. Clin. Exp. Pathol.* **7**, 552–564 (2014).

231. Guo, X. Y. *et al.* Transcriptome profile of rat genes in bone marrow-derived macrophages at different activation statuses by RNA-sequencing. *Genomics* **111**, 986–996 (2019).

232. Tang, L. *et al.* M2A and M2C Macrophage Subsets Ameliorate Inflammation and Fibroproliferation in Acute Lung Injury Through Interleukin 10 Pathway. *Shock* **48**, 119–129 (2017).

233. Tu, G. wei *et al.* Glucocorticoid attenuates acute lung injury through induction of type 2 macrophage. *J. Transl. Med.* **15**, (2017).

234. Lurier, E. B. *et al.* Transcriptome analysis of IL-10-stimulated (M2c) macrophages by next-generation sequencing. *Immunobiology* **222**, 847–856 (2017).

235. Elias, J. A. Tumor necrosis factor interacts with interleukin-1 and interferons to inhibit fibroblast proliferation via fibroblast prostaglandin-dependent and -independent mechanisms. *Am. Rev. Respir. Dis.* **138**, 652–658 (1988).

236. Vu, T. N., Chen, X., Foda, H. D., Smaldone, G. C. & Hasaneen, N. A. Interferon-γenhances the antifibrotic effects of pirfenidone by attenuating IPF lung fibroblast activation and differentiation. *Respir. Res.* **20**, (2019).

237. Li, W., Liang, R., Huang, H., Wu, B. & Zhong, Y. Effects of IFN-γ on cell growth and the expression of ADAM33 gene in human embryonic lung Mrc-5 fibroblasts in vitro. *J. Asthma* **55**, 15–25 (2018).

238. DiProspero, N. A., Meiners, S. & Geller, H. M. Inflammatory cytokines interact to modulate extracellular matrix and astrocytic support of neurite outgrowth. *Exp. Neurol.* **148**, 628–639 (1997).

239. Saito, A., Okazaki, H., Sugawara, I., Yamamoto, K. & Takizawa, H. Potential action of IL-4 and IL-13 as fibrogenic factors on lung fibroblasts in vitro. *Int. Arch. Allergy Immunol.* **132**, 168–176 (2003).

240. White Sergei Atamas, B. P., Luzina, I. G. & Dai, H. Receptor Signaling Fibroblast Proliferation Involves IL-4 Synergy Between CD40 Ligation and IL-4 on. (2002) doi:10.4049/jimmunol.168.3.1139.

241. Feghali, C. A., Bost, K. L., Boulware, D. W. & Levy, L. S. Human recombinant interleukin-4 induces proliferation and interleukin-6 production by cultured human skin fibroblasts. *Clin. Immunol. Immunopathol.* **63**, 182–187 (1992).

242. Postlethwaite, A. E., Holness, M. A., Katai, H. & Raghow, R. Human fibroblasts synthesize elevated levels of extracellular matrix proteins in response to interleukin 4. *J. Clin. Invest.* **90**, 1479–1485 (1992).

243. Liu, T. *et al.* The in vivo fibrotic role of FIZZ1 in pulmonary fibrosis. *PLoS One* **9**, (2014).

244. La Flamme, A. C. *et al.* Type II-Activated Murine Macrophages Produce IL-4. *PLoS One* **7**, e46989 (2012).

245. Julien, O. & Wells, J. A. Caspases and their substrates. *Cell Death and Differentiation* vol. 24 1380–1389 (2017).

246. Sjöstrand, M. & Rylander, R. Enzymes in lung lavage fluid after inhalation exposure to silica dust. *Environ. Res.* **33**, 307–311 (1984).

247. Kasper, M., Lackie, P., Haase, M., Schuh, D. & Müller, M. Immunolocalization of cathepsin D in pneumocytes of normal human lung and in pulmonary fibrosis. *Virchows Arch.* **428**, 207–215 (1996).

248. Kasper, M. & Fehrenbach, H. Immunohistochemical evidence for the occurrence of similar epithelial phenotypes during lung development and radiation-induced fibrogenesis. in *International Journal of Radiation Biology* vol. 76 493–501 (Taylor and Francis Ltd, 2000).

249. Koslowski, R., Knoch, K., Kuhlisch, E., Seidel, D. & Kasper, M. Cathepsins in bleomycin-induced lung injury in rat. *Eur. Respir. J.* **22**, 427–435 (2003).

250. Uhal, B. D. *et al.* Abrogation of ER stress-induced apoptosis of alveolar epithelial cells by angiotensin 1-7. *Am. J. Physiol. - Lung Cell. Mol. Physiol.* **305**, (2013).

251. Zhong, S. & Khalil, R. A. A Disintegrin and Metalloproteinase (ADAM) and ADAM with thrombospondin motifs (ADAMTS) family in vascular biology and disease. *Biochemical Pharmacology* vol. 164 188–204 (2019).

252. Hendrix, A. Y. & Kheradmand, F. The Role of Matrix Metalloproteinases in Development, Repair, and Destruction of the Lungs. in *Progress in Molecular Biology and Translational Science* vol. 148 1–29 (Elsevier B.V., 2017).

253. Woodcock, H. V., Molyneaux, P. L. & Maher, T. M. Reducing lung function decline in patients with idiopathic pulmonary fibrosis: Potential of nintedanib. *Drug Des. Devel. Ther.* **7**, 503–510 (2013).

254. Murray, L. A. *et al.* Antifibrotic role of vascular endothelial growth factor in pulmonary fibrosis. *JCI insight* **2**, (2017).

255. Gibbons, M. A. *et al.* Ly6Chi monocytes direct alternatively activated profibrotic macrophage regulation of lung fibrosis. *Am. J. Respir. Crit. Care Med.* **184**, 569–581 (2011).

256. Das, A. *et al.* Monocyte and Macrophage Plasticity in Tissue Repair and Regeneration. *Am. J. Pathol.* **185**, 2596 (2015).

257. Epelman, S., Lavine, K. J. & Randolph, G. J. Origin and functions of tissue macrophages. *Immunity* **41**, 21–35 (2014).

258. Besner, G., Higashiyama, S. & Klagsbrun, M. Isolation and characterization of a macrophage-derived heparin-binding growth factor. *Cell Regul.* **1**, 811 (1990).

259. Hult, E. M., Gurczynski, S. J. & Moore, B. B. M2 macrophages have unique transcriptomes but conditioned media does not promote profibrotic responses in lung fibroblasts or alveolar epithelial cells in vitro. *Am. J. Physiol. Lung Cell. Mol. Physiol.* **321**, L518–L532 (2021).

260. Poumay, Y. & De Rouvroit, C. L. HB-EGF, the growth factor that accelerates keratinocyte migration, but slows proliferation. *Journal of Investigative Dermatology* vol. 132 2129–2130 (2012).

261. Yang, J., Su, Y., Zhou, Y. & Besner, G. E. Heparin-Binding EGF-like Growth Factor (HB-EGF) Therapy for Intestinal Injury: Application and Future Prospects. *Pathophysiology* **21**, 95 (2014).

262. Su, Y., Luo, H. & Yang, J. Heparin-binding EGF-like growth factor attenuates lung inflammation and injury in a murine model of pulmonary emphysema. *Growth Factors* **36**, 246–262 (2018).

263. Cockayne, D. A. *et al.* Systemic biomarkers of neutrophilic inflammation, tissue injury and repair in COPD patients with differing levels of disease severity. *PLoS One* **7**, (2012).

264. Ashley, S. L. *et al.* Six-SOMAmer Index Relating to Immune, Protease and Angiogenic Functions Predicts Progression in IPF. *PLoS One* **11**, (2016).

265. Iwamoto, R. *et al.* Heparin-binding EGF-like growth factor and ErbB signaling is essential for heart function. *Proc. Natl. Acad. Sci. U. S. A.* **100**, 3221–3226 (2003).

266. Coomes, S. M., Farmen, S., Wilke, C. A., Laouar, Y. & Moore, B. B. Severe Gammaherpesvirus-Induced Pneumonitis and Fibrosis in Syngeneic Bone Marrow Transplant Mice Is Related to Effects of Transforming Growth Factor-β. *Am. J. Pathol.* **179**, 2382 (2011).

267. Gurczynski, S. J., Zhou, X., Flaherty, M., Wilke, C. A. & Moore, B. B. Bone Marrow Transplant Induced Alterations in Notch Signaling Promote Pathologic Th17 Responses to γ-Herpesvirus Infection. *Mucosal Immunol.* **11**, 881 (2018).

268. Hubbard, L. L. N., Ballinger, M. N., Wilke, C. A. & Moore, B. B. Comparison of conditioning regimens for alveolar macrophage reconstitution and innate immune function post bone marrow transplant. *Exp. Lung Res.* **34**, 263–275 (2008).

269. Cui, T. X. *et al.* CCR2 Mediates Chronic LPS-Induced Pulmonary Inflammation and Hypoalveolarization in a Murine Model of Bronchopulmonary Dysplasia. *Front. Immunol.* **11**, (2020).

270. Henrot, P., Prevel, R., Berger, P. & Dupin, I. Chemokines in COPD: From Implication to Therapeutic Use. *Int. J. Mol. Sci.* **20**, (2019).

271. Belchamber, K. B. R. & Donnelly, L. E. Macrophage Dysfunction in Respiratory Disease. *Results Probl. Cell Differ.* **62**, 299–313 (2017).

272. Clausen, B. E., Burkhardt, C., Reith, W., Renkawitz, R. & Förster, I. Conditional gene targeting in macrophages and granulocytes using LysMcre mice. *Transgenic Res.* **8**, 265–277 (1999).

273. Miyake, Y. *et al.* Protective role of macrophages in noninflammatory lung injury caused by selective ablation of alveolar epithelial type II Cells. *J. Immunol.* **178**, 5001–5009 (2007).

274. McCubbrey, A. L., Allison, K. C., Lee-Sherick, A. B., Jakubzick, C. V. & Janssen, W. J. Promoter Specificity and Efficacy in Conditional and Inducible Transgenic Targeting of Lung Macrophages. *Front. Immunol.* **8**, (2017).

275. Desai, T. J., Brownfield, D. G. & Krasnow, M. A. Alveolar progenitor and stem cells in lung development, renewal and cancer. *Nature* **507**, 190 (2014).

276. Radigan, K. A. *et al.* Impaired Clearance of Influenza A Virus in Obese, Leptin Receptor Deficient Mice Is Independent of Leptin Signaling in the Lung Epithelium and Macrophages. *PLoS One* **9**, (2014).

277. Habermann, A. C. *et al.* Single-cell RNA sequencing reveals profibrotic roles of distinct epithelial and mesenchymal lineages in pulmonary fibrosis. *Sci. Adv.* **6**, (2020).

278. Ayaub, E. *et al.* Single Cell RNA-seq and Mass Cytometry Reveals a Novel and a

Targetable Population of Macrophages in Idiopathic Pulmonary Fibrosis. *bioRxiv* 2021.01.04.425268 (2021) doi:10.1101/2021.01.04.425268.

279. Adams, T. S. *et al.* Single-cell RNA-seq reveals ectopic and aberrant lung-resident cell populations in idiopathic pulmonary fibrosis. *Sci. Adv.* **6**, (2020).

280. Morse, C. *et al.* Proliferating SPP1/MERTK-expressing macrophages in idiopathic pulmonary fibrosis. *Eur. Respir. J.* **54**, (2019).

281. McDonough, J. E. *et al.* Transcriptional regulatory model of fibrosis progression in the human lung. *JCI Insight* **4**, (2019).

282. Xie, T. *et al.* Single-Cell Deconvolution of Fibroblast Heterogeneity in Mouse Pulmonary Fibrosis. *Cell Rep.* **22**, 3625–3640 (2018).

283. O'Dwyer, D. N., Ashley, S. L. & Moore, B. B. Biomarkers in Lung Diseases: from Pathogenesis to Prediction to New Therapies: Influences of innate immunity, autophagy, and fibroblast activation in the pathogenesis of lung fibrosis. *Am. J. Physiol. - Lung Cell. Mol. Physiol.* **311**, L590 (2016).

284. Goodman, R. B. *et al.* Inflammatory cytokines in patients with persistence of the acute respiratory distress syndrome. *Am. J. Respir. Crit. Care Med.* **154**, 602–611 (1996).

285. Antoniades, H. N. *et al.* Expression of monocyte chemoattractant protein 1 mRNA in human idiopathic pulmonary fibrosis. *Proc. Natl. Acad. Sci. U. S. A.* **89**, 5371–5375 (1992).

286. McCubbrey, A. L., Allison, K. C., Lee-Sherick, A. B., Jakubzick, C. V. & Janssen, W. J. Promoter Specificity and Efficacy in Conditional and Inducible Transgenic Targeting of Lung Macrophages. *Front. Immunol.* **8**, (2017).

287. Riemondy, K. A. *et al.* Single cell RNA sequencing identifies TGFβ as a key regenerative cue following LPS-induced lung injury. *JCI insight* **5**, (2019).

288. Bocchino, M., Zanotta, S., Capitelli, L. & Galati, D. Dendritic Cells Are the Intriguing Players in the Puzzle of Idiopathic Pulmonary Fibrosis Pathogenesis. *Front. Immunol.* **12**, (2021).

289. Warheit-Niemi, H. I. *et al.* Fibrotic lung disease inhibits innate immune responses to Staphylococcal pneumonia via impaired neutrophil and macrophage function. *JCI insight* (2022) doi:10.1172/JCI.INSIGHT.152690.

290. Takemasa, A., Ishii, Y. & Fukuda, T. A neutrophil elastase inhibitor prevents bleomycin-induced pulmonary fibrosis in mice. *Eur. Respir. J.* **40**, 1475–1482 (2012).

291. Ishikawa, G., Liu, A. & Herzog, E. L. Evolving Perspectives on Innate Immune

Mechanisms of IPF. *Front. Mol. Biosci.* **8**, (2021).

292. Prednisone, Azathioprine, and N -Acetylcysteine for Pulmonary Fibrosis . *N. Engl. J. Med.* **366**, 1968–1977 (2012).

293. Vannella, K. M. & Wynn, T. A. Mechanisms of Organ Injury and Repair by Macrophages *. *Annu. Rev. Physiol* **79**, 593–617 (2017).

294. Moore, B. B. *et al.* Inflammatory leukocyte phenotypes correlate with disease progression in idiopathic pulmonary fibrosis. *Front. Med.* **1**, (2014).

295. Duffield, J. S. *et al.* Selective depletion of macrophages reveals distinct, opposing roles during liver injury and repair. *J. Clin. Invest.* **115**, 56–65 (2005).

296. Zhang, M. Z. *et al.* CSF-1 signaling mediates recovery from acute kidney injury. *J. Clin. Invest.* **122**, 4519–4532 (2012).

297. Murthy, S. *et al.* Alternative activation of macrophages and pulmonary fibrosis are modulated by scavenger receptor, macrophage receptor with collagenous structure. *Wiley Online Libr.* **29**, 3527–3536 (2015).

298. Gratchev, A. *et al.* Alternatively activated macrophages differentially express fibronectin and its splice variants and the extracellular matrix protein βIG-H3. *Scand. J. Immunol.* **53**, 386–392 (2001).

299. Osterholzer, J. J. *et al.* Implicating exudate macrophages and Ly-6C(high) monocytes in CCR2-dependent lung fibrosis following gene-targeted alveolar injury. *J. Immunol.* **190**, 3447–3457 (2013).

300. Wynn, T. A. & Barron, L. Macrophages: master regulators of inflammation and fibrosis. *Semin. Liver Dis.* **30**, 245–257 (2010).

301. Murray, P. J. & Wynn, T. A. Protective and pathogenic functions of macrophage subsets. *Nat. Rev. Immunol.* **11**, 723–737 (2011).

302. Young, L. R. *et al.* Epithelial-macrophage interactions determine pulmonary fibrosis susceptibility in Hermansky-Pudlak syndrome. *JCI insight* **1**, (2016).

303. Schupp, J. C. *et al.* Macrophage activation in acute exacerbation of idiopathic pulmonary fibrosis. *PLoS One* **10**, (2015).

304. Garibaldi, B. T. *et al.* Regulatory T cells reduce acute lung injury fibroproliferation by decreasing fibrocyte recruitment. *Am. J. Respir. Cell Mol. Biol.* **48**, 35–43 (2013).

305. Chapman, H. A. Epithelial-mesenchymal interactions in pulmonary fibrosis. *Annu. Rev. Physiol.* **73**, 413–435 (2011).

306. Zhou, Y. *et al.* Chitinase 3-like 1 suppresses injury and promotes fibroproliferative responses in Mammalian lung fibrosis. *Sci. Transl. Med.* **6**, (2014).

307. Hult, E. M., Warheit-Niemi, H. & Moore, B. B. Animal Models of Fibrotic Interstitial Lung Disease. *Encycl. Respir. Med.* 169–181 (2022) doi:10.1016/B978-0-12-801238-3.11286-3.

308. Sauer, B. Inducible gene targeting in mice using the Cre/lox system. *Methods* **14**, 381–392 (1998).

309. Rawlins, E. L. & Perl, A. K. The a"MAZE"ing World of Lung-Specific Transgenic Mice. *Am. J. Respir. Cell Mol. Biol.* **46**, 269 (2012).

310. De Lange, W. J., Halabi, C. M., Beyer, A. M. & Sigmund, C. D. Germ line activation of the Tie2 and SMMHC promoters causes noncell-specific deletion of floxed alleles. *Physiol. Genomics* **35**, 1–4 (2008).

311. Nathan, S. D. *et al.* The association between white blood cell count and outcomes in patients with idiopathic pulmonary fibrosis. *Respir. Med.* **170**, (2020).

312. Nathan, S. D. *et al.* Changes in neutrophil–lymphocyte or platelet–lymphocyte ratios and their associations with clinical outcomes in idiopathic pulmonary fibrosis. *J. Clin. Med.* **10**, 1427 (2021).

313. Duffield, J. S., Lupher, M., Thannickal, V. J. & Wynn, T. A. Host responses in tissue repair and fibrosis. *Annu. Rev. Pathol.* **8**, 241–276 (2013).

314. Gundra, U. M. *et al.* Alternatively activated macrophages derived from monocytes and tissue macrophages are phenotypically and functionally distinct. *Blood* **123**, e110 (2014).

315. Vannella, K. M. *et al.* Incomplete deletion of IL-4Rα by LysM(Cre) reveals distinct subsets of M2 macrophages controlling inflammation and fibrosis in chronic schistosomiasis. *PLoS Pathog.* **10**, (2014).

316. Schneider, C. *et al.* Induction of the nuclear receptor PPAR-γ by the cytokine GM-CSF is critical for the differentiation of fetal monocytes into alveolar macrophages. *Nat. Immunol. 2014 1511* **15**, 1026–1037 (2014).

317. Flodby, P. *et al.* Directed Expression of Cre in Alveolar Epithelial Type 1 Cells. *Am. J. Respir. Cell Mol. Biol.* **43**, 173 (2010).

318. Taylor, S. R., Markesbery, M. G. & Harding, P. A. Heparin-binding epidermal growth factor-like growth factor (HB-EGF) and proteolytic processing by a disintegrin and metalloproteinases (ADAM): A regulator of several pathways. *Seminars in Cell and Developmental Biology* vol. 28 22–30 (2014).

319. Lin, J., Hutchinson, L., Gaston, S. M., Raab, G. & Freeman, M. R. BAG-1 is a novel cytoplasmic binding partner of the membrane form of heparin-binding EGF-like growth factor: a unique role for proHB-EGF in cell survival regulation. *J. Biol. Chem.* **276**, 30127–30132 (2001).

320. Iwamoto, R. & Mekada, E. Heparin-binding EGF-like growth factor: a juxtacrine growth factor. *Cytokine Growth Factor Rev.* **11**, 335–344 (2000).

321. Hieda, M. *et al.* Membrane-anchored growth factor, HB-EGF, on the cell surface targeted to the inner nuclear membrane. *J. Cell Biol.* **180**, 763–769 (2008).

322. Elenius, K., Paul, S., Allison, G., Sun, J. & Klagsbrun, M. Activation of HER4 by heparin-binding EGF-like growth factor stimulates chemotaxis but not proliferation. *EMBO J.* **16**, 1268 (1997).

323. Prenzel, N. *et al.* EGF receptor transactivation by G-protein-coupled receptors requires metalloproteinase cleavage of proHB-EGF. *Nature* **402**, 884–888 (1999).

324. Forrester, S. J. *et al.* EGFR transactivation: mechanisms, pathophysiology and potential therapies in cardiovascular system. *Annu. Rev. Pharmacol. Toxicol.* **56**, 627 (2016).